AFRL-VA-WP-TR-2003-3079

COOPERATIVE DECEPTION OF RADAR NETWORKS BY USING ELECTRONIC COMBAT AIR VEHICLES (ECAV) TEAMS TO CREATE COHERENT PHANTOM TRACKS

Keith B. Purvis

Control Theory Optimization Branch (AFRL/VACA)
Control Sciences Division
Air Vehicles Directorate
Air Force Research Laboratory, Air Force Materiel Command
Wright-Patterson Air Force Base, OH 45433-7542

SEPTEMBER 2003

Final Report for 01 June 2003 – 01 September 2003

STINFO FINAL REPORT

AIR VEHICLES DIRECTORATE
AIR FORCE RESEARCH LABORATORY
AIR FORCE MATERIEL COMMAND
WRIGHT-PATTERSON AIR FORCE BASE, OH 45433-7542

NOTICE

USING GOVERNMENT DRAWINGS, SPECIFICATIONS, OR OTHER DATA INCLUDED IN THIS DOCUMENT FOR ANY PURPOSE OTHER THAN GOVERNMENT PROCUREMENT DOES NOT IN ANY WAY OBLIGATE THE U.S. GOVERNMENT. THE FACT THAT THE GOVERNMENT FORMULATED OR SUPPLIED THE DRAWINGS, SPECIFICATIONS, OR OTHER DATA DOES NOT LICENSE THE HOLDER OR ANY OTHER PERSON OR CORPORATION; OR CONVEY AND RIGHTS OR PERMISSION TO MANUFACTURE, USE, OR SELL ANY PATENTED INVENTION THAT MAY RELATE TO THEM.

THIS REPORT HAS BEEN REVIEWED BY THE OFFICE OF PUBLIC AFFAIRS (ASC/PA) AND IS RELEASABLE TO THE NATIONAL TECHNICAL INFORMATION SERVICE (NTIS). AT NTIS, IT WILL BE AVAILABLE TO THE GENERAL PUBLIC, INCLUDING FOREIGN NATIONS.

THIS TECHNICAL REPORT HAS BEEN REVIEWED AND IS APPROVED FOR PUBLICATION.

/s/
REID A. LARSON, 2d Lt, USAF
Flight Controls Engineer
Control Theory Optimization Branch
AFRL/VACA

/s/
PHILLIP R. CHANDLER
Lead, UAV Cooperative Control Team
Control Theory Optimization Branch
AFRL/VACA

/s/
DEBORAH S. GRISMER, PhD
Branch Chief
Control Theory Optimization Branch
AFRL/VACA

COPIES OF THIS REPORT SHOULD NOT BE RETURNED UNLESS RETURN IS REQUIRED BY SECURITY CONSIDERATIONS, CONTRACTUAL OBLIGATIONS, OR NOTICE ON A SPECIFIC DOCUMENT.

REPORT DOCUMENTATION PAGE

Form Approved
OMB No. 0704-0188

1. REPORT DATE *(DD-MM-YY)*	2. REPORT TYPE	3. DATES COVERED *(From - To)*
September 2003	Final	06/01/2003 – 09/01/2003

4. TITLE AND SUBTITLE
COOPERATIVE DECEPTION OF RADAR NETWORKS BY USING ELECTRONIC COMBAT AIR VEHICLES (ECAV) TEAMS TO CREATE COHERENT PHANTOM TRACKS

5a. CONTRACT NUMBER
IN-HOUSE

5b. GRANT NUMBER

5c. PROGRAM ELEMENT NUMBER
N/A

6. AUTHOR(S)
Keith B. Purvis

5d. PROJECT NUMBER
N/A

5e. TASK NUMBER
N/A

5f. WORK UNIT NUMBER
N/A

7. PERFORMING ORGANIZATION NAME(S) AND ADDRESS(ES)
Control Theory Optimization Branch (AFRL/VACA)
Control Sciences Division
Air Vehicles Directorate
Air Force Research Laboratory, Air Force Materiel Command
Wright-Patterson Air Force Base, OH 45433-7542

8. PERFORMING ORGANIZATION REPORT NUMBER
AFRL-VA-WP-TR-2003-3079

9. SPONSORING/MONITORING AGENCY NAME(S) AND ADDRESS(ES)
Air Vehicles Directorate
Air Force Research Laboratory
Air Force Materiel Command
Wright-Patterson Air Force Base, OH 45433-7542

10. SPONSORING/MONITORING AGENCY ACRONYM(S)
AFRL/VACA

11. SPONSORING/MONITORING AGENCY REPORT NUMBER(S)
AFRL-VA-WP-TR-2003-3079

12. DISTRIBUTION/AVAILABILITY STATEMENT
Approved for public release; distribution is unlimited.

13. SUPPLEMENTARY NOTES
This report contains color.

14. ABSTRACT ***(Maximum 200 Words)***
Electronic Combat Air Vehicles (ECAV) are used to generate phantom radar tracks in a single or multiple radar air defense network. The vehicles use a range delay deception transponder, which sends a delayed pulse back to the radar and causes the radar to calculate an erroneous target range. This paper provides two-dimensional analyses of scenarios involving a single ECAV deceiving a single radar and multiple ECAVs deceiving an integrated network of radars using range delay deception. Closed form solutions are provided for the various cases along with graphical representations of vehicle and phantom track trajectories.

15. SUBJECT TERMS
RADAR PHANTOM TRACKS RANGE DELAY DECEPTION, ELECTRONIC DECEPTION RADAR SYSTEM, ARBITRARY RADAR AND AIRCRAFT

16. SECURITY CLASSIFICATION OF:			17. LIMITATION OF ABSTRACT:	18. NUMBER OF PAGES	19a. NAME OF RESPONSIBLE PERSON (Monitor)
a. REPORT	b. ABSTRACT	c. THIS PAGE			Reid A. Larson
Unclassified	Unclassified	Unclassified	SAR	90	19b. TELEPHONE NUMBER *(Include Area Code)* (937) 255-6301

Standard Form 298 (Rev. 8-98)
Prescribed by ANSI Std. Z39-18

Cooperative Deception of Radar Networks by Using ECAV Teams to Create Coherent Phantom Tracks

Prepared by:
Keith B. Purvis
Summer Research Intern
Air Force Research Laboratory
AFRL/VACA

September 12, 2003

Mentors:
Phil Chandler, AFRL/VACA
Meir Pachter, AFIT/ENG

Table of Contents

I. Introduction

The scope of this project is using Electronic Combat Air Vehicles (ECAVs) to cooperatively deceive a network of radars by creating phantom tracks in two dimensions – range and azimuth. A network of radars is defined as a geometric arrangement (possibly changing with time) of two or more radars, which are able to communicate with each other; hence, two or more radars may be used to track and correlate the same target. The methods by which a team of ECAVs might create one or more phantom tracks for a network of radars include mainlobe deception using range delay techniques and sidelobe deception using range delay and angle-based techniques. Before explaining these deceptive methods for creating phantom tracks and how ECAVs might accomplish such a task, some essential radar fundamentals are presented.

II. Radar Fundamentals

All of the theory on radar presented in this paper was obtained from "Introduction to Airborne Radar" by George Stimson. To keep its transmitter from interfering with reception, a radar usually transmits radio waves in pulses and only turns on its receiver in between pulses to listen for the echoes (see Figure I below).

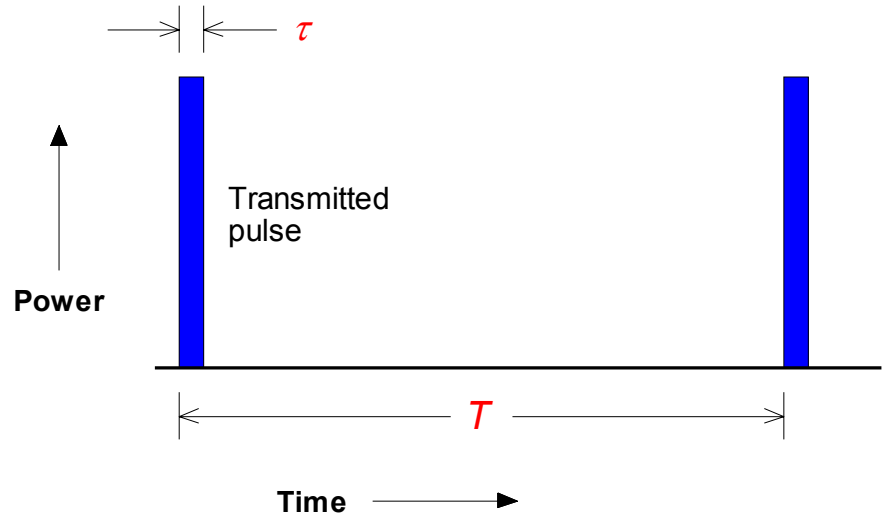

Figure I: Transmitted power of a pulsed radar over time

The parameters of interest in Figure I and some useful combinations of these parameters are defined as follows.

τ	~	Pulse width
T	~	Interpulse period or pulse repetition interval
$\frac{1}{T} = f_r$	~	Rate of pulse transmission or pulse repetition frequency (PRF)
$\frac{\tau}{T}$	~	Fraction of time the radar is transmitting or duty factor of the transmitter

Since radio waves travel at approximately the speed of light, the range (distance from radar) of a target can be determined using a measurement of the round-trip time, t, for a pulse to be transmitted and its echo from the target received. A rule of thumb is that a round-trip time of 10 microseconds corresponds to a range of 1.5 kilometers. This method of range measurement, known as pulse-delay ranging, is simple and accurate; it is valid for radars operating at a low PRF where the interpulse period is longer than the round-trip time for a given target (see Figure II below).

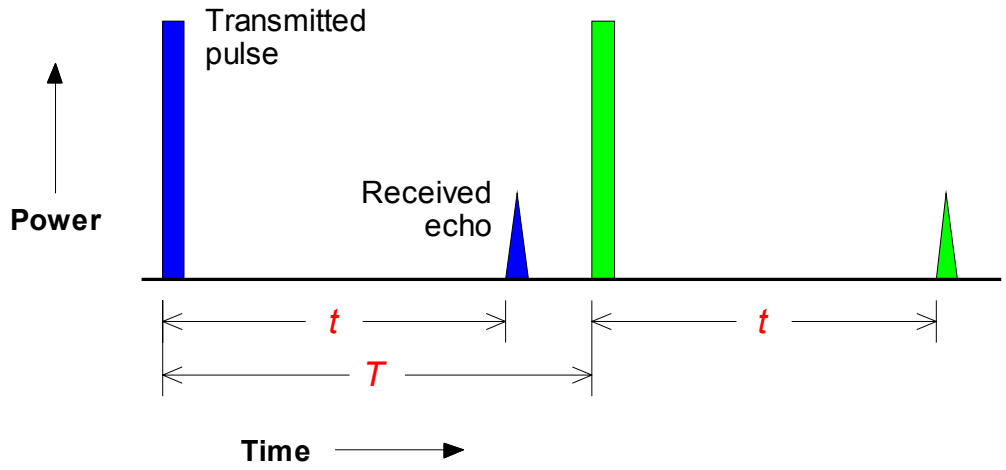

Figure II: Pulsed radar operating at a low PRF with $t < T$, making pulse-delay ranging possible

Observing Figure II shows that, for a target's range, *R*, to be accurately measurable using pulse-delay ranging, the following inequality must hold.

$$R = \frac{1}{2} t\, c < \frac{1}{2} T\, c = \frac{c}{2 f_r} \tag{1}$$

Applying (1) and with the speed of light, *c*, equal to 300,000 kilometers per second, a low PRF of one kilohertz would allow radar to accurately measure ranges less than 150 kilometers using pulse-delay ranging; a PRF of five kilohertz would reduce this value to 30 kilometers. Figure II also helps illustrate that a given range observed by radar becomes more ambiguous as PRF increases. For, as *T* decreases below *t*, the number of transmitted pulses an echo could belong to increases.

Because of the Doppler effect, a target's range rate can be determined by comparing the frequency of transmitted pulses to that of their echoes from the moving target; the resulting difference is known as the target's Doppler frequency. Range rates are miniscule compared to the speed of light; hence, Doppler frequencies are extremely small and are measured in terms of a progressive phase shift from cycle to cycle, which requires that the pulses are coherent. To detect Doppler frequencies, radars use a bank of narrowband filters, each tuned to a specific frequency. Unfortunately, because pulsed signals are discontinuous, a received echo will pass through a filter tuned not only to its frequency but also above/below its frequency by multiples of the PRF. These frequencies passed by the filter are called spectral lines and make Doppler frequency measurement difficult if the PRF is lower than the Doppler frequency (see Figure III below).

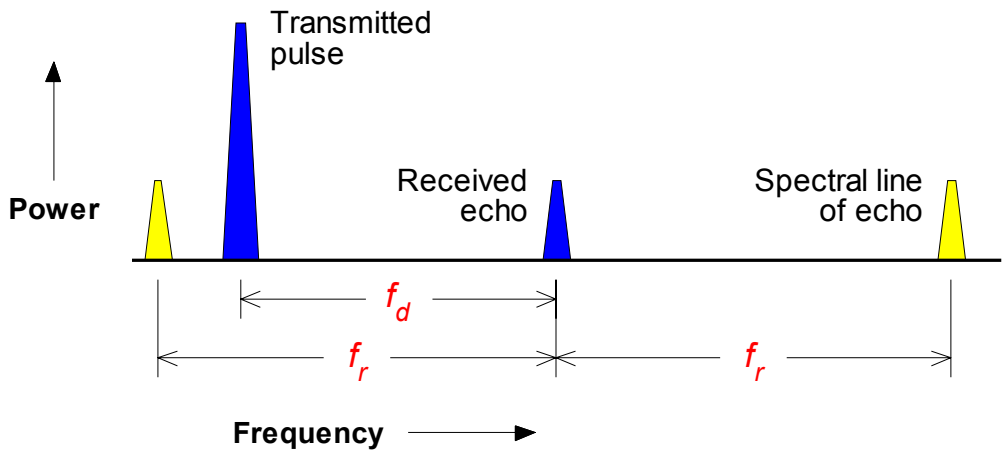

Figure III: Pulsed radar operating at a high PRF with $f_d < f_r$, making Doppler frequency measurement possible

To obtain accurate measurements of a target's Doppler frequency and hence its range rate, $\dot{R}$, Figure III makes apparent the necessary inequality,

$$-2\dot{R}\frac{f}{c} = f_d < f_r, \tag{2}$$

where f is the frequency of the transmitted pulse. The minus sign correlates a negative range rate or closing target with a positive Doppler frequency. Using (2) and assigning values of 300,000 kilometers per second and 10 gigahertz for c and f, respectively, a high PRF of 100 kilohertz would allow radar to accurately measure range rates below 1500 meters per second; a PRF of five kilohertz would reduce this value to 75 meters per second.

Contrasting the increase of range ambiguities with an *increase* in PRF, Figure III helps to show that a given range rate or Doppler frequency observed by radar becomes more ambiguous as PRF *decreases*. For, as f_r decreases below f_d, spectral lines of the echo appear between the transmitted pulse and the received echo, and there is no direct way to distinguish between these frequencies and the true Doppler frequency of the received echo. Figure IV below summarizes the effect of PRF on range and range rate measurements. It is important to note that this tradeoff of accurate range and range rates with PRF is idealized. Tracking radars can operate at medium PRF where range and range rate ambiguities are both a factor, but can shift between low and high PRF's to compensate for these limitations and obtain accurate ranges and range rates for targets. In any case, PRF is a key characteristic of pulsed radar.

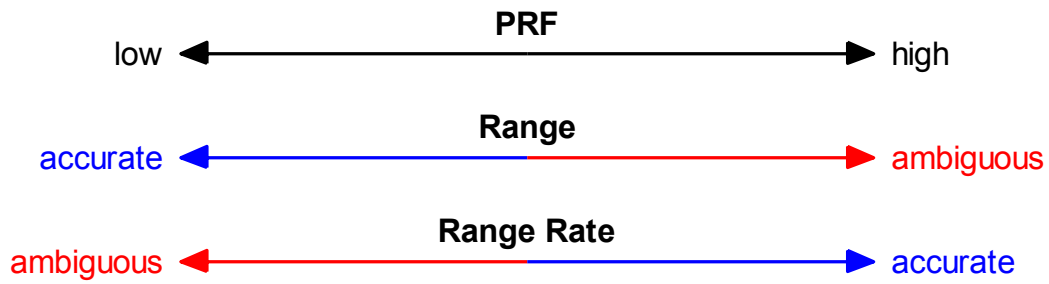

Figure IV: How PRF affects range and range rate measurements

A second key characteristic for any radar is its antenna radiation pattern or distribution of radiated power, P, in angle, θ. For radars with a planar array antenna, which contains rows of closely spaced radiators, the radiation pattern can be approximated by the following equation.

$$P = \left(\frac{\sin x}{x} \right)^2 \text{, where} \qquad (3)$$

$$x = \pi \frac{L}{\lambda} \sin\theta$$

L ~ Horizontal length or diameter of the antenna

λ ~ Operational wavelength

An idealized radiation pattern for a planar array antenna, using eq. (3), is shown below in Figure V. The specific parameters used to plot this pattern are two meters and 30 centimeters for L and λ, respectively.

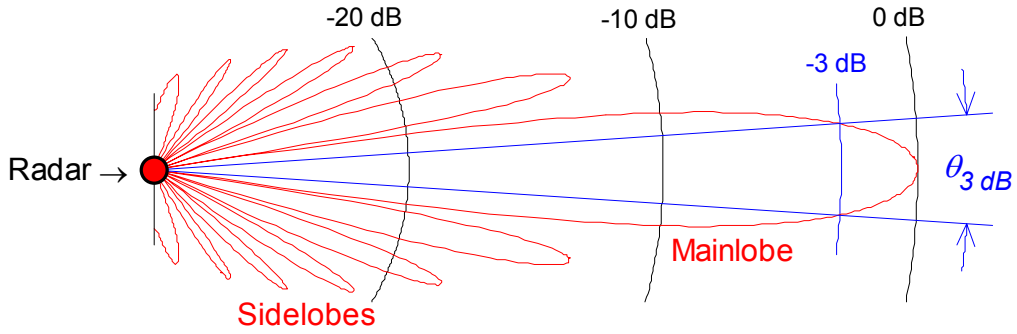

Figure V: Idealized radiation pattern for radar with a planar array antenna

In Figure V, the mainlobe of the radar is the region where most of the radiated power is concentrated. The sidelobes are much weaker and are caused by cancellation and addition of waves from the antenna's individual radiators as the waves' relative phases change with angle. The radar's beamwidth, $\theta_{3\text{ dB}}$, has edges defined by points where the power has dropped to ½ of that at the center of the beam (-3 decibels). Only the beamwidth is used to search for targets; radiated power outside this area is generally not desired. The radiation pattern describes not only how transmitted power is distributed in angle but also how received power is attenuated with angle; this characteristic is called reciprocity.

III. Mainlobe Deception

Assuming that an ECAV is not detected and knows the maximum operational range, R_{max}, and location of a radar with pulse-to-pulse agility, the ECAV can intercept and appropriately delay the return of the radar's transmitted pulses so that the radar sees a phantom target beyond the ECAV but closer than R_{max}. The capability of digitally storing, altering, and returning encoded pulses so that they correspond to a desired range and range rate is formally known as Digital Radio Frequency Memory (DRFM), but will often be referred to simply as range delay since it is assumed that digital means will be used to accomplish this task. To deceive the radar using only range delay requires that the ECAV be in the radar's mainlobe; of course, the phantom target will also be on the line of sight (LOS) from the radar to the ECAV. Thus, the phantom target's track is a function of the ECAV's range delay and bearing from the radar. If the radar operates at a low PRF so that pulse-delay ranging is possible, then accurately delaying the radar's pulses is crucial. If the radar operates at a medium or high PRF and is in tracking mode, then accurate range information is still important, and the ECAV should also focus on sending returns with accurate Doppler frequencies for the phantom target (see Figure IV above). Keep in mind that a phantom track flying roughly perpendicular to a radar will not produce significant Doppler frequencies and may even get filtered out or ignored by some radars. Figure VI below illustrates how four ECAVs could cooperatively create a single phantom track to deceive a network of four radars by using range delay techniques. Unless all radars see the same phantom track, the track is dismissed as spurious.

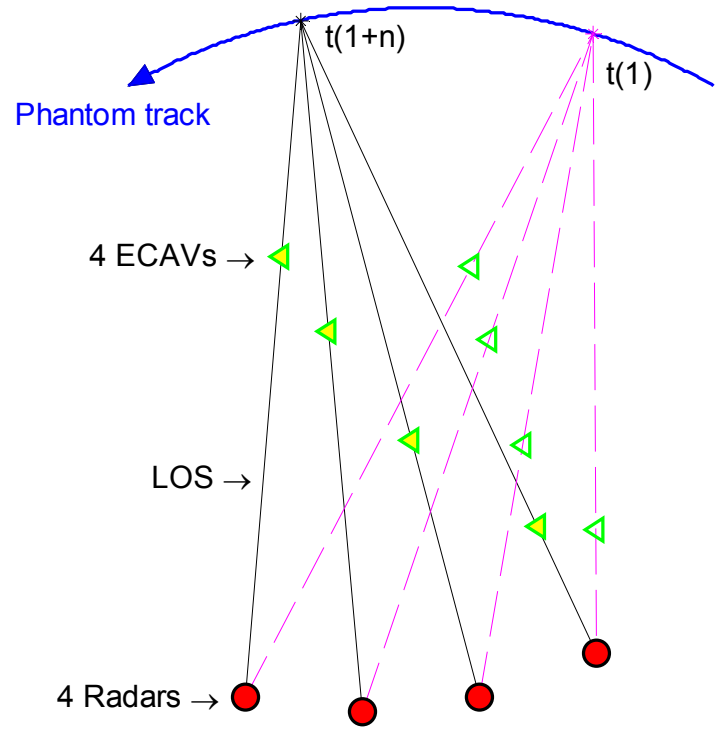

Figure VI: Cooperative mainlobe deception of a radar network by creation of a phantom track

One problem of interest is to determine the allowable trajectories for the ECAVs given their initial conditions and a time-dependent phantom track. Observing Figure VI, one can see

that each ECAV behaves much like a bead on a string that is rotating at some variable rate; the ECAV may slide up and down freely but must rotate with the LOS from the radar to the phantom track. If the speed, heading, or another variable of the ECAV is limited, then it can no longer slide freely; in fact, an allowable trajectory for the ECAV may not exist.

Assuming that the number of ECAVs equals the number of radars, then the inherent limits of mainlobe deception on an ECAV trajectory can be assessed using degrees of freedom (DOF). Any general phantom track specified in the x-y plane has two DOF, which can be represented by R and θ or alternately by υ_T and ϕ_T (see Figure VII below). Likewise, two DOF also represent any free ECAV trajectory in the same plane and can be represented by r and θ or alternately by υ_E and ϕ_E. Thus, an ECAV trying to generate a given phantom track will have one constraint, θ, and one DOF. This DOF is constrained by setting any other variable of the ECAV, including r, υ_E, or ϕ_E.

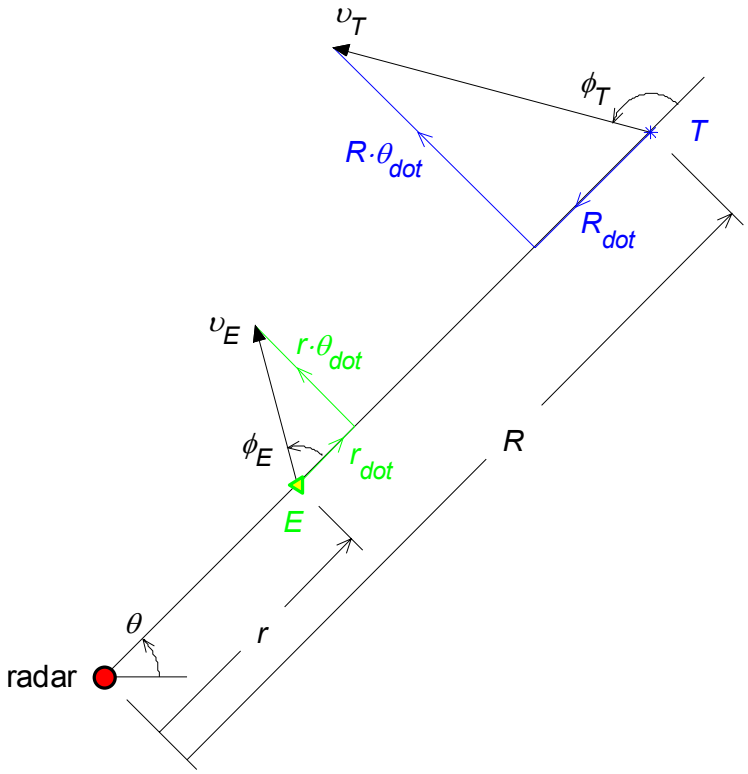

E ~ ECAV
υ_E ~ ECAV speed
ϕ_E ~ ECAV course
r ~ ECAV range from radar
θ ~ ECAV/phantom target bearing from radar
T ~ phantom target
R ~ phantom target range from radar
υ_T ~ phantom target speed
ϕ_T ~ phantom target course

Figure VII: ECAV and phantom track variables and their relations

In general, if the number of ECAVs is greater than or equal to the number of radars, then the following two equations relate the number of ECAVs, e, required to generate a desired number of tracks with a desired total DOF for the combined tracks.

$$if\ n = 2,\ e = \sum (prime\ factorization\ numbers\ of\ T), \text{ where} \tag{4}$$

n ~ Number of radars voting
$T \geq 1$ ~ Number of phantom tracks desired
$DOF = e$ ~ Total DOF constrained

$$if\ n \geq 3,\ e = nT + (DOF - 2T), \text{ where} \tag{5}$$

n	~	Number of radars voting
$T \geq 1$	~	Number of phantom tracks desired
$2 \leq DOF \leq 2t$	~	Total DOF desired

For eq. (4) and values of T not having a prime factorization other than 1 and T itself, use the next highest value of T that does. With two radars voting and four phantom tracks desired, eq. (4) shows that only four ECAVs are required and the phantom tracks will have a combined four DOF. If instead twelve phantom tracks are desired, then only three additional ECAVs must be supplied. If three radars vote and four phantom tracks with 4 total DOF are again desired, eq. (5) equals eight ECAVs required. In the simple case where each phantom track desired has a full two DOF, eq. (5) reduces to e equal to n multiplied by T. The interesting result of eqs. (4) and (5) is that, if there are more ECAVs than radars available, additional phantom tracks – some having less than two DOF – may be generated using less than one ECAV per voting radar per additional track.

Mainlobe deception has the primary advantage that it is technically simpler to execute. The main disadvantage to mainlobe deception is that it is capable of producing only one phantom track when the number of ECAVs is equal to the number of radars voting. Other issues that need to be addressed for mainlobe deception include:

- Inaccuracy of radar/ECAV positions and time delay – an estimation problem
- Limitations on ECAV dynamics due to bounded ranges for υ_E, ϕ_E, and υ_T
- Choosing the "best" phantom track for a team of ECAVs – a decentralized cooperative control problem
- Dealing with bi-static (passive) receivers as part of a radar network
- Processing power required by DRFM – can be better at low PRF
- Electronic requirements for generating returns with sufficiently accurate range and Doppler frequency information

The first three issues listed above will be addressed later in more detail.

IV. Sidelobe Deception

If, in addition to the assumptions in Mainlobe Deception, an ECAV has certain information about the radiation pattern of a radar, it can intercept the radar's transmitted pulses through the sidelobes (see Figure V above). Returning the intercepted pulses using DRFM is interpreted by the radar as a return in the radar's mainlobe between the range of the ECAV and R_{max}. This deception assumes that the radar cannot distinguish between returns coming through its mainlobe and those coming through its sidelobes. In this case, the phantom target is not on the LOS from the radar to the ECAV. However, since the phantom target's bearing from the radar is offset from that of the ECAV by a constant angle, the phantom target's track is still a function of only the ECAV's bearing from the radar and range delay. As in mainlobe deception, if the radar operates at a low PRF, then accurately delaying the radar's pulses is key. If the radar operates at a medium or high PRF, then sending returns with accurate Doppler frequencies for the phantom target is important, as is continued accurate range information if the radar is in tracking mode (see Figure IV above).

An electronically steered array (ESA) antenna progressively shifts the phases coming from its individual radiators so that the antenna beam may be steered almost instantaneously to track multiple targets. Hence, an ECAV can use the multiple sidelobes of a radar with ESA capabilities to generate multiple phantom tracks. Figure VIII below presents an example where sidelobe and mainlobe deception could be used together to generate multiple phantom tracks for two radars.

Sidelobe deception is considered based on the premise that a tracking radar will lock on an ECAV emitting delayed returns through its sidelobe. This premise depends on the radiation patterns of the tracking radars and constrains an ECAV to operate in sidelobe peaks or on one line per sidelobe as in Figure VIII. As stated earlier, the ECAV must determine where it is in relation to the mainlobe as well as where the sidelobe peaks are, i.e. the characteristics of the radar's radiation pattern.

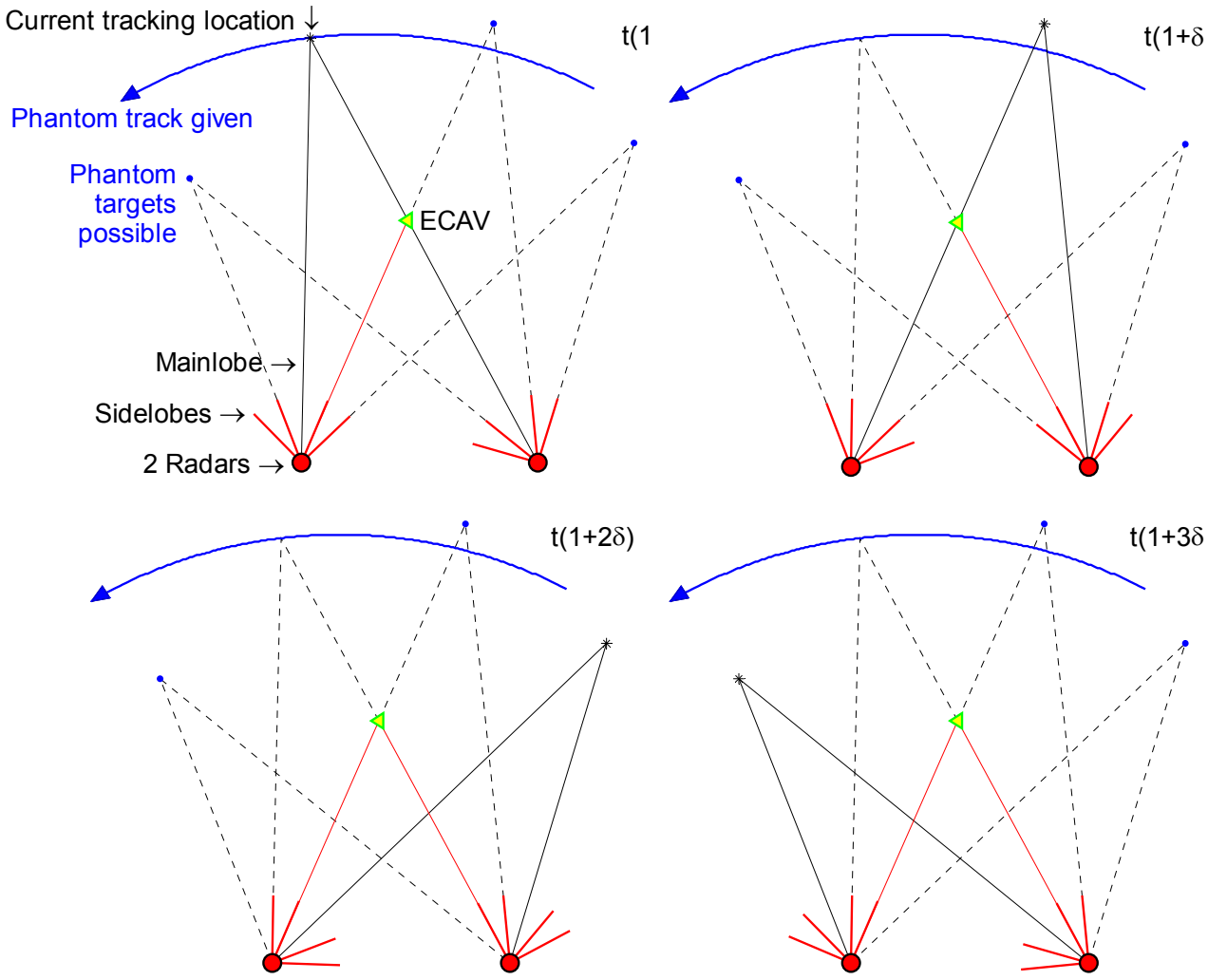

Figure VIII: Sidelobe and mainlobe deception of a radar network by using one ECAV to create multiple phantom tracks

Each picture in Figure VIII represents the two radars tracking a different phantom target; the time difference between each picture, δ, is the time required for the radars to send out a pulse, receive a return for the current phantom target being tracked, and electronically steer their beams to the next tracking location. Collectively, the four pictures correspond to one tracking cycle for the two radars – assuming no other targets are being tracked. As shown in Figure VIII, all the phantom tracks together share only two DOF: once one phantom track is given as a function of time, all remaining phantom targets possible for each tracking cycle are fully constrained points for any position of the ECAV. Clearly, the creation of these constrained phantom targets over time still generates continuous phantom tracks since the ECAV trajectory is continuous. The scenario in Figure VIII also fully constrains the ECAV trajectory once a phantom track is given because the ECAV must deceive radar one and radar two, constraining it to both θ_1 and θ_2.

If one radar is subtracted from the Figure VIII-scenario, then a given phantom track does not fully constrain the remaining phantom tracks possible. Each phantom track may have an independent range rate – one additional DOF. Continuing with the concept of DOF, each phantom track, T, may be represented as follows.

$i = 1 \ldots n$ ~ Number of radars voting
$j = 1 \ldots m$ ~ Number of sidelobes on one side of the mainlobe

$i = 1$
$T_{1,j} \rightarrow R_{1,j}, \theta_1 + \zeta_j$, where
ζ_j ~ Constant angle subtending the mainlobe and jth sidelobe

Thus, in the one-radar case, the first phantom track has two DOF and all remaining phantom tracks have one constraint, θ_1, and one DOF, $R_{1,j}$. The following equation determines how many tracks and total DOF are possible for any one radar.

$$\begin{aligned} &if\ e = n = 1,\ T = 2m + 1 \\ &DOF = 2m + 2 \end{aligned} \tag{6}$$

For the two-radar case, with i, j, and ζ_j defined as before, the phantom tracks are represented as follows.

$i = 1$
$T_{1,j} \rightarrow R_{1,j}, \theta_1 + \zeta_j$
$i = 2$
$T_{2,j} \rightarrow R_{2,j}, \theta_2 + \zeta_j$

Adding the second radar, $i = 2$, adds the set of phantom tracks, T_2, with an additional "free" DOF given by eq. (6); however, two constraints per track are also added since T_2 must be equal to T_1. Indeed, if a third radar were added, similar DOF and constraints would again be added. Thus, the following equation generalizes the phantom tracks possible, T, and their total DOF for any number of voting radars.

$$\begin{aligned} &if\ e = n \geq 1,\ T = 2m + 1 \\ &DOF = n(2m + 2) - 2(n - 1)(2m + 1) = 2[m(2 - n) + 1] \end{aligned} \tag{7}$$

Eq. (7) reveals the surprising result that for two radars, all the phantom tracks combined are reduced to having only two total DOF as in Figure VIII above. For three radars, the combined phantom tracks share zero DOF and are over-constrained; at best, one phantom track with two DOF may be generated as in mainlobe deception.

In summary, for sidelobe deception the problem geometry and dynamics depend on the ratio of ECAVs to radars and the number of radars voting. Specifically, the number of radars voting determines how many phantom tracks are possible and their total DOF; the ratio of ECAVs to radars affects the limitations on ECAV trajectories.

The big advantage to sidelobe deception is that multiple phantom tracks are possible when there are less than three radars voting. The main disadvantage to sidelobe deception is the increased technical complexity of the deception process and the additional information necessary for success. So, in addition to those listed for mainlobe deception, issues for sidelobe deception include:

- Information needed on radar radiation patterns and their dependency on frequency
- Sidelobe attenuation techniques currently used by the radar

Only part of the first issue is now addressed: the dependency of radiation patterns on frequency.

Equation (3) in Section II describes an idealized radiation pattern for a planar array antenna and shows that this pattern depends on frequency through the term λ. Therefore, changing frequency alters the radiation pattern, which includes the sidelobes' characteristics. Figure IX below shows four radiation patterns, each plotted in polar coordinates for a different frequency. The blue value in degrees is $\theta_{3\,\mathrm{dB}}$, the radar's beamwidth.

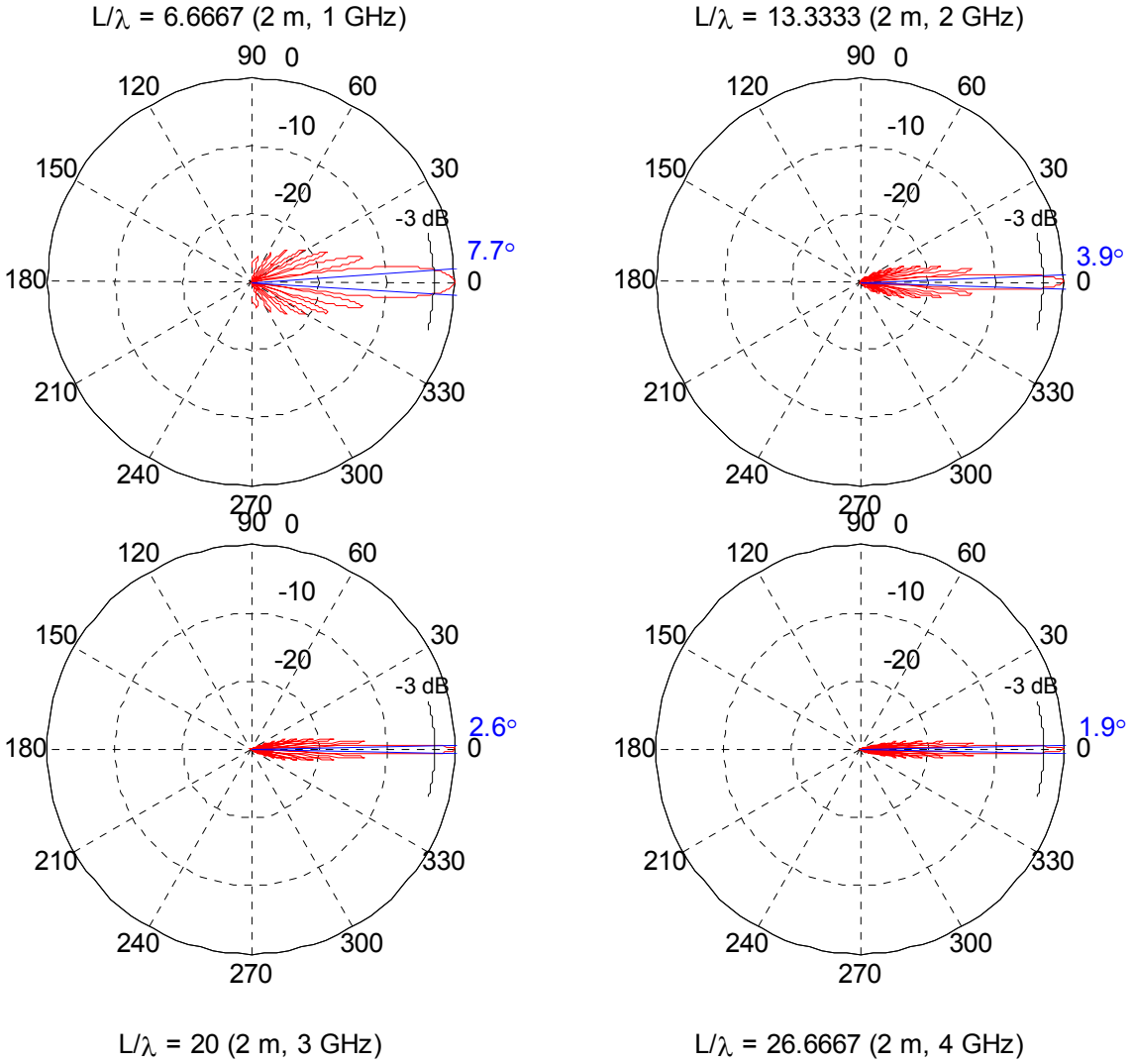

Figure IX: How the radiation pattern of a planar array antenna depends on frequency

From observing Figure IX, frequency has a significant effect on a radar's radiation pattern. As frequency increases, the following also occur, though not to the precision shown by Figure IX since these plots are idealized (real radiation patterns are not as neat or symmetric).

1. The number of sidelobes increases
2. The angles between sidelobe tips decrease
3. The bearings of sidelobes relative to the mainlobe change
4. The width of sidelobes decreases
5. The beamwidth decreases
6. The maximum power of each sidelobe remains constant

Possibly most detrimental to sidelobe deception is item three listed above; varying operational frequency causes the bearing location of sidelobes to change relative to the mainlobe. The most helpful observation could be item six; if a reference power in the mainlobe is known, then by measuring the power of a pulse coming through a sidelobe, an ECAV might be able to identify the sidelobe and even determine its own distance from the sidelobe peak.

The variation in frequency required to significantly change the bearing location of sidelobes appears to be about 20% at a frequency of two gigahertz. As shown in Figure X below, this change in frequency causes the first sidelobes to separate by approximately one degree while the sidelobes at –30 decibels are separated by approximately 10 degrees. Since it is assumed that an ECAV can only operate in sidelobe peaks, this amount of separation could be enough to place the ECAV in a null or cause a phantom track to break up as radar frequency varies.

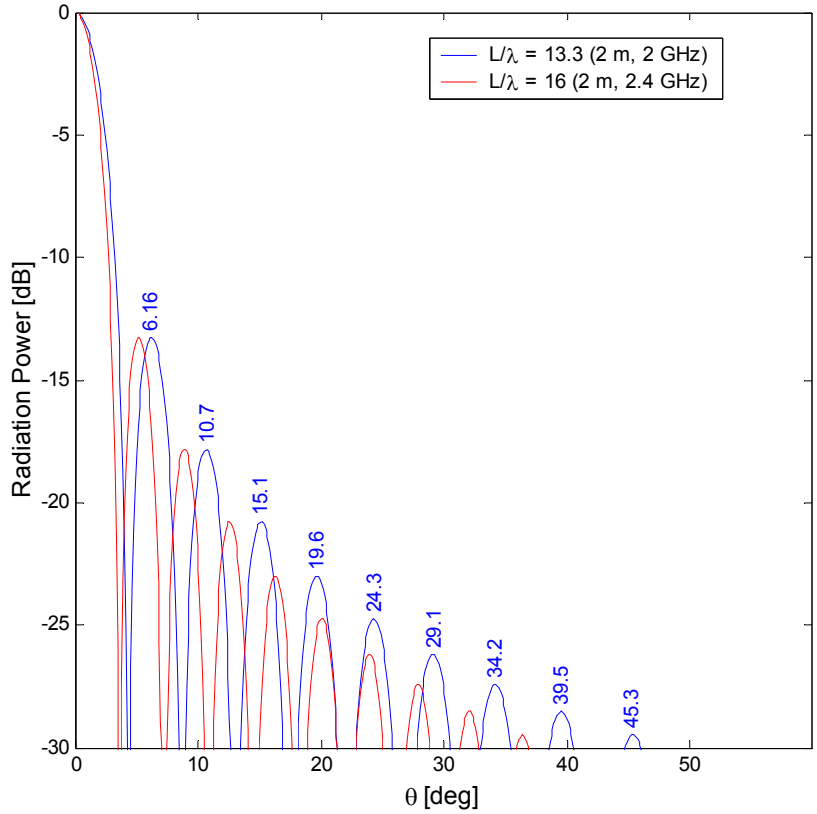

Figure X: Separation of sidelobes due to varying radar operational frequency

V. Uncertainty Analysis

One important issue of both mainlobe and sidelobe deception is the effect of the inaccuracies of radar position, ECAV position, and ECAV time delay. These inaccuracies contribute to a region of uncertainty around a "nominal" phantom target where the target may actually be placed by an unsuspecting ECAV. If the region is too large, then radars correlating tracks in a radar network may be able to discriminate between their respectively observed phantom targets and determine the track to be false. Therefore, given an uncertainty in radar position, Δrd, an uncertainty in ECAV position, Δr, and an uncertainty in the ECAV's time delay, Δt_d, the goal is to develop equations for the maximum deviations in range and azimuth, ΔR_{max} and $\Delta\theta_{max}$, for a nominal phantom target. Figure XI below shows the radar/ECAV configuration where the maximum range deviation occurs.

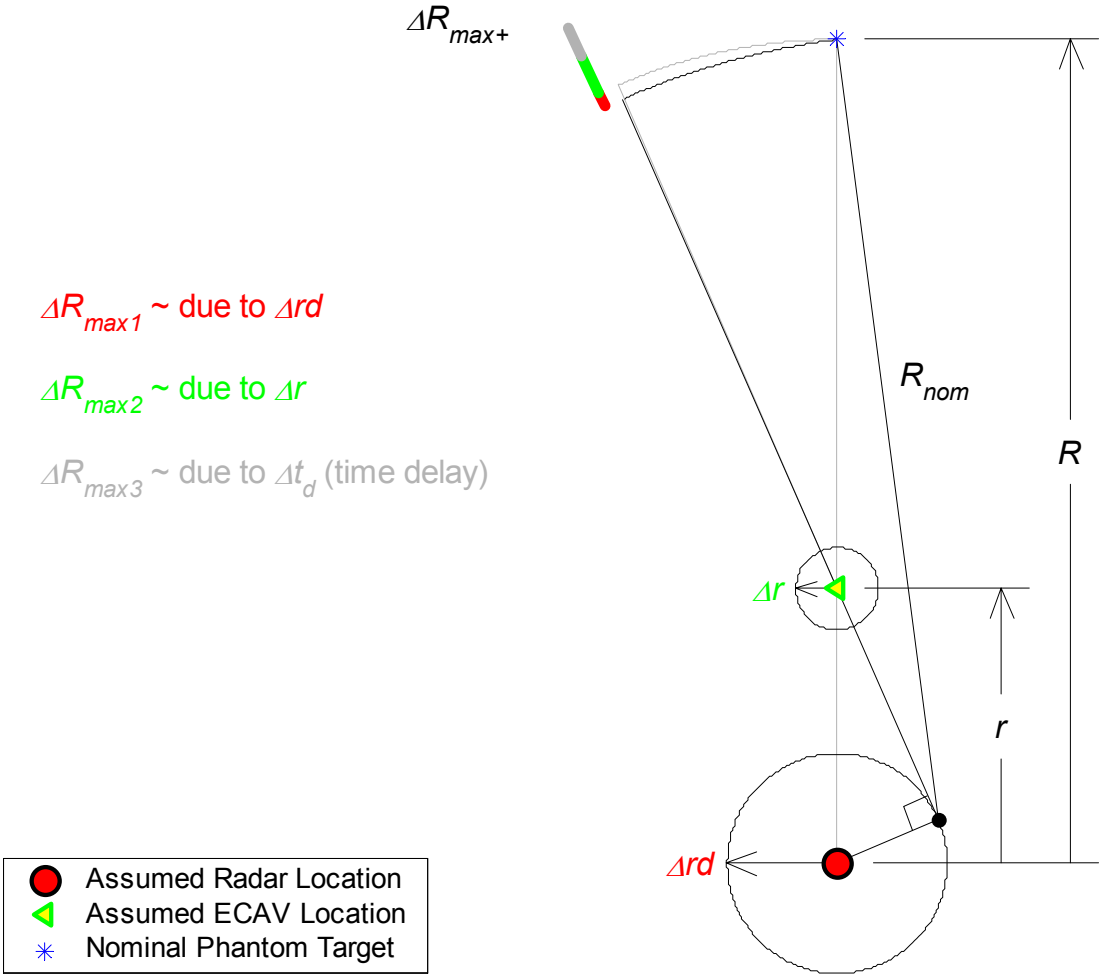

Figure XI: Radar/ECAV locations and geometry required to produce ΔR_{max+}

Based on Figure XI, the maximum positive deviation in range from that of a nominal phantom target, ΔR_{max+}, may be calculated as follows.

$$\Delta R_{\max +} = \Delta R_{\max 1} + \Delta R_{\max 2} + \Delta R_{\max 3}, \text{ where} \tag{8}$$

$$\Delta R_{\max 1} = \sqrt{r^2 - \Delta rd^2} + (R - r) - R_{nom}$$

$$\Delta R_{\max 2} = \Delta r$$

$$\Delta R_{\max 3} = \frac{1}{2} c \, \Delta t_d$$

$$R_{nom} = \sqrt{\Delta rd^2 \left(1 - \frac{2R}{r}\right) + R^2}$$

The maximum negative deviation in range, ΔR_{max-}, is similarly determined by the following equation, where the radar and ECAV are both moved away from but in line with the nominal phantom target – a different configuration than Figure XI.

$$\Delta R_{\max -} = \Delta R_{\max 2} + \Delta R_{\max 3}, \text{ where} \tag{9}$$

$$\Delta R_{\max 2} = \Delta r$$

$$\Delta R_{\max 3} = \frac{1}{2} c \, \Delta t_d$$

Surprising at first, ΔR_{max+} and $\Delta R_{\max -}$ are not affected significantly by Δrd because the ECAV's time delay depends on the distance $(R - r)$, and Δrd does not affect this quantity. For the maximum deviation in azimuth from a nominal phantom target to occur, a third radar/ECAV configuration is necessary, which is shown below in Figure XII.

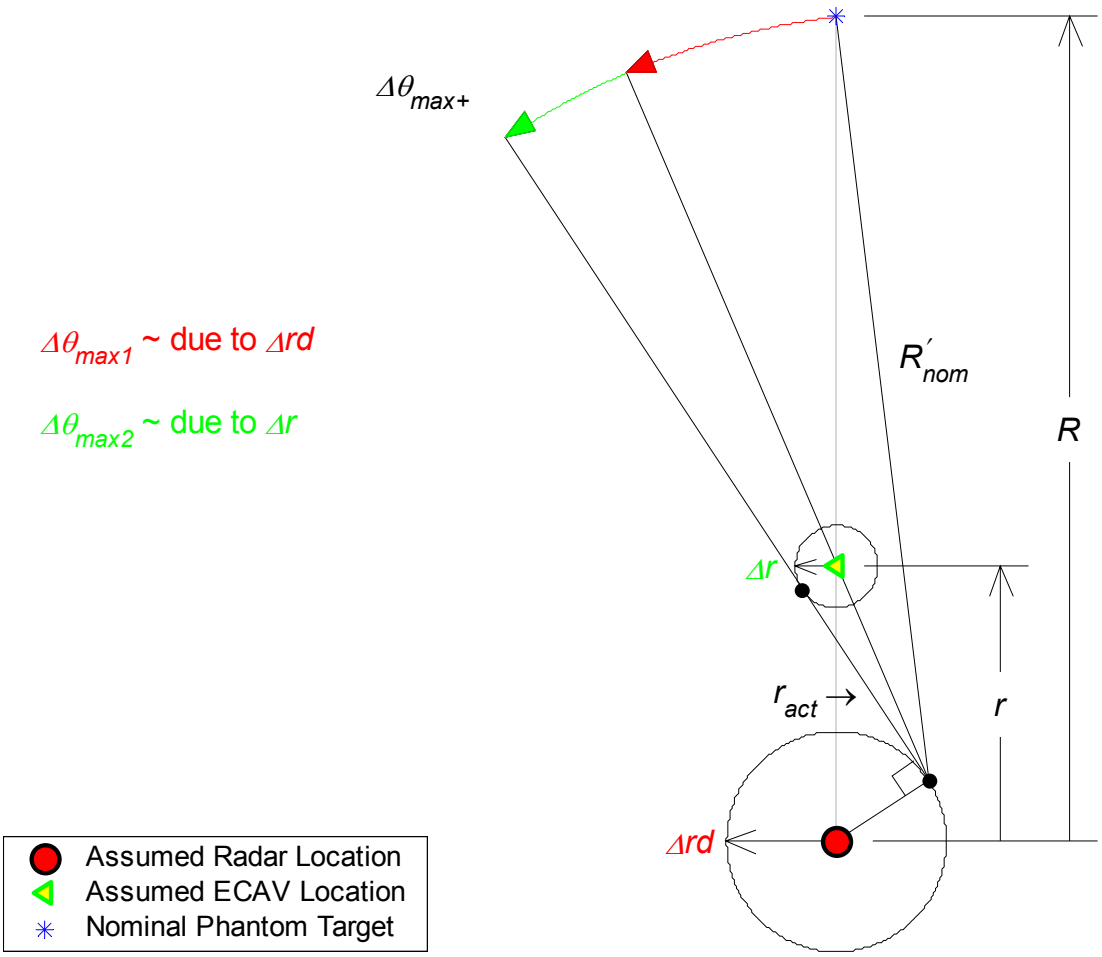

Figure XII: Radar/ECAV locations and geometry required to produce $\Delta\theta_{max+}$

Based on Figure XII, the maximum positive deviation in azimuth from that of a nominal phantom target, $\Delta\theta_{max+}$, may be calculated as follows.

$$\Delta\theta_{\max+} = \Delta\theta_{\max 1} + \Delta\theta_{\max 2}\text{, where} \tag{10}$$

$$\Delta\theta_{\max 1} = \arcsin\left(\frac{r_{act}\,\Delta rd\,(R-r)}{R_{nom}{}'\,r\sqrt{\Delta r^2 + r_{act}{}^2}}\right)$$

$$\Delta\theta_{\max 2} = \arctan\frac{\Delta r}{r_{act}}$$

$$r_{act} = \sqrt{r^2 - (\Delta r + \Delta rd)^2}$$

$$R_{nom}{}' = \sqrt{\frac{R}{r}\left(r^2 + \Delta r^2 + r_{act}{}^2 - \Delta rd^2\right) + R^2 - 2Rr + \Delta rd^2}$$

To calculate the radar resolutions needed to discriminate against correlated phantom targets, the following uncertainty values are used.

Δrd = 10 meters
Δr = 3 meters
Δt_d = 10 nanoseconds

An uncertainty in synchronization time was not included in this analysis because its effect on ΔR_{max} and $\Delta\theta_{max}$ is negligible. Even with a fast ECAV or phantom target of 300 meters per second and an uncertainty in synchronization time of 10 nanoseconds, the contribution to ΔR_{max} is only 0.000003 meters, and the contribution to $\Delta\theta_{max}$ is similarly small for any reasonable value of R. Figure XIII below shows the critical radar resolutions, given the above listed uncertainties, for two combinations of r and R using eqs. (8) - (10). Note that the one-way deviations from a nominal phantom target were combined to account for the worst case where two phantom targets are placed on opposite extremes of the nominal target.

ECAV/phantom target distances from radar	Critical resolution in range, $\Delta R_{max} = \Delta R_{max+} + \Delta R_{max-}$	Critical resolution in azimuth, $\Delta\theta_{max} = 2\ (\Delta\theta_{max+})$
r = 5 km R = 6 km	9.00 m	0.107 °
r = 5 km R = 30 km	9.01 m	0.260 °

Figure XIII: Critical radar resolutions for two values of R using eqs. (8) - (10)

This analysis could apply to sidelobe deception as well as mainlobe deception; offsetting the ECAV's bearing from the radar by a constant angle does not change the results. Given that targets are larger than nine meters, it seems reasonable that mainlobe deception may be able to present coherent phantom tracks. However, the critical resolution in azimuth of 0.260 degrees is 136 meters wide at R = 30 kilometers.

VI. Results of a Constant Speed ECAV

Before applying realistic bounded ranges for the speed of the ECAV, its course, and the speed of the phantom track, it is helpful to know the dynamic limitations on an ECAV when just a constant speed is assumed. With mainlobe deception as the focus for this section, the ECAV's one DOF is constrained by its constant speed. The inverse problem is now of interest: given a time-dependent phantom track and an ECAV's initial position, synthesize the ECAV trajectory required to create the desired phantom track. For ease of comparison, the following non-dimensional variables are used, with $\upsilon_E = 1$, $R_0 = 1$, and $\theta_0 = 0$.

$$t \to \frac{\upsilon_E}{R_0} t \qquad r \to \frac{r}{R_0}$$

$$\alpha \to \frac{\upsilon_T}{\upsilon_E} \qquad R \to \frac{R}{R_0}$$

Given these definitions and a constant-speed constant-course phantom track for this analysis, Figure XIV below illustrates the appropriate variables and their relations. For definitions of the basic ECAV and phantom track variables, see Figure VII above.

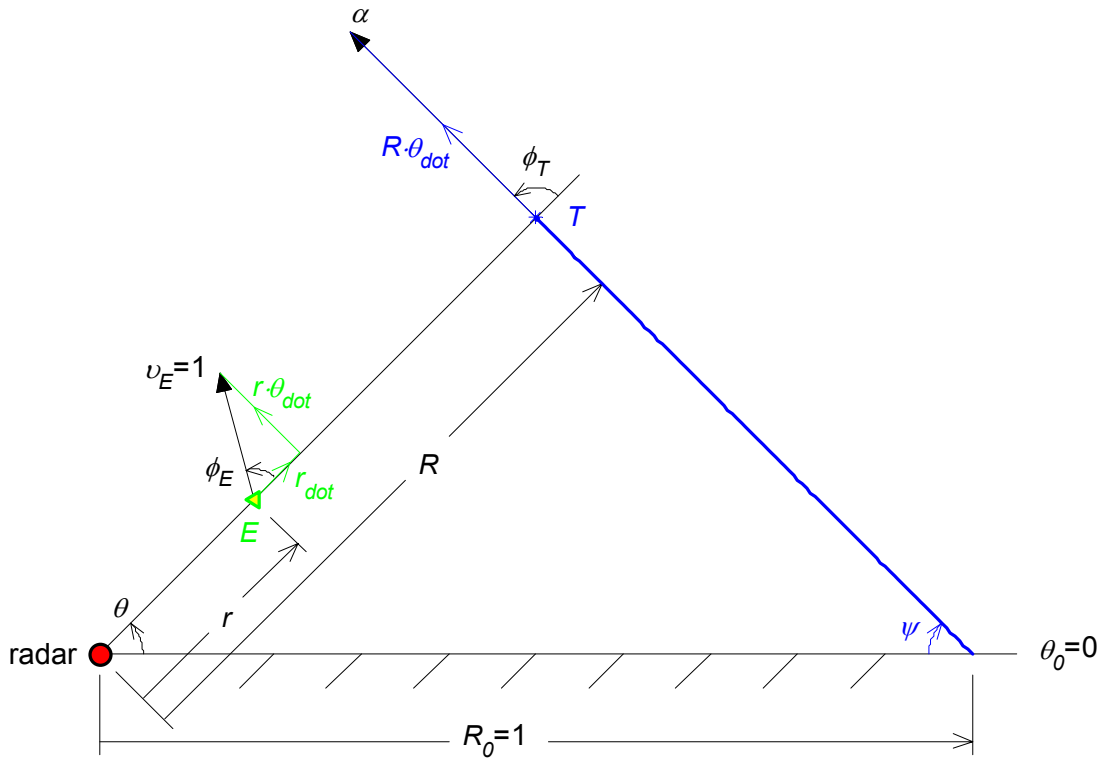

Figure XIV: Variables and relations for a constant speed ECAV and a constant-speed constant-course phantom track

The basic equations of motion for the ECAV and phantom target, using polar coordinates, are as follows. Every derivative is taken with respect to time.

$$\dot{r} = \cos\phi_E, \qquad r(0) = r_0 \tag{11}$$

$$\dot{\theta} = \frac{1}{r}\sin\phi_E, \quad \theta(0) = 0 \tag{12}$$

$$\dot{R} = \alpha\cos\phi_T, \quad R(0) = 1 \tag{13}$$

$$\dot{\theta} = \alpha\frac{1}{r}\sin\phi_T, \ \theta(0) = 0 \tag{14}$$

Without loss of generality, $\dot{\theta}$ is assumed positive. Manipulating eqs. (11) and (12) results in the following differential equations. These same equations easily follow by using the Pythagorean theorem on Figure XIV.

$$\dot{r} = \sqrt{1-(r\dot{\theta})^2}, \qquad r(0) = r_0 \tag{15}$$

$$\dot{r} = -\sqrt{1-(r\dot{\theta})^2}, \qquad r(0) = r_0 \tag{16}$$

For both equations, the ECAV's range, including r_0, must satisfy the following inequality for a solution to exist.

$$r(t) < \frac{1}{\dot{\theta}}, \qquad \forall t \tag{17}$$

If condition (17) is not satisfied, the solutions to eqs. (15) and (16) become imaginary. Physically, condition (17) makes it clear that an ECAV cannot fly at a constant speed of one when its range is such that $r\dot{\theta}$ is greater than one (see Figure XIV above). If $r\dot{\theta}$ is less than one, the ECAV may fly at a constant speed of one by having the correct $\dot{r}$ component via eq. (15) or (16). If either eq. (15) or (16) reaches zero in finite time at t_s, the necessary condition for switching from one equation to the other is as follows, assuming the second derivative of θ exists.

$$\ddot{\theta}(t_s) = 0 \tag{18}$$

Finally, the equations defining the constant-speed constant-course phantom track in polar coordinates are as follows (see Figure XIV above).

$$R(t) = \sqrt{1+\alpha^2 t^2 - 2\alpha t\cos\psi} \tag{19}$$

$$\theta(t) = \arcsin\left(\frac{\alpha t\sin\psi}{R(t)}\right) \tag{20}$$

$$\dot{\theta}(t) = \frac{\alpha\sin\psi}{1+\alpha^2 t^2 - 2\alpha t\cos\psi} \tag{21}$$

To solve for an ECAV trajectory given this phantom track, eq. (21) is inserted into eq. (15) or (16), and the solution, $r(t)$, is plotted versus $\theta(t)$, which is obtained from eq. (20) and (19). A good portion of the mathematical development above is from an internal document entitled "Cooperative Electronic Attack Using Range Delay-Based Deception" by M. Pachter and P. Chandler.

Figures XV and XVI below effectively explore eqs. (15) and (16) by plotting ECAV trajectories for various initial conditions. The equations are solved using the MATLAB function, ode45, with a constant time step. For each equation/figure, the initial conditions are carefully selected to show the minimum and maximum r_0 values yielding a flyable ECAV trajectory for a full 90 degrees, and one initial condition where the trajectory runs into the bound represented by (17) before $\theta = 90$ degrees is reached. Note that in both cases the maximum r_0 value yields an ECAV trajectory that switches from eq. (15) to (16) or vice versa at 45 degrees.

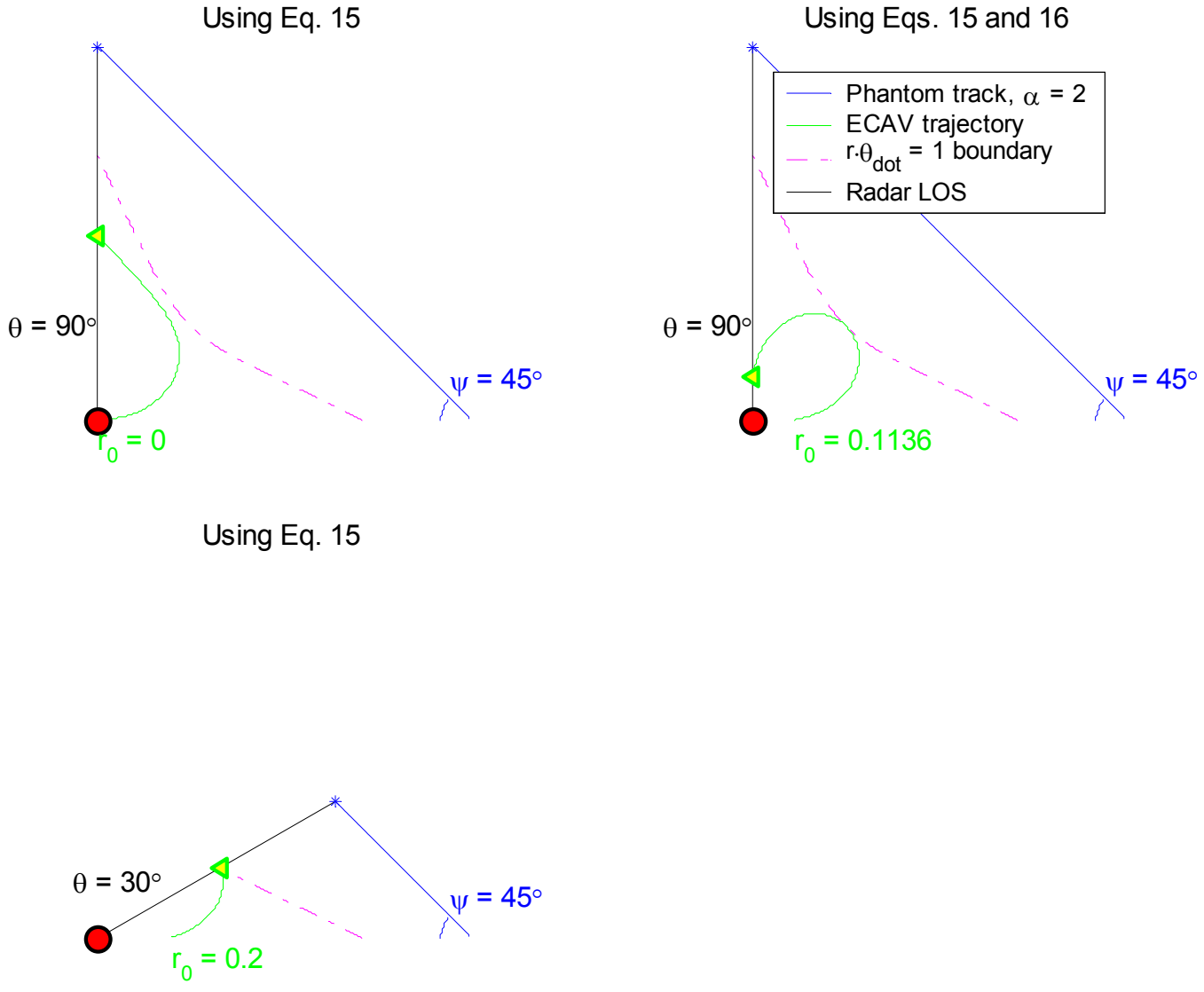

Figure XV: Constant speed ECAV trajectory solutions for a constant-speed, constant-course phantom track, starting with eq. (15)

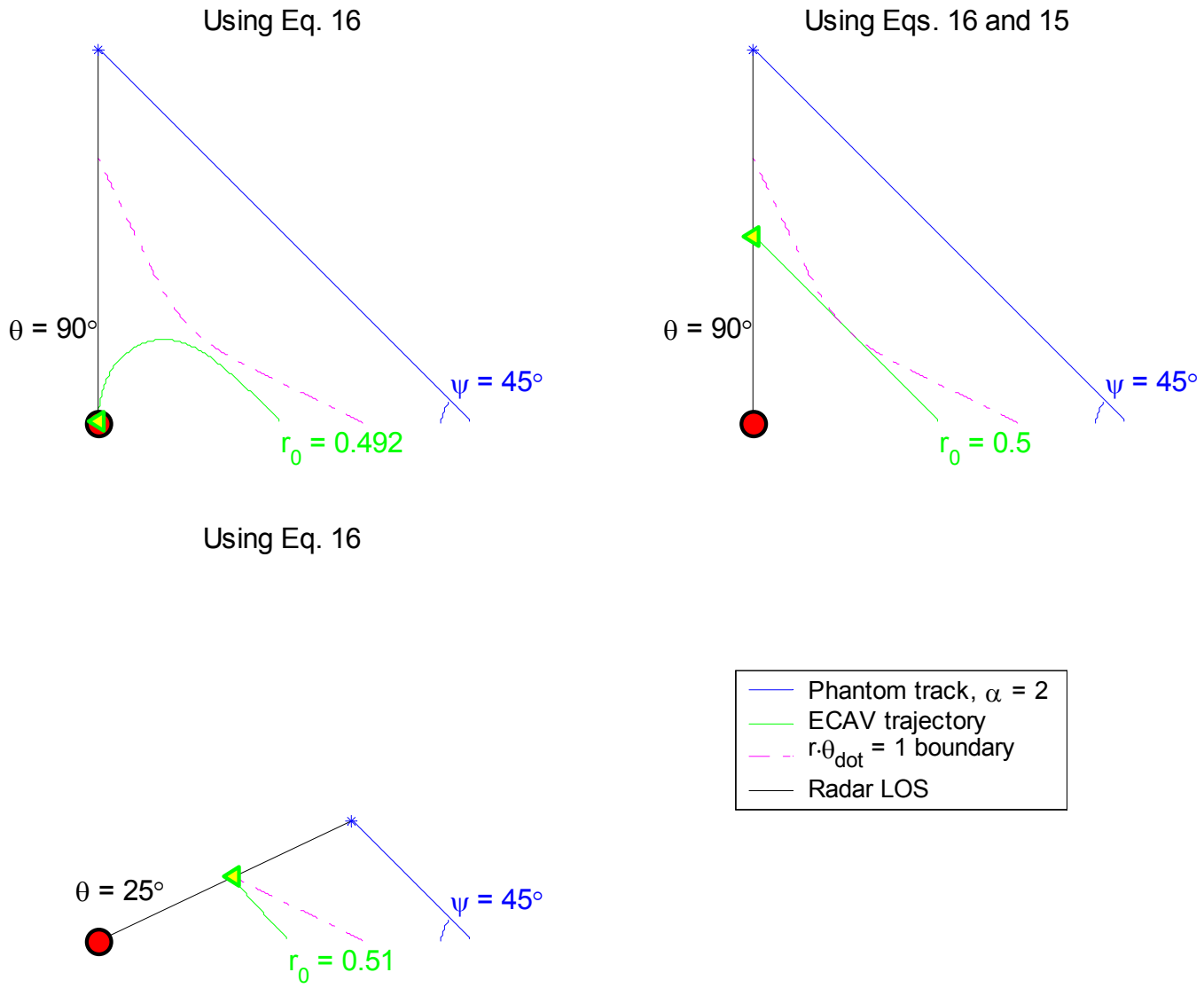

Figure XVI: Constant speed ECAV trajectory solutions for a constant-speed, constant-course phantom track, starting with eq. (16)

From observing Figures XV and XVI, the sizes of the sets of initial conditions yielding complete ECAV trajectories for a full 90 degrees are small compared to R_0, which is one. In addition, these results are for no additional limitations on the ECAV dynamics. Figures XVII and XVIII below show how the size of the sets of initial conditions yielding complete ECAV trajectories for a full 90 degrees (hereafter called valid initial conditions in this section) varies with both phantom track speed and heading, for both eq. (15) and eq. (16).

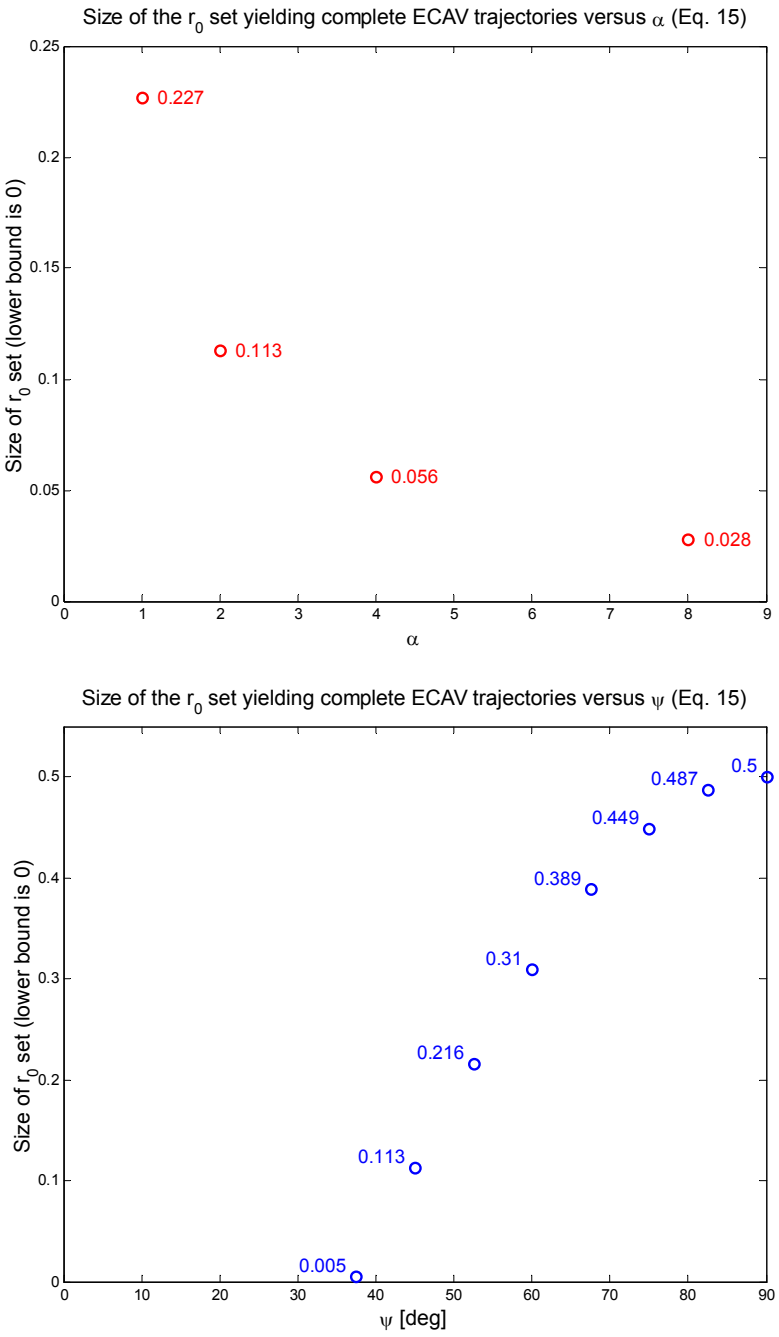

Figure XVII: How the set size of valid initial conditions varies with α and ψ for eq. (15)

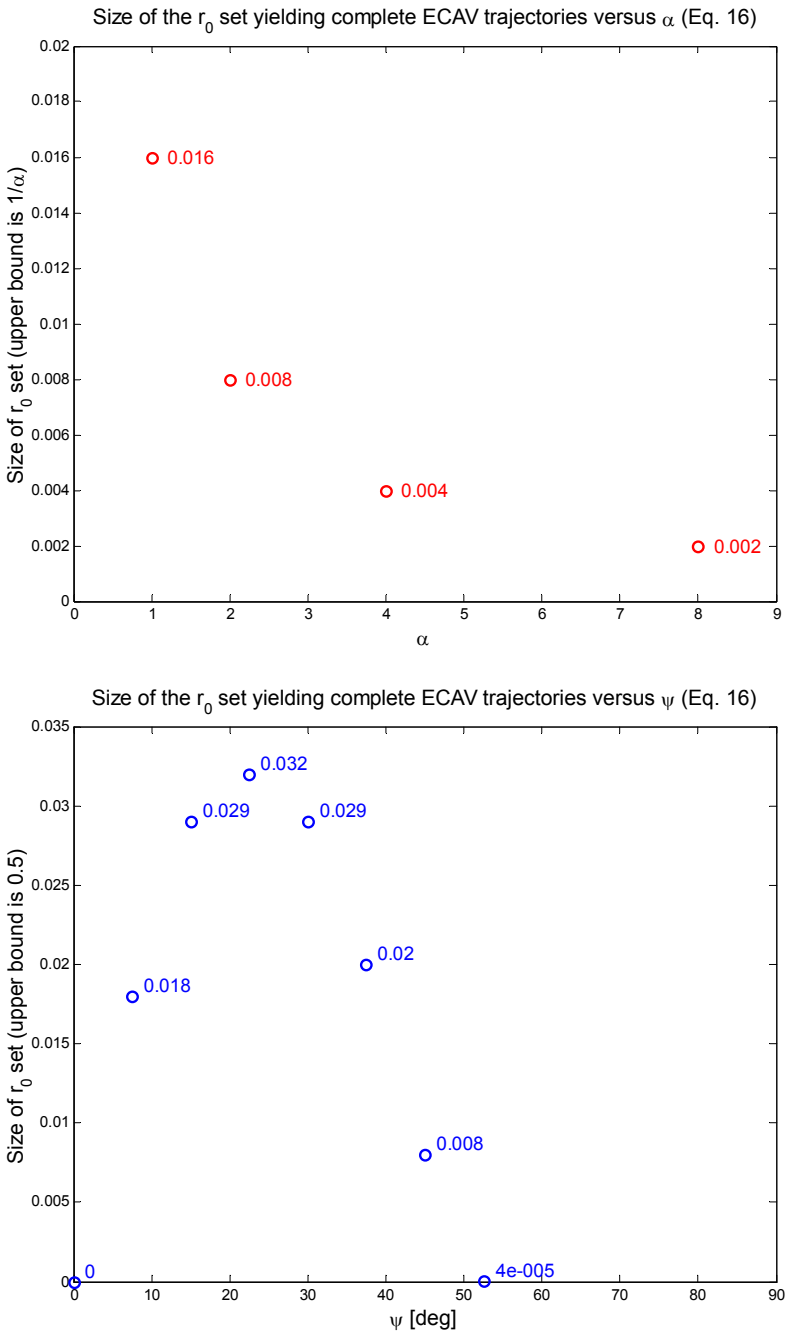

Figure XVIII: How the set size of valid initial conditions varies with α and ψ for eq. (16)

From observing Figures XVII and XVIII, the size of the sets of valid initial conditions is inversely proportional to the speed of the phantom track. The size dependence on the track's heading is more complicated. For eq. (15), the size is zero below 37.5 degrees and reaches a maximum at 90 degrees. For eq. (16), the size has a maximum at 22.5 degrees and reaches zero again at 52.5 degrees, which is 90 degrees minus 37.5 degrees. No further insight is forthcoming on why the size of the sets of valid initial conditions behaves the way it does since it depends on a numerical solution to eq. (15) and/or (16).

VII. General Theory for ECAV Trajectory Bounds and Solutions

Because the assumption of only a constant speed ECAV puts severe limitations on its valid initial conditions and trajectories, it is beneficial to move the scenario closer to reality by allowing the ECAV and phantom track speeds to vary within some bounded range. In addition, it is now assumed that the ECAV has two fixed antennas, each mounted on one side of the ECAV with less than a 90-degree look angle, ϕ_{Erange}, from its central axis (see Figure XIX below). Hence, the ECAV can no longer send pulse returns to a radar at any course angle, ϕ_E.

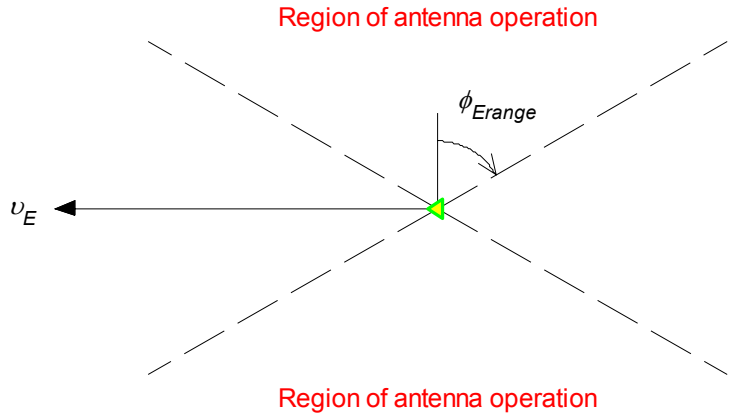

Figure XIX: ECAV with fixed antennas not covering a full 360 degrees

For the rest of this study, the following ranges are used in determining ECAV trajectory bounds and solutions.

$$\begin{aligned} \upsilon_E &\sim \pm 20\,\% \\ \phi_E &\sim 90^\circ \pm 60^\circ \\ \alpha &\sim \pm 20\% \end{aligned}$$

Mainlobe deception is again assumed, so the ECAV has one DOF, which will be constrained in different ways to create several ECAV dynamic systems for exploration of the ECAV's flyable range given a phantom track. For ease of comparison, the following non-dimensional variables are used, with $\upsilon_{Em} = 1$, $R_0 = 1$, and $\theta_0 = 0$.

$$t \to \frac{\upsilon_{Em}}{R_0} t \qquad r \to \frac{r}{R_0}$$

$$\alpha \to \frac{\upsilon_T}{\upsilon_{Em}} \qquad R \to \frac{R}{R_0}$$

$$\upsilon_E \to \frac{\upsilon_E}{\upsilon_{Em}}$$

Given these definitions and the ranges listed above for υ_E, ϕ_E, and α, the minimum and maximum values for these same variables are as follows.

$$\upsilon_{E\min} = 0.8 \qquad (22)$$
$$\upsilon_{E\max} = 1.2$$
$$\phi_{E\min} = \frac{\pi}{6}$$
$$\phi_{E\max} = \frac{5\pi}{6}$$
$$\alpha_{\min} = 0.8\alpha$$
$$\alpha_{\max} = 1.2\alpha$$

Given a generic phantom track and the previously defined non-dimensional variables, the appropriate variables and their relations for the track and for developing ECAV dynamic systems are shown below in Figure XX. For definitions of the basic ECAV and phantom track variables, see Figure VII above.

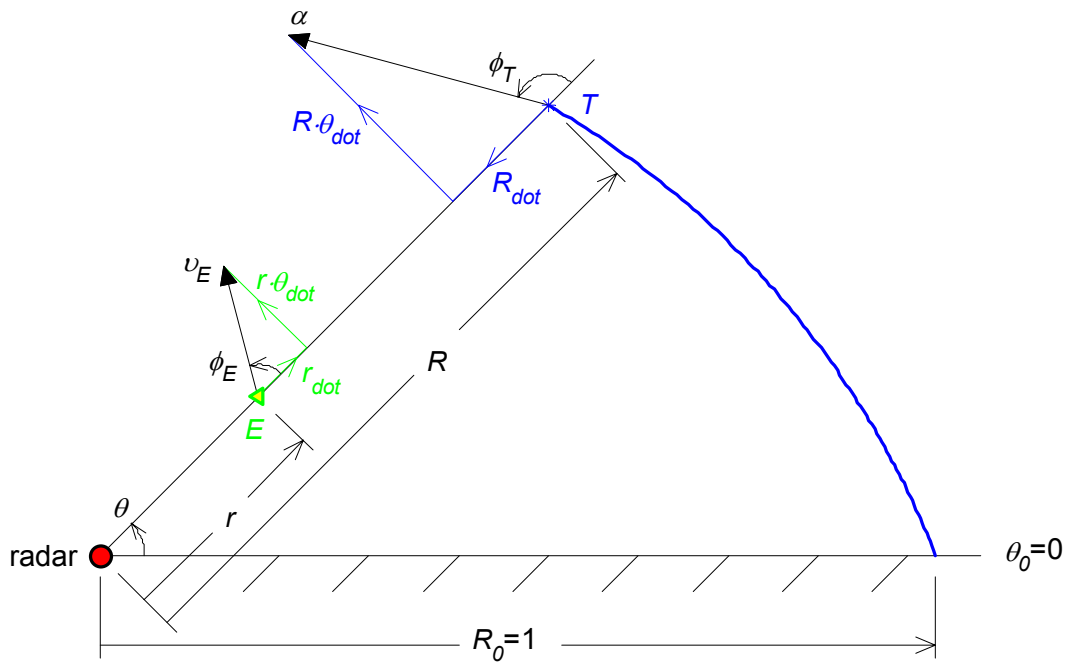

Figure XX: Variables and relations for an ECAV with variable speed and a generic phantom track with variable speed

The basic equations of motion for the ECAV and phantom target, using polar coordinates, are as follows. Every derivative is taken with respect to time. An equation for ECAV time delay, t_d, is also included.

$$\dot{r} = \upsilon_E \cos\phi_E, \quad r(0) = r_0 \qquad (23)$$

$$\dot{\theta} = \frac{\upsilon_E}{r}\sin\phi_E, \quad \theta(0) = 0 \qquad (24)$$

$$\dot{R} = \alpha\cos\phi_T, \quad R(0) = 1 \qquad (25)$$

$$\dot{\theta} = \frac{\alpha}{r}\sin\phi_T, \quad \theta(0) = 0 \tag{26}$$

$$t_d(t) = \frac{1}{2}c[(R(t) - r(t)] \tag{27}$$

Without loss of generality, $\dot{\theta}$ is assumed positive and given by some pre-determined phantom track. Six ECAV dynamic systems are now presented below, which can be developed from eqs. (23) and (24) by setting one ECAV variable. All systems include an algorithm for choosing initial conditions that satisfy the ranges in (22), differential equations necessary to solve for the ECAV trajectory, and bounds resulting from (22) that must be satisfied for all time. A subscript *c* indicates that the corresponding variable is constant.

a. Constant speed, υ_{Ec}

choose $\upsilon_{E\min} \le \upsilon_{Ec} \le \upsilon_{E\max}$

then choose $\dfrac{\upsilon_{Ec}\sin\phi_{E\min}}{\dot{\theta}_0} \le r_0 \le \dfrac{\upsilon_{Ec}}{\dot{\theta}_0}$

$$\dot{r} = \pm\sqrt{\upsilon_{Ec}{}^2 - (r\dot{\theta})^2}, \quad r(0) = r_0, \text{ where} \tag{28}$$

$s(t) = \upsilon_{Ec}{}^2 - [r(t)\dot{\theta}]^2 > 0, \ \forall t$ must be satisfied, or if $s(t) = 0$ condition (18) must be satisfied to switch from the (+) to (–) solution or vice versa, and

$\sin\phi_{E\min} \le \dfrac{r(t)\dot{\theta}}{\upsilon_{Ec}}, \ \forall t$ must be satisfied for course

b. Constant course, ϕ_{Ec}

choose $\phi_{E\min} \le \phi_{Ec} \le \phi_{E\max}$

then choose $\dfrac{\upsilon_{E\min}\sin\phi_{Ec}}{\dot{\theta}_0} \le r_0 \le \dfrac{\upsilon_{E\max}\sin\phi_{Ec}}{\dot{\theta}_0}$

$$\dot{r} = r\dot{\theta}\cot\phi_{Ec}, \quad r(0) = r_0, \text{ where} \tag{29}$$

$\upsilon_{E\min} \le \dfrac{r(t)\dot{\theta}}{\sin\phi_{Ec}} \le \upsilon_{E\max}, \ \forall t$ must be satisfied for speed

c. Constant heading, h_{Ec}

choose $\phi_{E\min} + \theta_0 \le h_{Ec} \le \phi_{E\max} + \theta_0$ and define $\phi_{E0} = h_{Ec} - \theta_0$

then choose $\dfrac{\upsilon_{E\min}\sin\phi_{E0}}{\dot\theta_0} \le r_0 \le \dfrac{\upsilon_{E\max}\sin\phi_{E0}}{\dot\theta_0}$

$\dot r = r\dot\theta\cot\phi_E(t),\ \ r(0) = r_0$, where (30)

$\phi_E(t) = h_E - \theta(t)$ and

$\upsilon_{E\min} \le \dfrac{r(t)\dot\theta}{\sin\phi_E(t)} \le \upsilon_{E\max},\ \ \forall t$ must be satisfied for speed

d. Constant speed rate, $\dot\upsilon_{Ec}$

choose $\dot\upsilon_{E\min} \le \dot\upsilon_{Ec} \le \dot\upsilon_{E\max}$
then choose $\upsilon_{E\min} \le \upsilon_{E0} \le \upsilon_{E\max}$
then choose $\dfrac{\upsilon_{E0}\sin\phi_{E\min}}{\dot\theta_0} \le r_0 \le \dfrac{\upsilon_{E0}}{\dot\theta_0}$
then calculate $\dot r_0 = \sqrt{{\upsilon_{E0}}^2 - (r_0\dot\theta_0)^2}$

$$\frac{d}{dt}\begin{bmatrix} r \\ \dot r \end{bmatrix} = \begin{bmatrix} \dot r \\ \dfrac{-r\dot\theta(r\ddot\theta + \dot r\dot\theta) + \sqrt{\dot r^2 + (r\dot\theta)^2}\,\dot\upsilon_{Ec}}{\dot r} \end{bmatrix},\ \begin{bmatrix} r(0) \\ \dot r(0) \end{bmatrix} = \begin{bmatrix} r_0 \\ \dot r_0 \end{bmatrix}, \text{ where} \qquad (31)$$

$s(t) = |\dot r| > 0,\ \ \forall t$ must be satisfied, or if $s(t) = 0$ can switch to $-\dot\upsilon_{Ec}$ and continue the solution by perturbing $\dot r$ across zero,

$\upsilon_{E\min} \le \sqrt{\dot r^2 + [r(t)\dot\theta]^2} \le \upsilon_{E\max},\ \ \forall t$ must be satisfied for speed, and
$\sin\phi_{E\min} \le \dfrac{r(t)\dot\theta}{\sqrt{\dot r^2 + [r(t)\dot\theta]^2}},\ \ \forall t$ must be satisfied for course

e. Constant turn rate, tr_{Ec}

choose tr_{Ec}
then choose $\phi_{E\min} \le \phi_{E0} \le \phi_{E\max}$
then choose $\dfrac{\upsilon_{E\min}\sin\phi_{E0}}{\dot\theta_0} \le r_0 \le \dfrac{\upsilon_{E\max}\sin\phi_{E0}}{\dot\theta_0}$
then calculate $\dot r_0 = r_0\dot\theta_0\cot\phi_{E0}$

$$\frac{d}{dt}\begin{bmatrix} r \\ \dot{r} \end{bmatrix} = \begin{bmatrix} \dot{r} \\ \dfrac{\dot{r}(r\ddot{\theta} + \dot{r}\dot{\theta}) - [\dot{r}^2 + (r\dot{\theta})^2]\dot{\phi}_E(t)}{r\dot{\theta}} \end{bmatrix}, \quad \begin{bmatrix} r(0) \\ \dot{r}(0) \end{bmatrix} = \begin{bmatrix} r_0 \\ \dot{r}_0 \end{bmatrix}, \text{ where} \tag{32}$$

$$\dot{\phi}_E(t) = tr_{Ec} - \dot{\theta},$$

$$\upsilon_{E\min} \le \sqrt{\dot{r}^2 + [r(t)\dot{\theta}]^2} \le \upsilon_{E\max}, \ \forall t \text{ must be satisfied for speed, and}$$

$$\sin\phi_{E\min} \le \frac{r(t)\dot{\theta}}{\sqrt{\dot{r}^2 + [r(t)\dot{\theta}]^2}}, \ \forall t \text{ must be satisfied for course}$$

f. Constant acceleration, a_E

choose a_{Ec}

then choose $\upsilon_{E\min} \le \upsilon_{E0} \le \upsilon_{E\max}$

then choose $\dfrac{\upsilon_{E0}\sin\phi_{E\min}}{\dot{\theta}_0} \le r_0 \le \dfrac{\upsilon_{E0}}{\dot{\theta}_0}$

then calculate $\dot{r}_0 = \sqrt{{\upsilon_{E0}}^2 - (r_0\dot{\theta}_0)^2}$

$$\frac{d}{dt}\begin{bmatrix} r \\ \dot{r} \end{bmatrix} = \begin{bmatrix} \dot{r} \\ r\dot{\theta}^2 \pm \sqrt{{a_{Ec}}^2 - (r\ddot{\theta} + 2\dot{r}\dot{\theta})^2} \end{bmatrix}, \quad \begin{bmatrix} r(0) \\ \dot{r}(0) \end{bmatrix} = \begin{bmatrix} r_0 \\ \dot{r}_0 \end{bmatrix}, \text{ where} \tag{33}$$

$$s(t) = {a_{Ec}}^2 - (r(t)\ddot{\theta} + 2\dot{r}\dot{\theta})^2 > 0, \ \forall t \text{ must be satisfied,}$$

$$\upsilon_{E\min} \le \sqrt{\dot{r}^2 + [r(t)\dot{\theta}]^2} \le \upsilon_{E\max}, \ \forall t \text{ must be satisfied for speed, and}$$

$$\sin\phi_{E\min} \le \frac{r(t)\dot{\theta}}{\sqrt{\dot{r}^2 + [r(t)\dot{\theta}]^2}}, \ \forall t \text{ must be satisfied for course}$$

System (a) simply contains a reformulation of eqs. (15) and (16) for a range of constant ECAV speeds. System (b) allows the choice of a constant ECAV course, which is actually relative to θ (see Figure XX above); a course of 90 degrees would result in a circular trajectory. Equation (29) in system (b) may actually be solved explicitly for $r(t)$, but this solution is not a concern. System (c) allows the choice of a constant ECAV heading, which means the ECAV will fly in a straight line with the specified heading. Equation (30) may also be solved explicitly for $r(t)$ if the system is autonomous, i.e. θ is not a function of time. System (d) allows the choice of a constant ECAV speed rate and is not too useful since $s(t)$ quickly reaches zero for most initial conditions. If autonomous, Equation (31) is singular on $\dot{r} = 0$ except when the constant speed rate is zero. System (e) allows the choice of a constant ECAV turn rate and is extremely useful because it can often be used to find the minimum and maximum initial conditions for which a

flyable ECAV trajectory exists for a specified range of θ. If autonomous, Equation (32) is singular on $r = 0$, and invariant on $\dot{r} = 0$ when the constant turn rate is zero. System (f) allows the choice of a constant ECAV acceleration (time derivative of ECAV velocity) and is more useful when a given phantom track is circular in form so that a constant acceleration greater (less) than the inherent centripetal acceleration causes the ECAV to spiral in (out) relative to the radar. Equation (33) works best with the minus sign in front of the square root and has a saddle when autonomous. If eqs. (30) - (33) are not autonomous but depend explicitly on time, they may still possess the autonomous system characteristics stated above.

The variable definitions and minimum/maximum values for ECAV speed and course in (22) give rise to the following $r\dot{\theta}$-boundary lines for the ECAV, which are similar in concept to condition (17) with a constant speed ECAV.

$$r(t) = \frac{\upsilon_{E\min}}{\dot{\theta}} = \frac{0.8}{\dot{\theta}} \tag{34}$$

$$r(t) = \frac{\upsilon_{E\max}}{\dot{\theta}} = \frac{1.2}{\dot{\theta}} \tag{35}$$

$$r(t) = \frac{\upsilon_{E\min}\sin\phi_{E\min}}{\dot{\theta}} = \frac{0.4}{\dot{\theta}} \tag{36}$$

$$r(t) = \frac{\upsilon_{E\max}\sin\phi_{E\min}}{\dot{\theta}} = \frac{0.6}{\dot{\theta}} \tag{37}$$

The ECAV's range may not exceed (34) at any time because this would require it to fly faster than its maximum speed. If the ECAV range decreases below (35), the ECAV may continue its trajectory, but may not fly perpendicular to its current LOS to the radar since it must have a nonzero $\dot{r}$-component to fly above its minimum speed. The ECAV's range may not decrease below (36) at any time because this would rotate its fixed antennas out of range of the radar even at minimum speed (see Figure XIX above). If the ECAV range decreases below (37), the ECAV may continue its trajectory, but only at a speed less than its maximum speed.

For this analysis on ECAV trajectory bounds, it is beneficial to convert the phantom target speed range into a larger pseudo-range for the ECAV speed with the phantom target speed resumed to constant. To make this conversion, the effect of changing α to α_{min} and α_{max} on the $r\dot{\theta}$-boundary lines (34) - (37) is determined and maximized to produce a new set of $r\dot{\theta}$-boundary lines for the ECAV speed pseudo-range. The effect of α on $\dot{\theta}$ for a straight-line phantom track is given as follows, using eqs. (19) – (21), with $\dot{\theta}$ solved explicitly as a function of θ.

$$\dot{\theta}(\theta) = \frac{\alpha\sin\psi}{1 + \dfrac{\sin^2\theta}{\sin^2(\pi-\psi-\theta)} - 2\cos\psi\dfrac{\sin\theta}{\sin(\pi-\psi-\theta)}} \tag{38}$$

Conveniently, $\dot{\theta}$ is directly proportional to α; therefore, the new $r\dot{\theta}$-boundary lines are as follows for a straight-line phantom track, where υ_{Epsmin} and υ_{Epsmax} are defined in eqs. (39) and (40), respectively.

$$r(t) = \frac{\upsilon_{E\min}}{(\alpha_{\max} - \alpha)\dot{\theta}} = \frac{\upsilon_{Eps\min}}{\dot{\theta}} = \frac{0.67}{\dot{\theta}} \tag{39}$$

$$r(t) = \frac{\upsilon_{E\max}}{(\alpha - \alpha_{\min})\dot{\theta}} = \frac{\upsilon_{Eps\max}}{\dot{\theta}} = \frac{1.5}{\dot{\theta}} \tag{40}$$

$$r(t) = \frac{\upsilon_{Eps\min} \sin\phi_{E\min}}{\dot{\theta}} = \frac{0.33}{\dot{\theta}} \tag{41}$$

$$r(t) = \frac{\upsilon_{Eps\max} \sin\phi_{E\min}}{\dot{\theta}} = \frac{0.75}{\dot{\theta}} \tag{42}$$

Figure XXI below is an exported frame from a MATLAB-generated video and illustrates visually how (34) and (35) have been changed to (39) and (40), respectively. This visual explanation is similar for the changes made to convert (36) and (37) to (41) and (42), respectively.

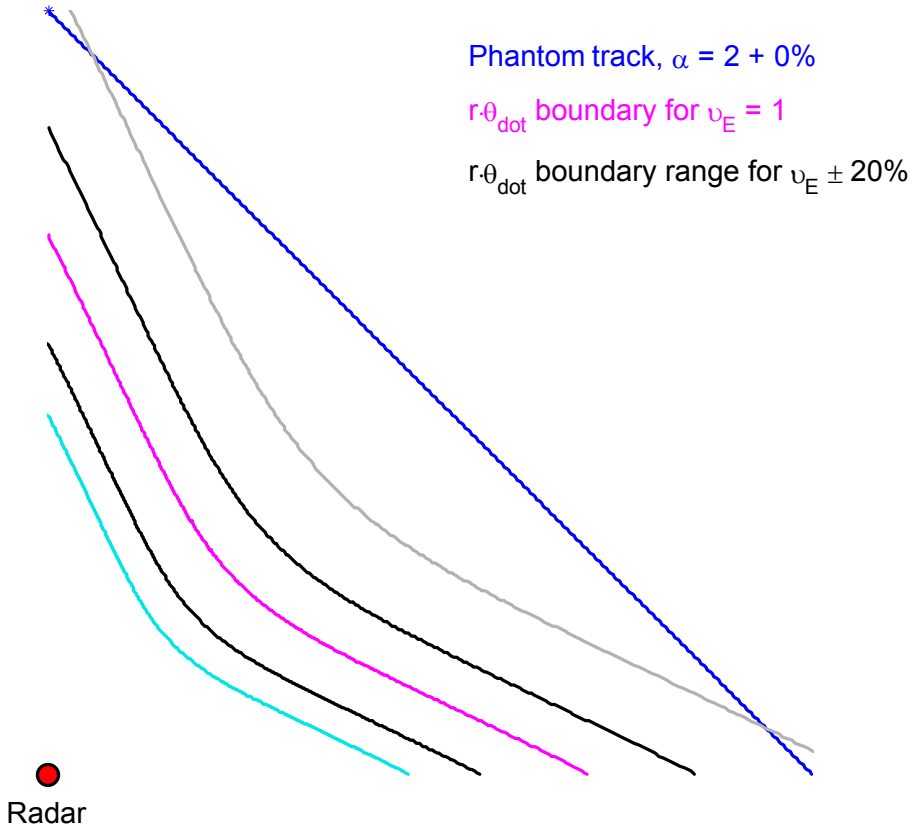

Figure XXI: Conversion of phantom track speed range into larger ECAV speed pseudo-range

In Figure XXI, the gray boundary represents the outer limit where α is decreased to α_{min}, which effectively moves the black boundary range for $\upsilon_E \pm 20$ % – both curves – out to the gray boundary; at this point, the outer black boundary coincides with the gray boundary. Likewise, the cyan boundary represents the inner limit where the black boundary range may be moved

when α is increased to α_{max}. It is important to realize that these lower and upper limits – the cyan and gray curves – may not coexist at any instant in time because α may only be one value at any time. This fact is important primarily in the case of multiple ECAVs and multiple radars because it constrains all ECAVs to be within the υ_E-boundary range at any given time, even though that range may move in and out as shown in Figure XXI. When changing α to accommodate an ECAV's desired position or speed, another consideration is that α will have to modulate in a continuous and believable fashion especially if the radar is operating at a high PRF (see Figure IV above).

To further enhance the assessment of an ECAV's flyable range given a phantom track and some range of θ, the following speed isolines may also be used, where $R(t)$ is given by the phantom track.

$$r(t) = \frac{\upsilon_{Eps\,\min}}{\alpha} R(t) \tag{43}$$

$$r(t) = \frac{\upsilon_{Eps\,\max}}{\alpha} R(t) \tag{44}$$

VIII. ECAV Bounds for a Straight-Line Phantom Track

The theory presented in the previous section for treating ranges on ECAV velocity, course, and the velocity of the phantom track is now utilized to conduct a survey of the ECAV bounds for a constant-course constant-speed phantom track. The equations for this type of phantom track, taken from the internal document by M. Pachter and P. Chandler, are shown below in polar coordinates and are identical to eqs. (19) - (21).

$$R(t) = \sqrt{1 + \alpha^2 t^2 - 2\alpha t \cos\psi} \tag{45}$$

$$\theta(t) = \arcsin\left(\frac{\alpha t \sin\psi}{R(t)}\right) \tag{46}$$

$$\dot{\theta}(t) = \frac{\alpha \sin\psi}{1 + \alpha^2 t^2 - 2\alpha t \cos\psi} \tag{47}$$

Using eqs. (45) - (47) and with $\alpha = 2$ and $\psi = 45$ degrees, a phantom track is plotted along with the boundaries and isolines corresponding to (39) - (42) and (43) - (44), respectively, in Figure XXII below. The yellow lines represent a flyable ECAV range for $\theta = 90$ degrees. This flyable range represents the union of all positions the ECAV could visit on certain trajectories and still be able to create a phantom track through 90 degrees.

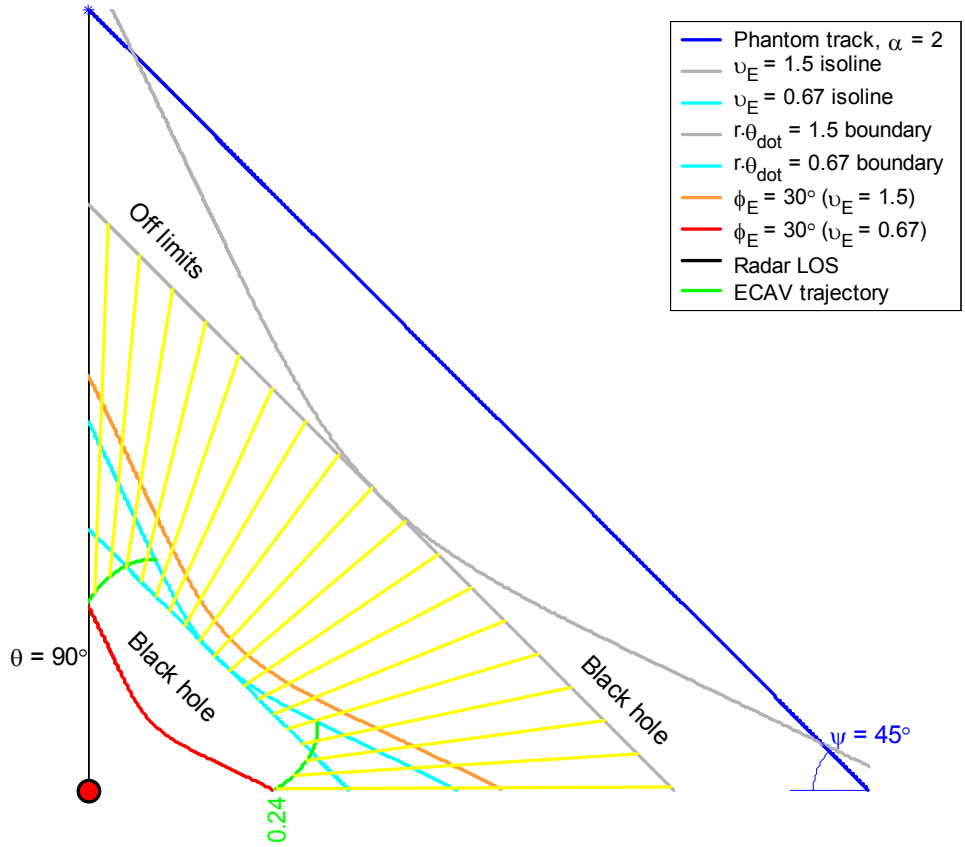

Figure XXII: ECAV flyable range for a constant-course constant-speed phantom track, $\theta = 90$ °

Many ECAV trajectories – solved using the six systems presented in the previous section – were used to test and verify the results shown in Figure XXII. Plots of some of these trajectories and the MATLAB code used to generate them are given in the Appendices. The flyable range bounded by the pseudo-speed isolines is valid since any trajectory parallel to and between these two isolines is within the ECAV speed pseudo-range and course range. The additional part of the flyable range, defined where the green curves are less than the $\upsilon_E = 0.67$ isoline, is actually bounded by a constant speed ECAV trajectory solution using system (a), where the ECAV is initially/finally on the red boundary, i.e. its course is at ϕ_{Emin}. For an ECAV starting on the right trajectory curve and running into the $r\dot{\theta} = 0.67$ boundary, it could then switch to a different system – such as system (b) with $\phi_E = 90$ degrees – to create a circular trajectory and switch back to the constant velocity system with $\upsilon_E = 0.67$ when it again crossed the $r\dot{\theta} = 0.67$ boundary. This line of reasoning as well as many flyable ECAV trajectories produced using a constant turn rate with system (e) provide ample evidence for the flyable range below the speed isolines in Figure XXII.

The right "black hole" in Figure XXII is an area that can be entered by the ECAV, but once the ECAV is in this region it cannot exit back into the flyable range; it will run into the $r\dot{\theta} = 1.5$ boundary and stop. To explain this mathematically, the following equation for the ECAV speed is used.

$$\upsilon_E = \sqrt{\dot{r}^2 + (r\dot{\theta})^2} \tag{48}$$

Taking a point on the $\upsilon_E = 1.5$ isoline that bounds the black hole, if the absolute value of $\dot{r}$ is decreased, which corresponds to entering the black hole, then eq. (48) says that υ_E will also decrease. This allows the ECAV to enter the black hole because in doing so it will be flying within its speed pseudo-range. However, for an ECAV to exit, the absolute value of $\dot{r}$ would have to increase, which by eq. (48) requires that the ECAV fly faster than its maximum pseudo-speed. A similar argument can be used to show that the region labeled "off limits" is an area that can be exited by the ECAV but not entered from its flyable range. The left "black hole" is an area that, once entered, will require that the ECAV turn in towards the radar at a progressive rate to stay within its speed pseudo-range; at some point in this process, the ECAV will reach its angle bound between the orange and red curves where its fixed antennas rotate out of range of the radar – all before $\theta = 90$ degrees is reached.

In addition to the speed and course bounds discussed above, there exist ultimate θ bounds for ECAV trajectories given a straight-line phantom track. Figure XXIII below shows a possibly conservative estimate for these bounds.

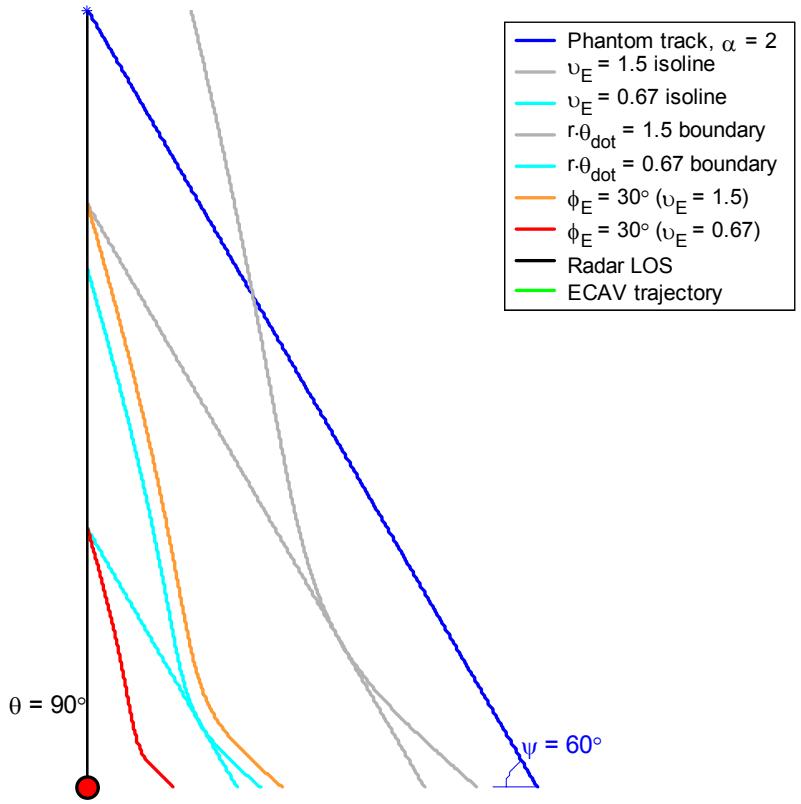

Figure XXIII: Ultimate θ bounds for ECAV trajectories given a constant-course constant-speed phantom track

From observing Figure XXIII, both speed isolines intersect their corresponding angle bounds when $\psi = 60$ degrees. If an ECAV were flying parallel to these isolines, it would reach its angle bound at this point – 60 degrees off of the shortest LOS from the radar to the phantom track. Note that this corresponds directly to the range chosen for ϕ_E, which was 90 ± 60 degrees. It may be possible for the ECAV to continue the phantom track for greater values of θ by starting on a high speed isoline and turning in towards the radar right before it reaches its angle bound; however, this possibility was not explored.

The analysis in this section is modular in that it is applicable to any number of ECAVs and the same number of radars, each on an individual basis. The parameter ψ of the phantom track is simply changed for each ECAV so that together the team creates one coherent straight-line phantom track with speed α.

IX. ECAV Bounds for a Simple Circular Phantom Track

The theory presented in Section VII is again utilized to conduct a survey of the ECAV bounds for a circular phantom track with the radar placed at the circle's center. The equations for this type of phantom track, taken from the Pachter and Chandler internal document, are shown below in polar coordinates.

$$R(t) \equiv 1 \tag{49}$$

$$\theta(t) = \alpha t \tag{50}$$

$$\dot{\theta}(t) \equiv \alpha \tag{51}$$

With eqs. (49) - (51) representing the circular phantom track, ECAV systems (a) through (f) are now autonomous and may be analyzed using phase-plane techniques if so desired. Because of this simplification, the simple circular phantom track presents a good opportunity to more thoroughly analyze the ECAV systems developed in Section VII. Using eqs. (49) - (51) and with $\alpha = 2$, a phantom track is plotted along with the boundaries and isolines corresponding to (39) - (42) and (43) - (44), respectively, in Figure XXIV below. The yellow lines represent a flyable ECAV range for $\theta = 180$ degrees. This flyable range represents the union of all positions the ECAV could visit on certain trajectories and still be able to create a phantom track through 180 degrees.

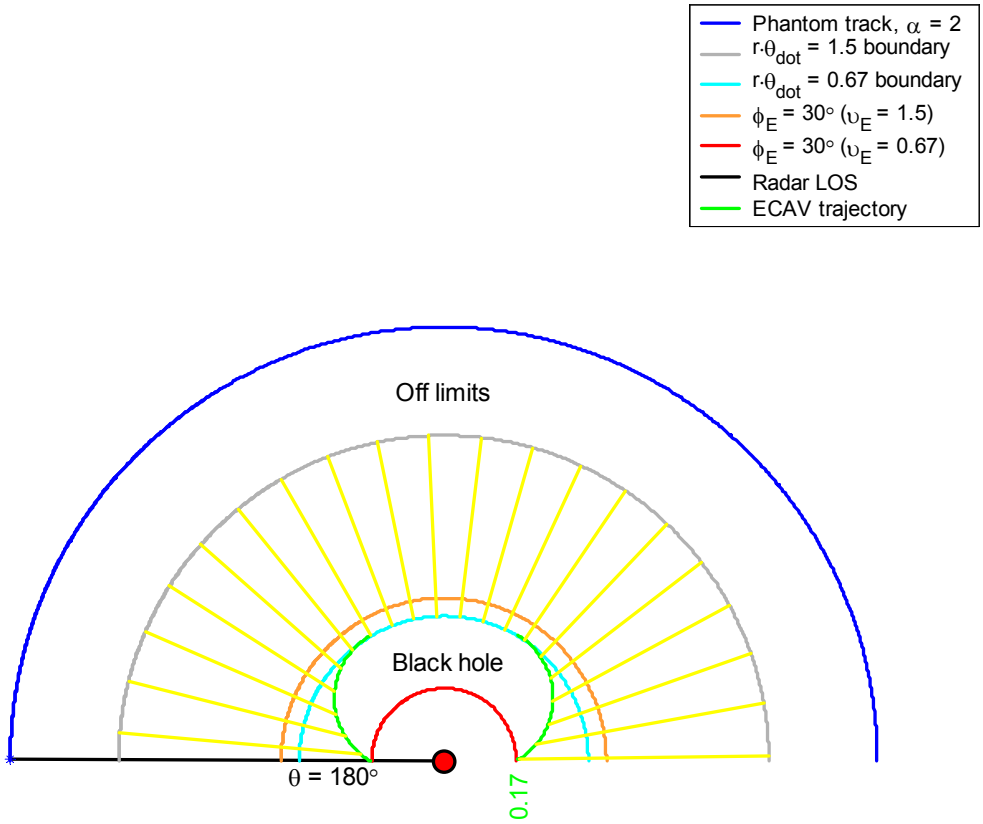

Figure XXIV: ECAV flyable range for a simple circular phantom track and $\theta = 180$ degrees

Many ECAV trajectories – solved using the six systems presented in Section VII – were used to test and verify the results shown in Figure XXIV. Some of these trajectories are given in the Appendices. For the simple circular phantom track, the minimum and maximum pseudo-speed isolines are not identified because they coincide with the $r\dot{\theta} = 0.67$ and $r\dot{\theta} = 1.5$ boundaries; this is advantageous because it means the ECAV has no ultimate θ bounds as with the straight-line phantom track (see Figure XXIII above). The flyable range bounded by the speed isolines is valid since any circular ECAV trajectory concentric with these isolines will be within the ECAV speed pseudo-range and course range. The additional part of the flyable range, defined where the green curves are less than the $\upsilon_E = 0.67$ isoline, is actually bounded by a constant speed ECAV trajectory solution using system (a), where the ECAV is initially/finally on the red boundary, i.e. its course is at ϕ_{Emin}. For an ECAV starting on the right trajectory curve and running into the $r\dot{\theta} = 0.67$ boundary, it could then switch to a different system to create a circular trajectory and switch back to the constant velocity system with $\upsilon_E = 0.67$ when it reaches the second trajectory curve on the left. This line of reasoning as well as many flyable ECAV trajectories produced using a constant turn rate with system (e) provide ample evidence for the flyable range below the speed isolines in Figure XXIV.

The region labeled "off limits" in Figure XXIV is an area that cannot be entered or exited by the ECAV because it is bounded by $r\dot{\theta} = 1.5$. Taking a point on this boundary, to enter or exit the off limits region requires $\dot{r}$ to be nonzero, which increases the ECAV speed above its pseudo-maximum according to eq. (48). The "black hole" is an area that, once entered, will require that the ECAV turn in towards the radar at a progressive rate to stay within its speed pseudo-range; at some point in this process, the ECAV will reach its angle bound between the orange and red curves where its fixed antennas rotate out of range of the radar – all before $\theta =$ 180 degrees is reached.

Although simple and useful for understanding ECAV systems and trajectory bounds, the analysis in this section alone is not modular. It is applicable at most to only one ECAV trying to deceive a radar located at the center of the circular phantom track. However, this information combined with the general circular phantom track analysis presented in the next section will provide the modularity needed for a team of ECAVs to create one coherent circular phantom track.

X. ECAV Bounds for a General Circular Phantom Track

The theory presented in Section VII is once more utilized to conduct a survey of the ECAV bounds for a circular phantom track with the radar placed arbitrarily with reference to the circle's center. The equations for this type of phantom track, taken from the Pachter and Chandler internal document and modified for corrections, are shown below in polar coordinates. Only two of the phantom track's three additional parameters, a, b, and ρ, must be specified.

$$R(t) = \sqrt{1 + 2a\rho - 2a\rho\cos\frac{\alpha}{\rho}t - 2b\rho\sin\frac{\alpha}{\rho}t} \tag{52}$$

$$\theta(t) = \left[\operatorname{sgn}\left(\xi - \frac{\alpha}{\rho}t\right)\right][x(t) - \pi] + \xi, \;\; \pi - \xi \le t \le \pi + \xi \text{, where} \tag{53}$$

$$\xi = \arg(b, a)$$

$$x(t) = \arg\left(\rho\left|a\sin\frac{\alpha}{\rho}t - b\cos\frac{\alpha}{\rho}t\right|, a^2 + b^2 - a\rho\cos\frac{\alpha}{\rho}t - b\rho\sin\frac{\alpha}{\rho}t\right)$$

$$\dot{\theta}(t) = \frac{\alpha}{R^2(t)}\left(\rho - a\cos\frac{\alpha}{\rho}t - b\sin\frac{\alpha}{\rho}t\right), \text{ where} \tag{54}$$

$$\rho = a + \sqrt{1 - b^2}$$

a ~ Distance from circle center to radar in x-direction (horizontal)
b ~ Distance from circle center to radar in y-direction (vertical)
ρ ~ Radius of the circular phantom track

Using eqs. (52) - (54) and with $\alpha = 2$, $a = -0.38$, and $b = 0.22$ (radar placed inside the circle), a phantom track is plotted along with the boundaries and isolines corresponding to (39) - (42) and (43) - (44), respectively, in Figure XXV below. The yellow lines represent a flyable ECAV range for a circular phantom track of 180 degrees, which corresponds to $\theta = 227$ degrees. This flyable range represents the union of all positions the ECAV could visit on certain trajectories and still be able to create a 180-degree circular phantom track. Application of the ECAV speed pseudo-range developed in Section VII is questionable here since the proportional dependence of $\dot{\theta}$ on α was not verified mathematically for eq. (54); in fact, it may not be possible to solve for $\dot{\theta}$ as a function of θ for the general circular phantom track. However, the form of the equation and $\dot{\theta}_0$ both suggest that this dependence still holds.

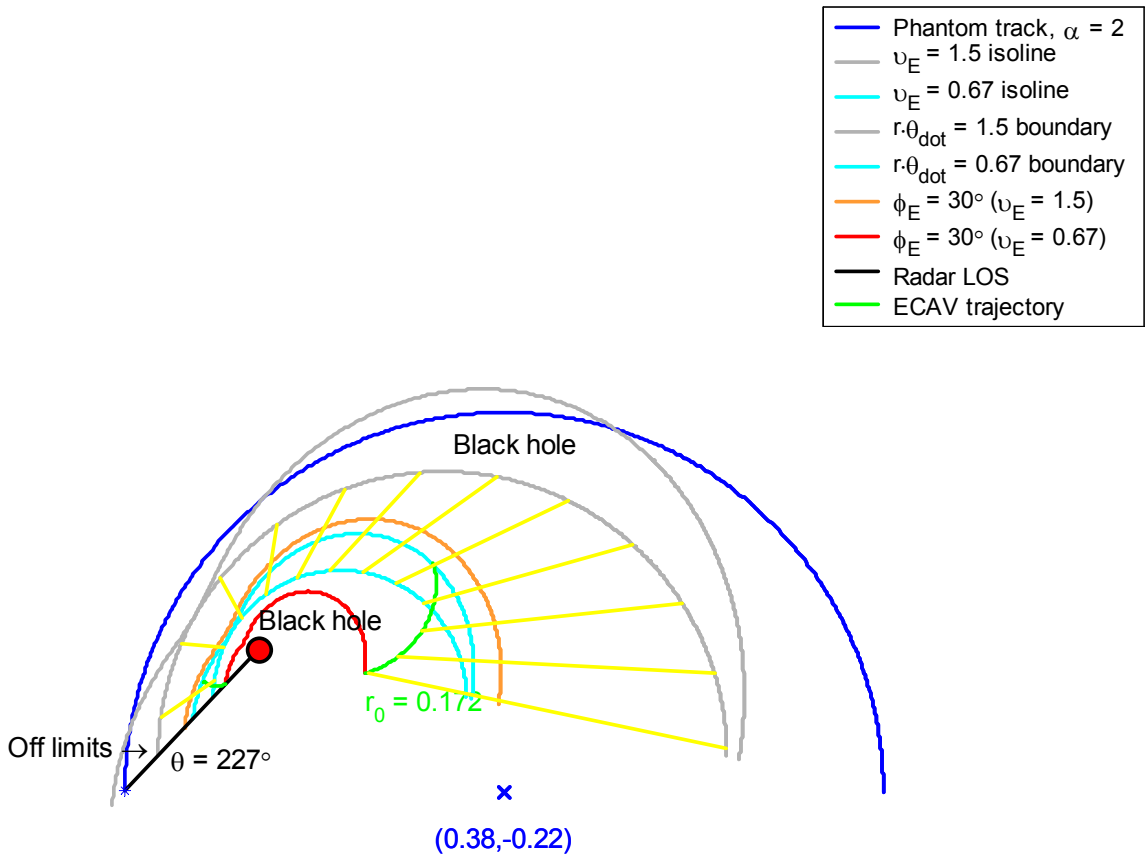

Figure XXV: ECAV flyable range for a general 180-degree circular phantom track with the radar placed inside the circle

Many ECAV trajectories – solved using the systems (a) and (e) presented in Section VII – were used to test and verify the results shown in Figure XXV. Some of these trajectories are given in the Appendices. For the general circular phantom track, the relevant isolines and boundaries plotted in Figure XXV look a good deal like those plotted for the straight-line phantom track (see Figure XXII above) except curved around in sort of an egg-shape. The flyable range bounded by the speed isolines is valid since any ECAV trajectory coinciding with a υ_E isoline between these two will fly at a constant speed and be within the ECAV speed pseudo-range and course range. The additional part of the flyable range, defined where the green curves are less than the $\upsilon_E = 0.67$ isoline, is actually bounded by a constant speed ECAV trajectory solution using system (a), where the ECAV is initially/finally on the red boundary, i.e. its course is at ϕ_{Emin}. For an ECAV starting on the right trajectory curve and running into the $r\dot{\theta} = 0.67$ boundary, it could turn into an appropriate speed isoline in between the minimum and maximum isolines and switch back to the constant velocity system with $\upsilon_E = 0.67$ when it again reaches the $r\dot{\theta} = 0.67$ boundary. This line of reasoning as well as some flyable ECAV trajectories produced using a constant turn rate with system (e) provide evidence for the flyable range below the speed isolines in Figure XXV. It has been verified that mirroring the radar's location about the phantom circle center's y-axis (vertical) produces symmetric bounds and flyable ECAV trajectories about this axis.

The "black hole" and "off limits" regions are analogous to those shown for the straight-line track in Figure XXII above. Their explanations are likewise similar and so are omitted here.

Using eqs. (52) - (54) and with $\alpha = 2$, $a = -0.6$, and $b = 0$ (radar placed outside the circle), a phantom track is plotted along with the boundaries and isolines corresponding to (39) - (42) and (43) - (44), respectively, in Figure XXVI below. The yellow lines represent a flyable ECAV range for a circular phantom track of approximately 120 degrees, which corresponds to $\theta = 40$ degrees; the phantom track can be generated no further given the placement of the radar. This flyable range represents the union of all positions the ECAV could visit on certain trajectories and still be able to create a 180-degree circular phantom track.

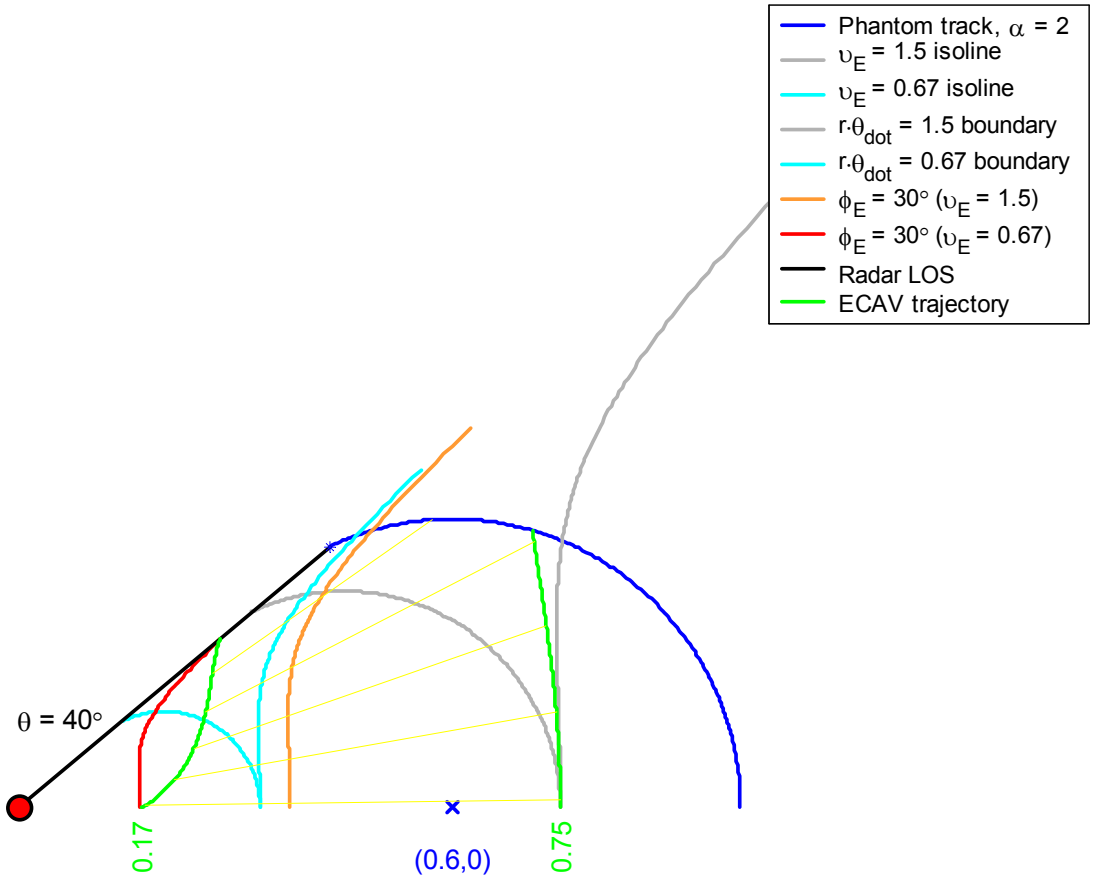

Figure XXVI: ECAV flyable range for a general circular phantom track with the radar placed outside the circle

ECAV trajectories solved using system (a) from Section VII were used to test and verify the results shown in Figure XXVI. The flyable range bounded by the green constant speed ECAV trajectory curves was validated by choosing several initial conditions in between 0.17 and 0.75 and solving the constant speed ECAV trajectory. Note that the upper bound on the flyable range now consists partly of the phantom track itself. The $\upsilon_E = 0.67$ isoline does not provide a lower bound for the flyable range because it intersects its own angle bound before $\theta = 40$ degrees. Unfortunately, the main result of placing the radar outside the circular phantom track is a severe limitation on how long the phantom track may be generated. This result is due mainly

to the angle/antenna bounds imposed on the ECAV; otherwise, the ECAV could generate a 180-degree circular phantom track and remain within its speed pseudo-range.

The analysis in this section, combined with that for the simple circular phantom track in the previous section, now provides a modular approach for a circular phantom track applicable to any number of ECAVs and the same number of radars, each on an individual basis. The parameters *a* and *b* of the phantom track are simply changed for each ECAV so that together the team creates one coherent circular phantom track. However, if any radar is placed outside the circular phantom track, it will be generated for less than 180 degrees due to the ECAV's antenna limitations (see Figure XIX above).

XI. Generalized Bounds for ECAV Initial Conditions and Flyable Range

Given the ECAV flyable ranges developed for modular straight-line and circular phantom tracks and presented in Figures XXII through XXVI above, the following equations define the range of valid initial conditions for an individual i[th] ECAV to start from and generate a desired phantom track for a desired range of θ, where $(R_0)_i$ is a dimensional length.

$$(r_{0\min})_i = \frac{\upsilon_{Eps\min} \sin\phi_{E\min}}{(\dot{\theta}_0)_i}(R_0)_i \tag{55}$$

$$(r_{0\max})_i = \min\left(\frac{\upsilon_{Eps\max}}{\alpha},1\right)(R_0)_i \tag{56}$$

Due to the conversion of the phantom track speed range into a larger ECAV speed pseudo-range in Section VII, the initial conditions of multiple ECAVs are constrained to stay within the original $r\dot{\theta}$ boundary range corresponding to their specified υ_E range of ± 20 % (see Figure XXI above) for whatever value α actually is within its range of ± 20 %. Therefore, eqs. (55) and (56) specify a maximum range, in which the selected initial conditions for each ECAV must also satisfy the following condition, where *I* contains an ordered set of index numbers for each ECAV participating.

$$\begin{aligned} &\textit{if } (r_0)_i > \frac{\upsilon_{E\max}}{\alpha}(R_0)_i \quad \textit{for any } i \in I, \\ &\textit{then } (r_0)_i > \max_{j\in I}\left(\frac{(r_0)_j}{(R_0)_j}\right)\frac{\upsilon_{E\min}}{\upsilon_{E\max}}(R_0)_i \quad \forall i \in I \end{aligned} \tag{57}$$

$$\begin{aligned} &\textit{if } (r_0)_i < \frac{\upsilon_{E\min}}{\alpha}(R_0)_i \quad \textit{for any } i \in I, \\ &\textit{then } (r_0)_i < \min_{j\in I}\left(\frac{(r_0)_j}{(R_0)_j}\right)\frac{\upsilon_{E\max}}{\upsilon_{E\min}}(R_0)_i \quad \forall i \in I \end{aligned} \tag{58}$$

In addition to the range of valid initial conditions, the time-dependent upper and lower bounds on the flyable range of an individual i[th] ECAV generating a desired phantom track for some range of θ are given below, where $R_i(t)$ is dimensional.

$$[r_{\min}(t)]_i = \min\left(\frac{\upsilon_{Eps\min}}{\alpha}R_i(t),[r^*(t)]_i,[r^{**}(t)]_i\right), \text{ where} \tag{59}$$

$[r^*(t)]_i$ solves eq. (28) with $\upsilon_{Ec} = \upsilon_{Epsmin}$, $\dot{\theta} = \dot{\theta}_i$, $t_0 = 0$, and $r_0 = (r_{0\min})_i$

$[r^{**}(t)]_i$ solves eq. (28) with $\upsilon_{Ec} = \upsilon_{Epsmin}$, $\dot{\theta} = \dot{\theta}_i$, $t_0 = (\cos\psi)/\alpha$ and $r_0 = (r_{\mathrm{fmin}})_i$

$$[r_{\max}(t)]_i = \min\left(\frac{\upsilon_{Eps\max}}{\alpha},1\right)R_i(t) \tag{60}$$

Equations (59) and (60) specify a maximum time-dependent flyable range, in which each ECAV's position must also satisfy conditions (57) and (58) for all time, with the following substitutions.

$$r_i(t) \to (r_0)_i$$

$$R_i(t) \to (R_0)_i$$

XII. Decentralized Cooperative Control Problem Formulation

As a first cut, the decentralized cooperative control problem – one of team coordination – is posed using the concept of coordination functions and illustrated for a team of three ECAVs using mainlobe deception on three radars by creating a straight-line phantom track. To begin, assume a constant-course constant-speed phantom track from right to left is desired, and that bounded ranges for υ_E, ϕ_E, and α have already been given. Let n be the number of radars – equal to the number of ECAVs – and define the following parameters.

$i = 1, 2, \ldots, n, \;\; I = [1, n] \in \mathrm{N}$, *natural numbers*

$rd_i = (rd_{ix}, rd_{iy}) \in R^2$, *real number plane* ~ location of ith radar

$(R_{\max})_i$ ~ maximum range of ith radar

$circle_i(x) = \pm\sqrt{(R_{\max})_i^{\,2} - (x - rd_{ix})^2} + rd_{iy}$ ~ maximum-range circle centered at rd_i

β ~ absolute course of the phantom track

$cone_i = \left(\beta + \frac{\pi}{2}\right) \pm \left(\frac{\pi}{2} - \phi_{E\min}\right)$ ~ ultimate θ bounds centered at rd_i

Given the above parameters, the following function can be defined, which maps these parameters into the set of functions that will later be used as inputs for each ECAV's coordination function.

$$h_T(rd_{i\in I}, (R_{\max})_{i\in I}, \beta, \phi_{E\min}) \rightarrow \textit{set } T_B \textit{ consisting of all functions, } f(x) \textit{ such that}$$

$$(x, f(x)) \in \left(\bigcap_{i\in I} circle_i\right) \bigcap \left(\bigcap_{i\in I} cone_i\right) = B \; (\textit{definition})$$

$$\frac{df}{dx} \equiv \tan\beta$$

Figure XXVII illustrates the mathematics introduced so far, where n = 3 radars. The blue lines represent functions in T_B and are all possible candidates for the team-optimal phantom track, i.e. each may be generated given the three-radar situation and taking into account each radar's maximum range and the angle/antenna bounds associated with the ECAVs.

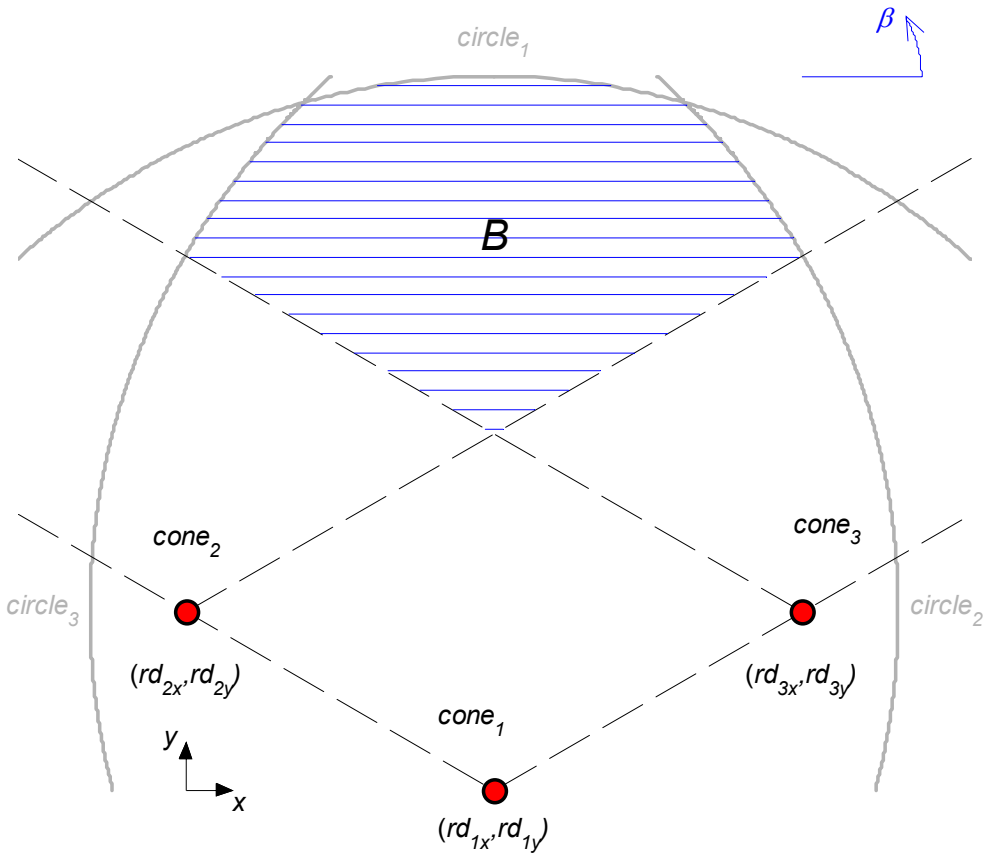

Figure XXVII: Decentralized Cooperative Control Problem for three radars and a straight-line phantom track, stage one

Three variables have yet to be chosen before a given phantom track is decided for the ECAV team. These variables and the approach to choosing them for now are given below.

- $f(x)$ ~ Choice of the phantom track as a function of x is determined by the cooperative control process
- x_0 ~ For simplicity, assume that the longest length phantom track is desirable, so choose x_0 by using the right-side boundary of B, $x_0(y)$, and set $x_0(y) > x$ by the right-to-left assumption
- α ~ Since the phantom target speed already has a built-in range of ± 20 %, assume its nominal value is fixed by the type of phantom target being created, but ensure $\alpha > 1.5$ to use the full ECAV speed and phantom target speed ranges

Given the variables $f(x)$, x_0, and α, the following function may be defined, which can use these variables to determine a valid initial condition range and/or time-dependent bounds for the flyable range of each ECAV.

$$h_r(rd_i, f(x), x_0, \alpha) \rightarrow \quad \begin{matrix} [r_{0\min}, r_{0\max}]_i = r_0 - range_i, (\bar{\theta}_0)_i \\ [r_{\min}(t), r_{\max}(t)]_i = r(t) - range_i, \theta_i(t) \end{matrix}, \text{ where}$$

$$(R_0)_i = \left\| (x_0, f(x_0)) - rd_i \right\|$$

$$(\bar{\theta}_0)_i = \arg(f(x_0) - rd_{iy}, x_0 - rd_{ix})$$

$$\psi_i = (\bar{\theta}_0)_i - \arctan\frac{df}{dx}$$

$$(\dot{\theta}_0)_i = \alpha \sin\psi_i$$

$$R_i(t) = (R_0)_i \sqrt{1 + \alpha^2 t^2 - 2\alpha t \cos\psi_i}$$

$$\theta_i(t) = \arcsin\left(\frac{\alpha t \sin\psi_i}{R_i(t)} \right)$$

$$\dot{\theta}_i(t) = \frac{\alpha \sin\psi_i}{1 + \alpha^2 t^2 - 2\alpha t \cos\psi_i}$$

The last five equations shown above are specific to the straight-line phantom track case. Conditions (57) and (58) must be applied to the choice of initial conditions and positions over time for each ECAV as in Section XI. Two cost functions may be defined for each ECAV as follows, where the price could depend on a variety of factors such as fuel or radiated power required.

$$ic_i(r_0 - range_i, (\bar{\theta}_0)_i) \rightarrow initialprice_i$$

$$tc_i(r_0 - range_i, (\bar{\theta}_0)_i, r(t) - range_i, \theta_i(t)) \rightarrow timeprice_i(t)$$

Note that the time-dependent price of each ECAV is not defined to depend on the positions of other ECAVs despite conditions (57) and (58); rather the price simply depends on the maximum flyable range of each ECAV before conditions (57) and (58) are applied to actual positions. Finally, a price based on initial conditions and the flyable ranges of each ECAV can be computed as a function of the track choice, $f(x)$, which leads to the following coordination function for each ECAV with three variations possible.

$$h_i(f(x)) \rightarrow \quad \begin{array}{l} initialprice_i \quad or \\ timeprice_i(t) \quad or \\ initialprice_i + timeprice_i(t) \end{array}$$

Each ECAV passes only a coordination function, h_i, to the team leader. The team leader then uses all n coordination functions to find the function, $f(x)$, that will minimize the total cost of the team and specify the team-optimal phantom track for the ECAVs to create. If the first version of

the coordination function is used, then each ECAV must know its own radar's location and maximum range, $x_0(y)$, and the phantom track speed. If the second or third versions of the coordination function are used, then each ECAV must additionally know the locations and maximum ranges of all additional radars involved because its time-dependent flyable range depends on where the phantom track stops as well as starts. If the flyable ranges were defined to be only the space in between minimum and maximum pseudo-speed isolines, then the flyable range for each ECAV would only be a function of x. In addition, if version two of the coordination function were used, then each ECAV would only need to know its own radar's location and maximum range.

Figure XXVIII below illustrates the situation once the necessary variables, $f(x)$, x_0, and α, are chosen to specify a team-optimal phantom track as discussed above. The bold blue line represents the phantom track chosen optimally by way of $f(x)$, and the yellow lines represent the resulting range of valid initial conditions from which each corresponding ECAV may start at time zero. Time-dependent flyable ranges for each ECAV are not shown in the figure.

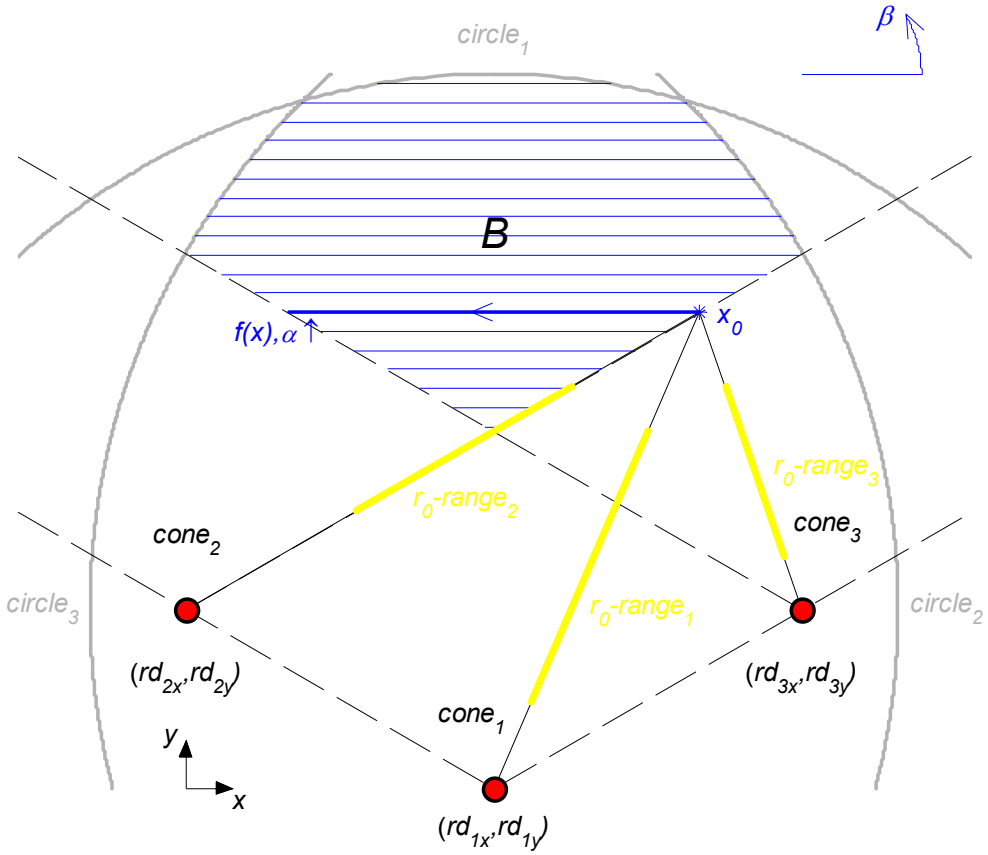

Figure XXVIII: Decentralized Cooperative Control Problem for three radars and a straight-line phantom track, stage two

Besides using coordination functions, several other methods are available in treating the decentralized cooperative control problem. The common goal is to use the minimum amount of communication – or minimum amount of the team state information, such as individual ECAV positions – to achieve the desired level of performance in choosing a team-optimal phantom track. One thing to remember is that an estimation problem may also be buried in this control problem due to the inaccuracies of ECAV and radar locations.

XIII. Conclusion

The feasibility of both mainlobe and sidelobe deception has been considered. Mainlobe deception is technically easier to accomplish but will only create one phantom track if the number of ECAVs equals the number of radars voting. Sidelobe deception is more complex but will allow multiple phantom tracks to be generated according to the number of sidelobes within range. However, if there are three or more radars voting, only one phantom track is possible. In addition, operational frequency may significantly alter a radar's sidelobes. For both mainlobe and sidelobe deception, uncertainty analysis based on inaccuracies in ECAV/radar locations and ECAV time delay indicates that both deception methods could probably work at fine resolutions in a radar network. The problem of estimating ECAV and radar locations will probably have to be solved together with the cooperative control problem.

For mainlobe deception, assuming ECAV speed to be constant severely limits the size of the sets of initial conditions yielding complete ECAV trajectories for a given range of θ. Therefore, assuming ranges for the ECAV and phantom track speeds and including an angle bound to account for the ECAV having fixed antennas produces a more realistic flyable range for the ECAV given a desired range of θ for the phantom track. ECAV trajectories and bounds can be computed given a straight-line or circular phantom track – all in a modular way for n radars and ECAVs. The ECAV trajectory solutions also require setting one ECAV variable whether it be speed, course, heading, turn rate, speed rate, or acceleration; systems are developed for this approach and some resulting ECAV trajectory solutions are shown in the Appendices for straight-line, simple circular, and general circular phantom tracks.

Based on the general theory for computing initial condition ranges and time-dependent flyable ranges for a given phantom track, the decentralized cooperative control problem may be solved under certain assumptions using coordination functions. Of course, there are other ways such as optimalization to solve this partial-information team coordination challenge. The "tallest pole" or biggest challenge in actually solving the decentralized cooperative control problem for a desired level of performance is yet to be clearly identified; it could be the dynamic coupling of the ECAVs, communication, or the estimation problem of determining ECAV and radar locations while trying to generate a coherent team-optimal phantom track.

XIV. References

Pachter, M.; Chandler, P. R. "Cooperative electronic attack using range delay-based deception." Air Force Institute of Technology and Air Force Research Laboratory Internal Document; June 25, 2003.

Stimson, G.W. Introduction to Airborne Radar. 2nd Ed. Scitech publishing; 1998.

XV. Appendices

Appendix A: ECAV trajectory solutions for a straight-line phantom track

ECAV Constant Speed Trajectory Solution for a Given Phantom Track

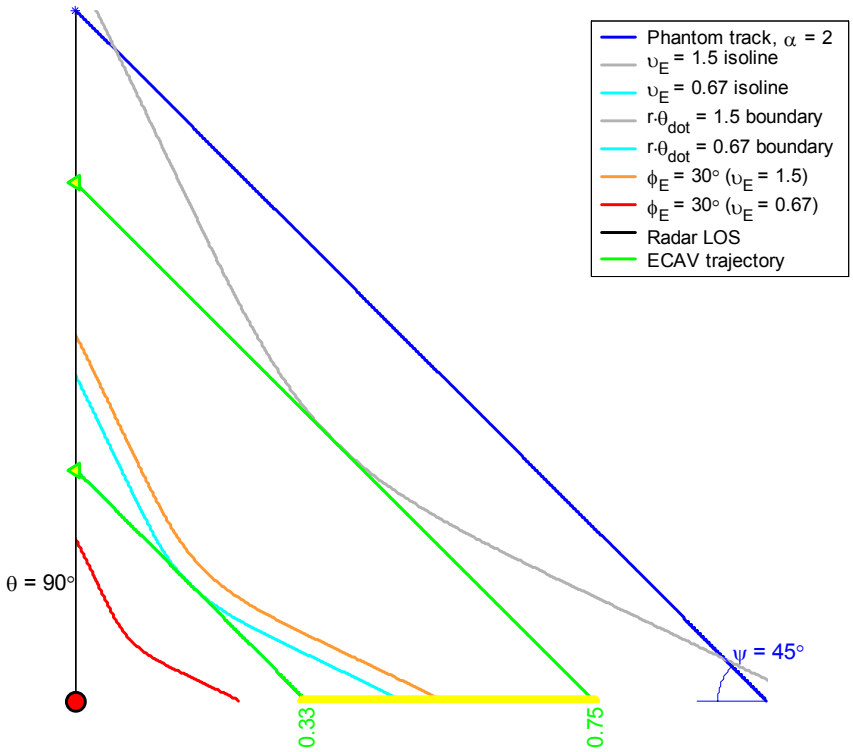

ECAV Constant Heading Trajectory Solution for a Given Phantom Track

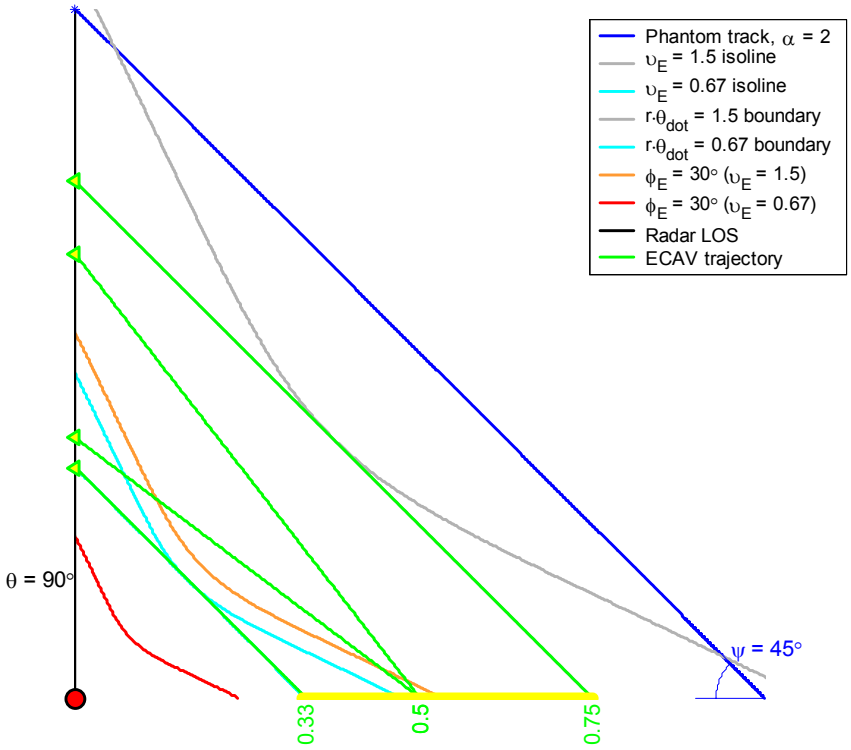

ECAV Constant Speed Rate Trajectory Solution for a Given Phantom Track

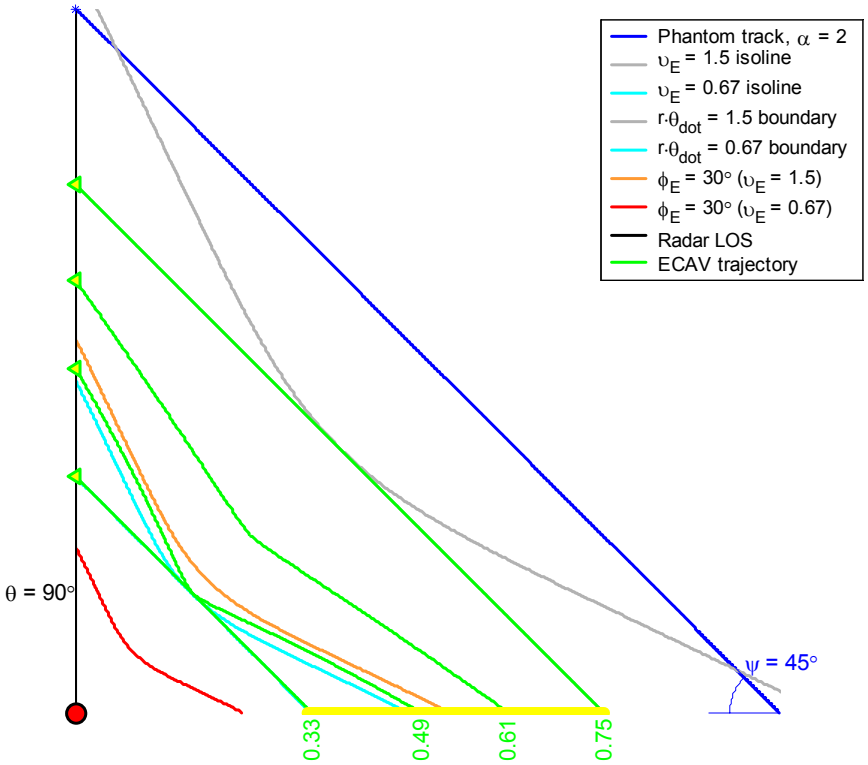

ECAV Constant Course Trajectory Solution for a Given Phantom Track

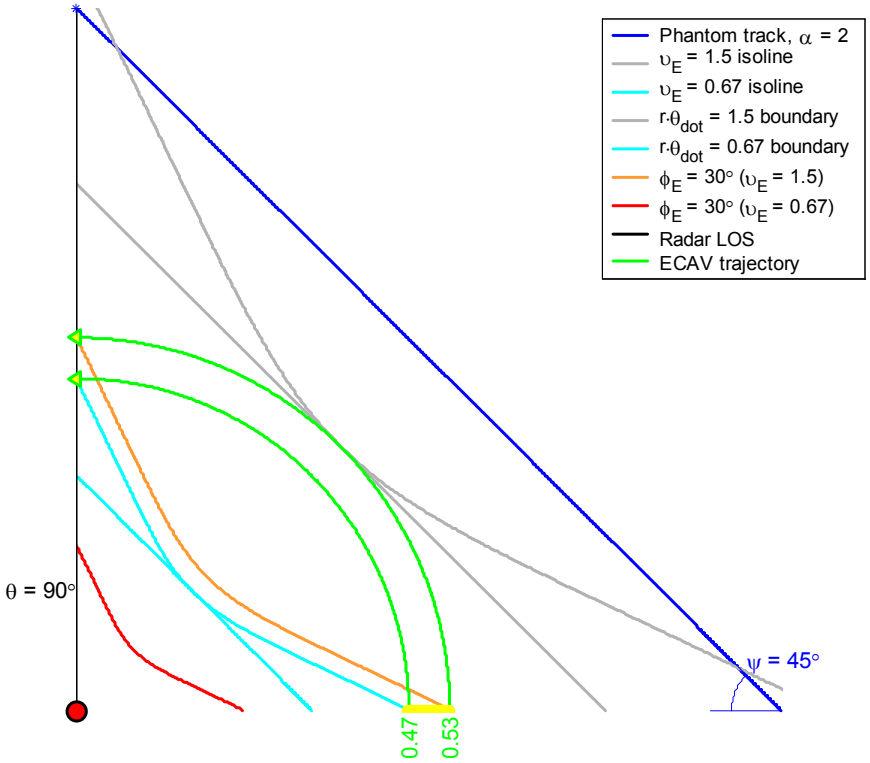

ECAV Constant Turn Rate Trajectory Solution for a Given Phantom Track

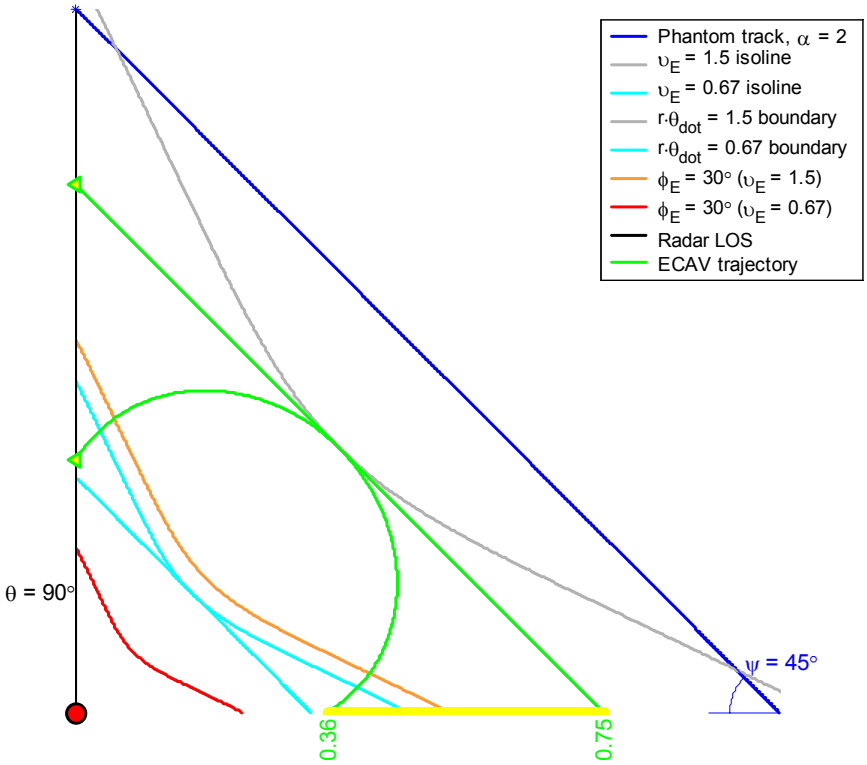

ECAV Constant Turn Rate Trajectory Solution for a Given Phantom Track

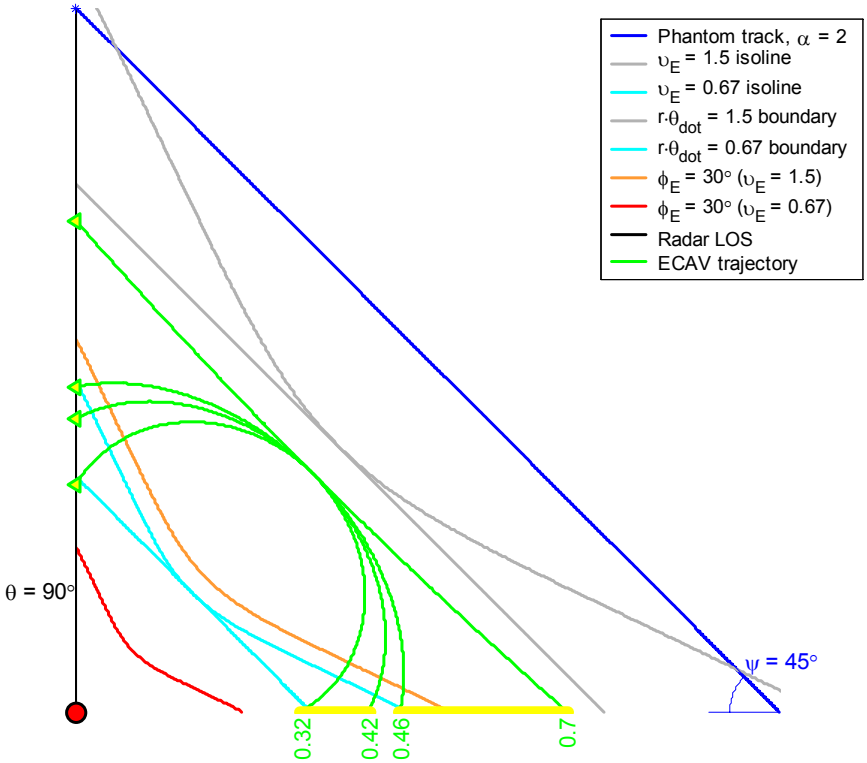

ECAV Constant Turn Rate Trajectory Solution for a Given Phantom Track

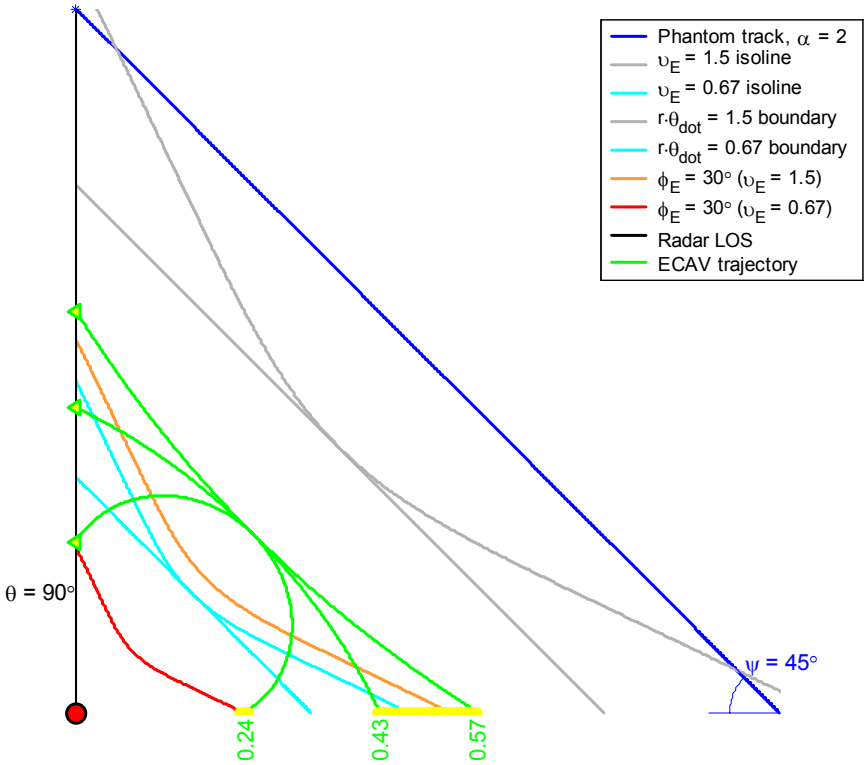

ECAV Constant Turn Rate Trajectory Solution for a Given Phantom Track

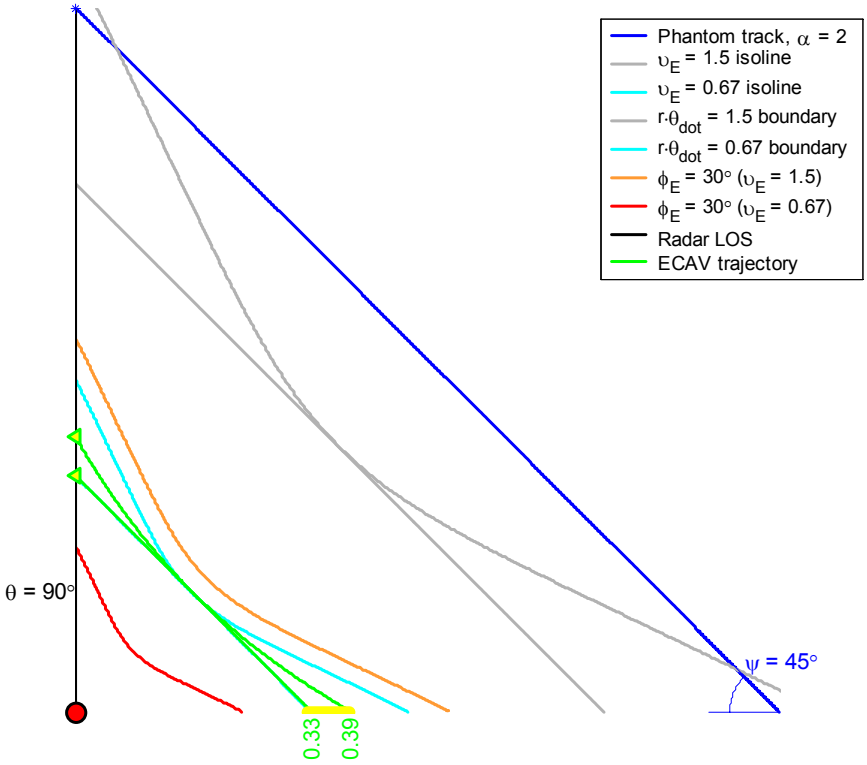

Appendix B: ECAV trajectory solutions for a simple circular phantom track

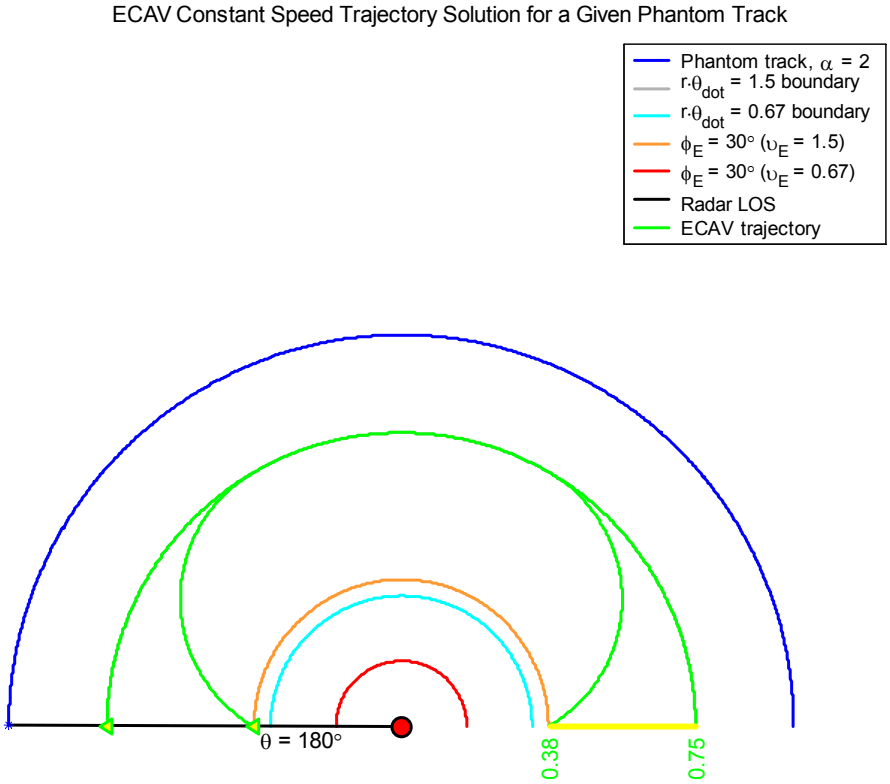

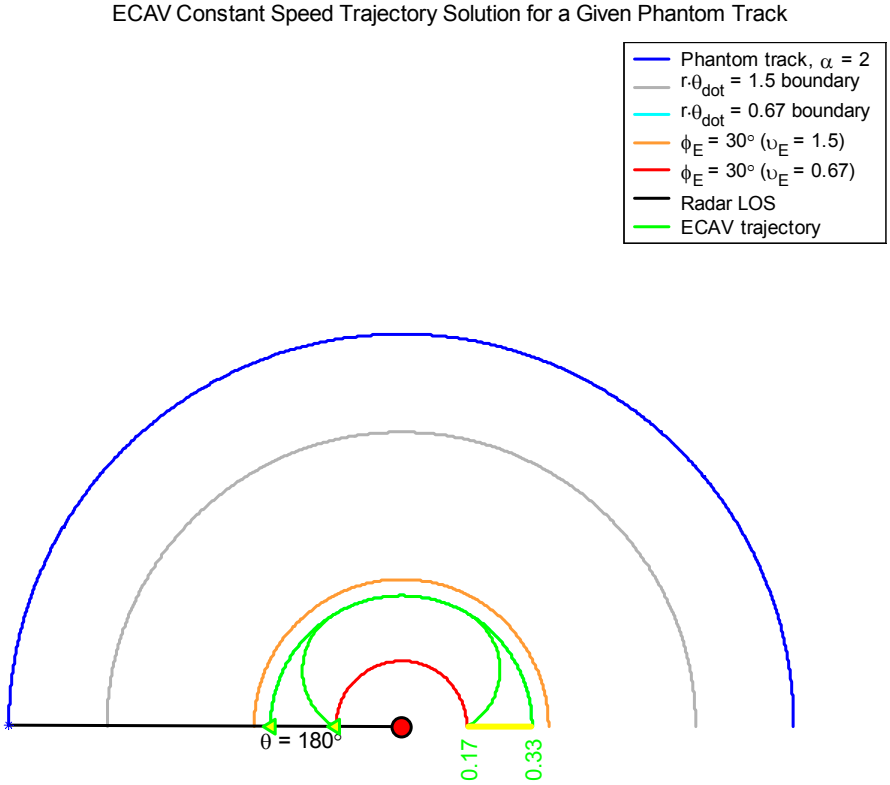

ECAV Constant Course Trajectory Solution for a Given Phantom Track

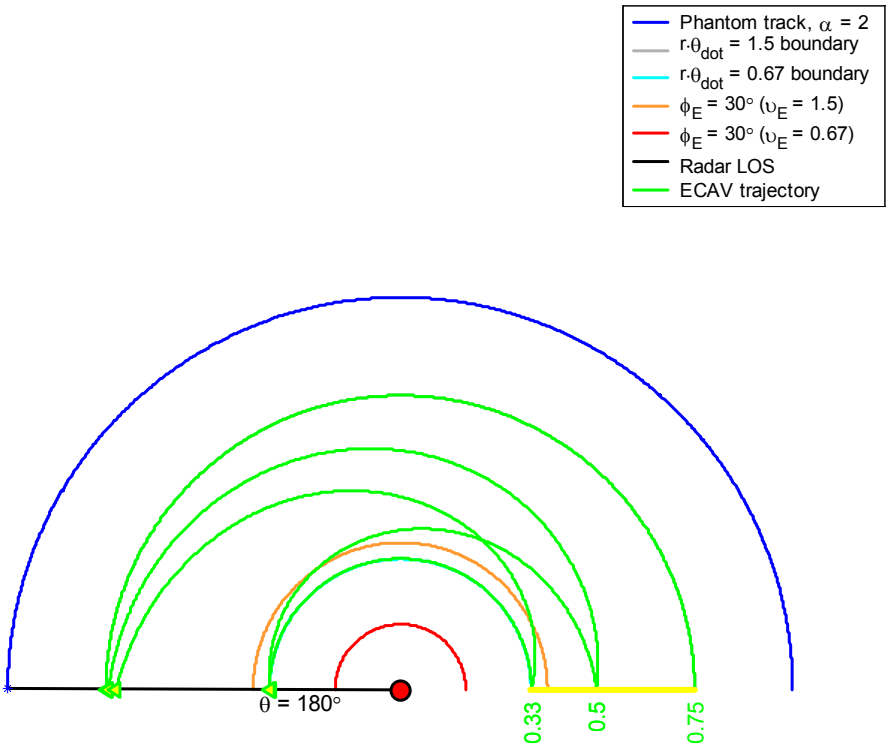

ECAV Constant Speed Rate Trajectory Solution for a Given Phantom Track

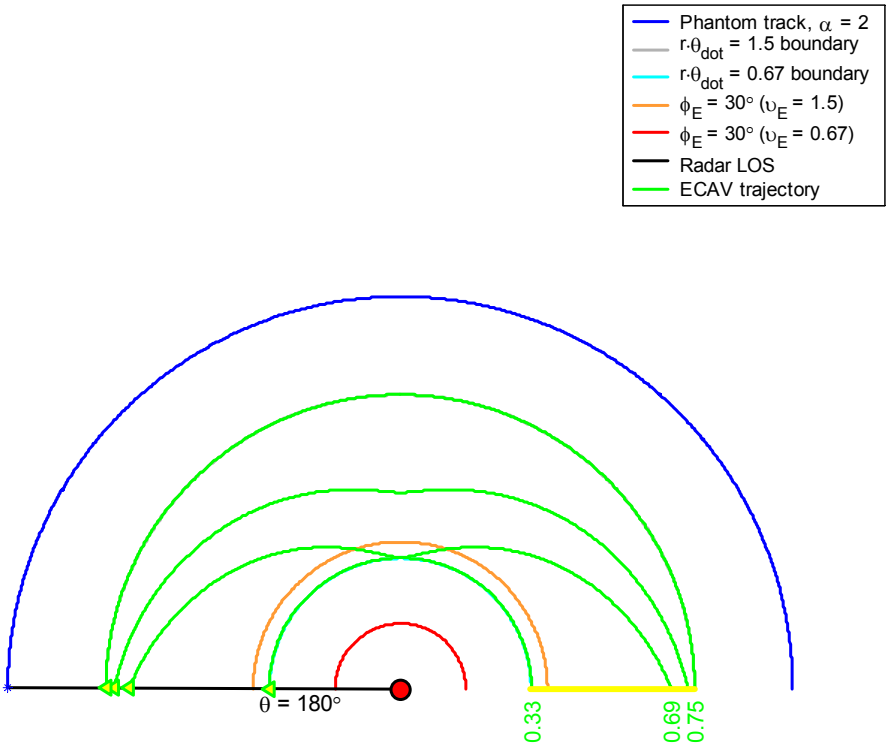

ECAV Constant Heading Trajectory Solution for a Given Phantom Track

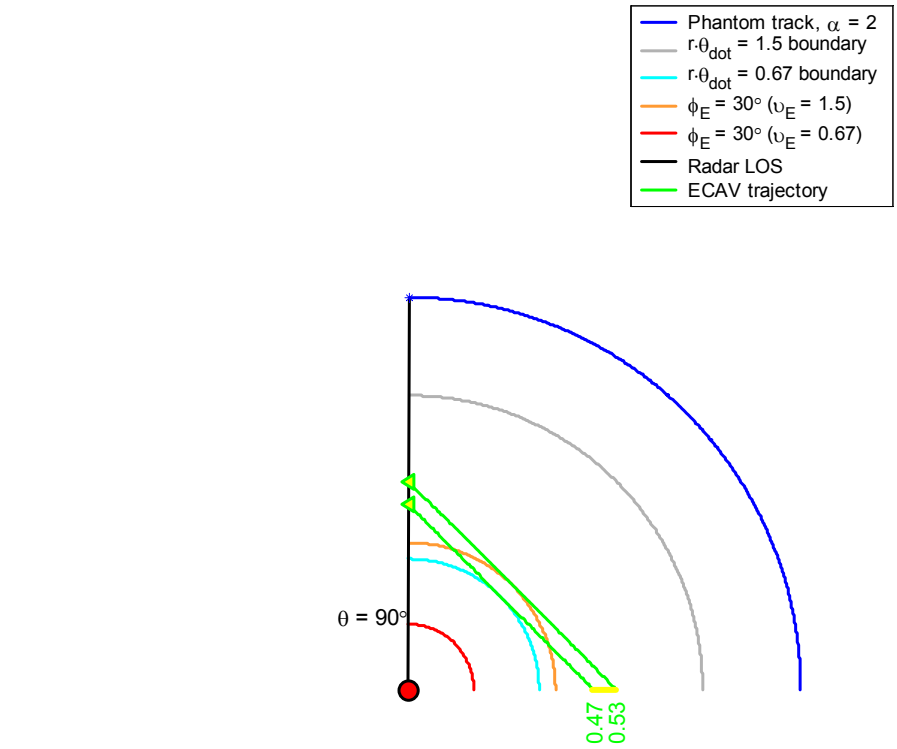

ECAV Constant Acceleration Trajectory Solution for a Given Phantom Track

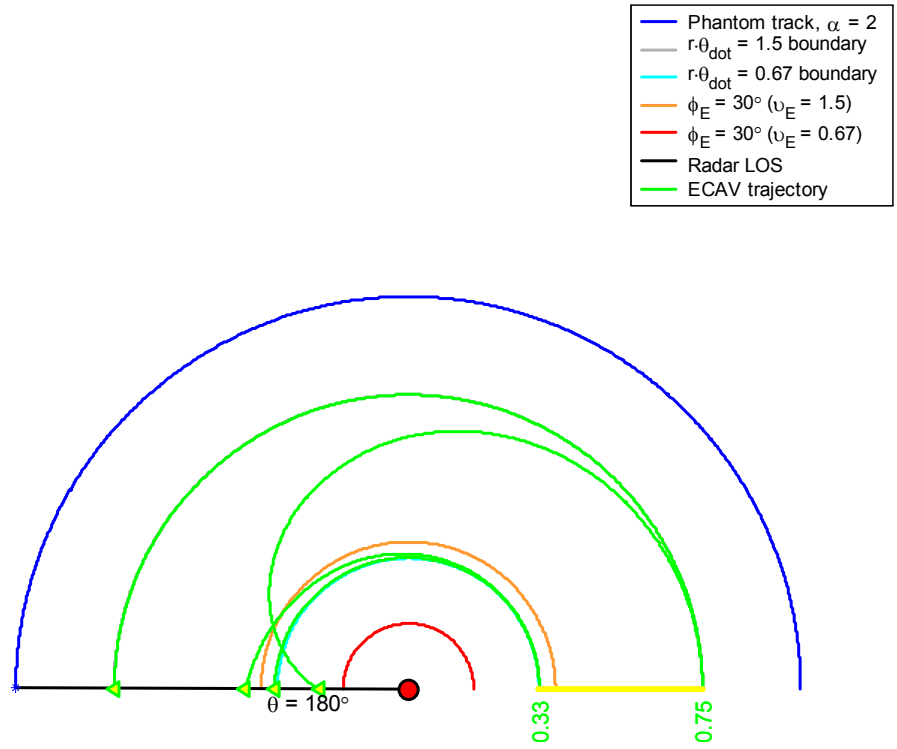

ECAV Constant Turn Rate Trajectory Solution for a Given Phantom Track

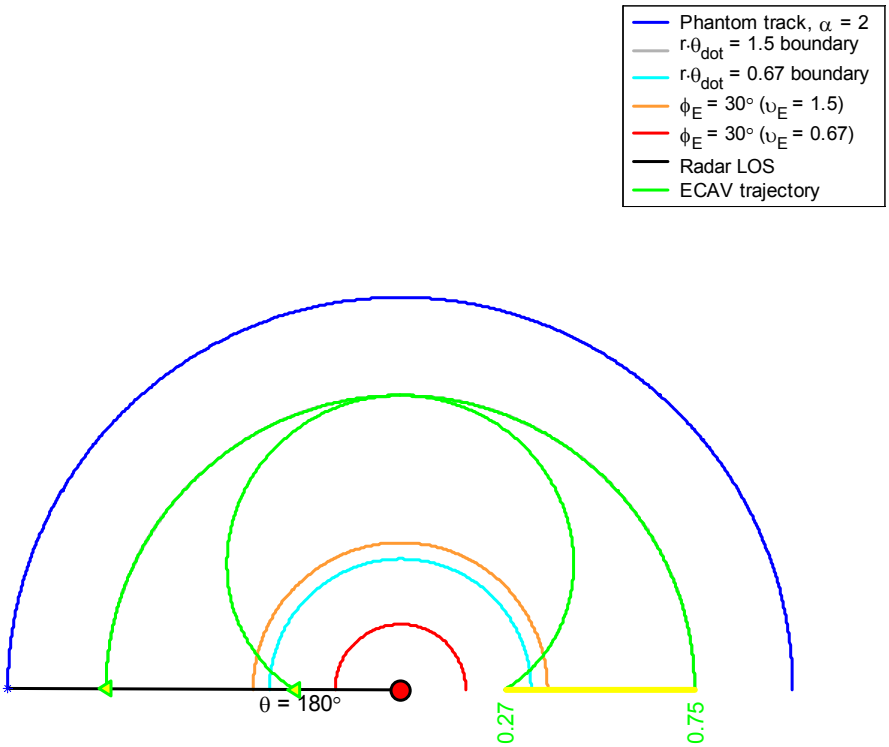

ECAV Constant Turn Rate Trajectory Solution for a Given Phantom Track

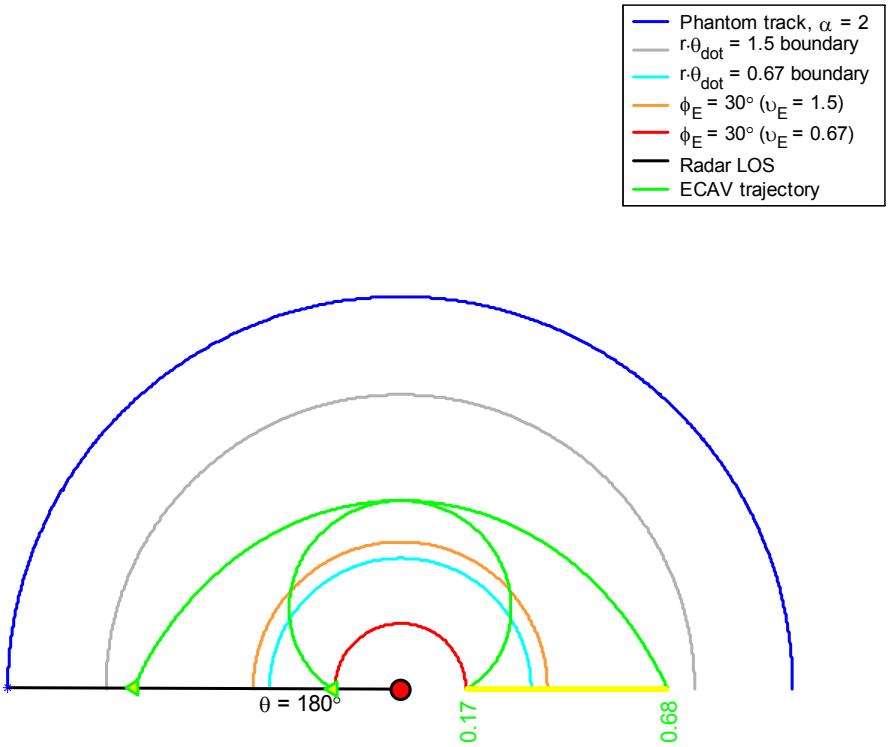

ECAV Constant Turn Rate Trajectory Solution for a Given Phantom Track

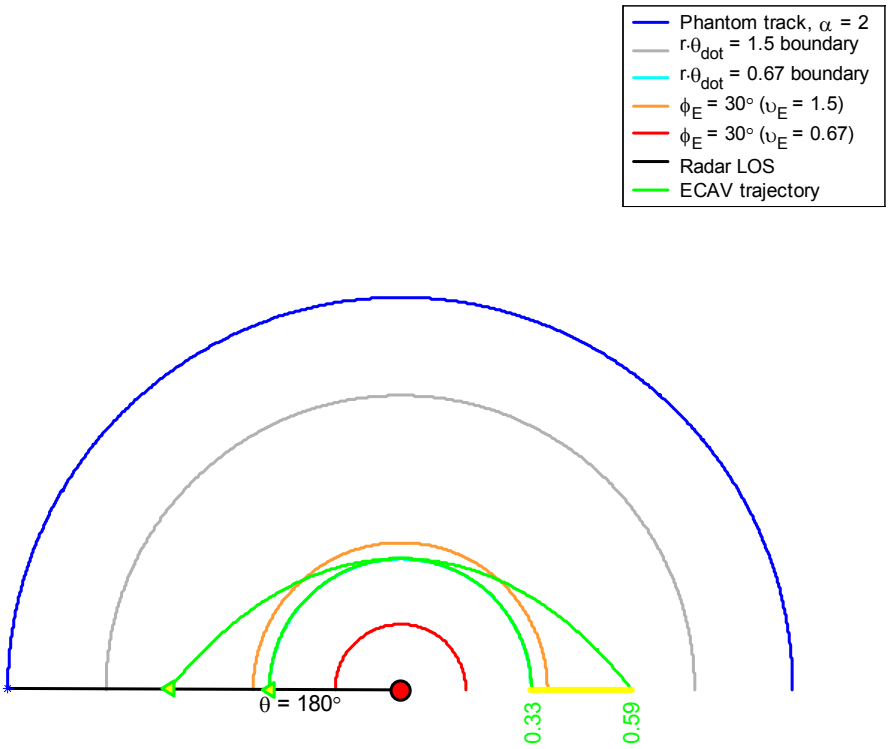

Appendix C: Theoretical ECAV trajectory solutions for a simple circular phantom track with no antenna/angle limitations applied to the ECAV

ECAV Constant Speed Trajectory Solution for a Given Phantom Track

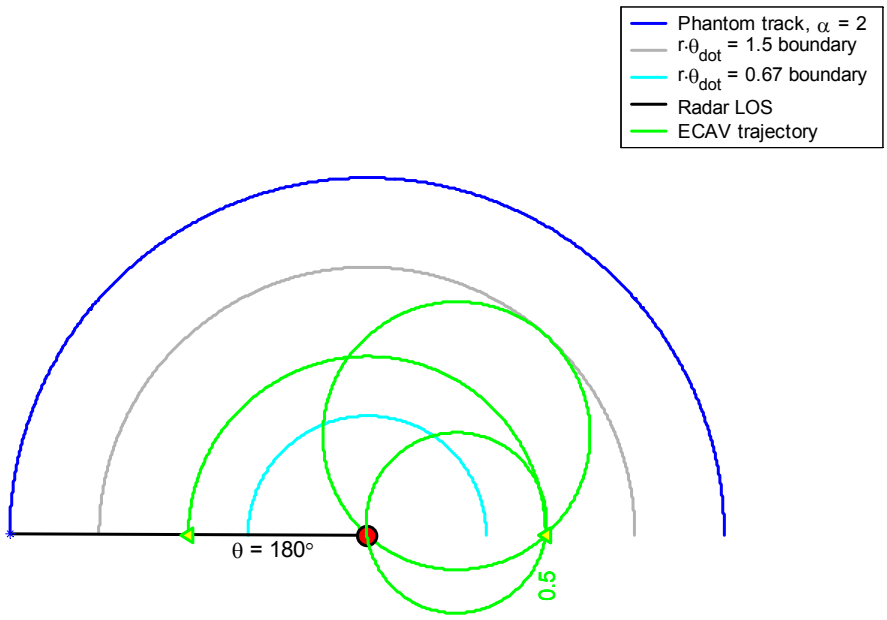

ECAV Constant Acceleration Trajectory Solution for a Given Phantom Track

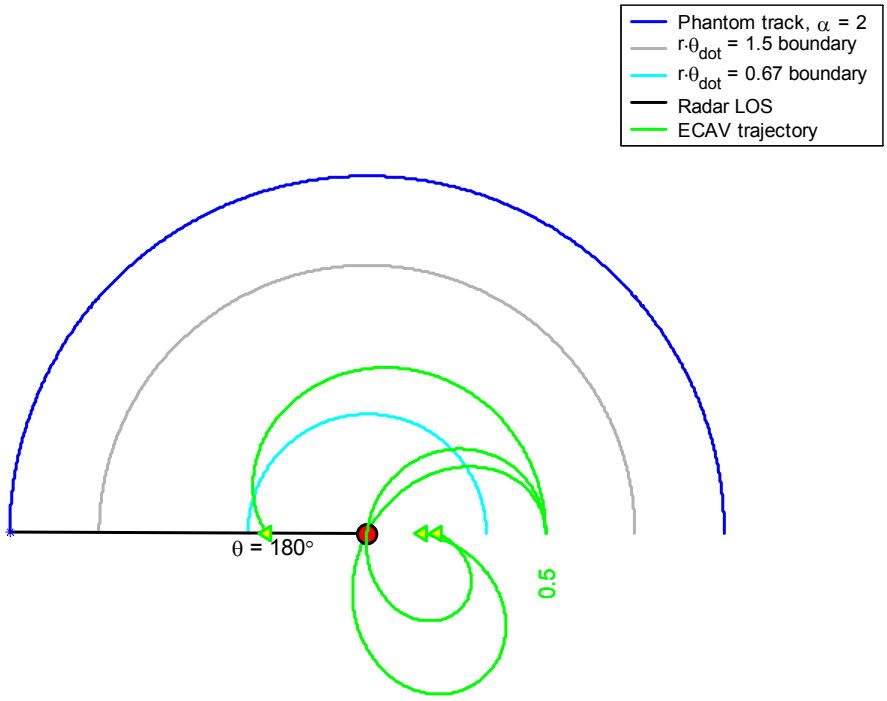

Appendix D: ECAV trajectory solutions for a general circular phantom track

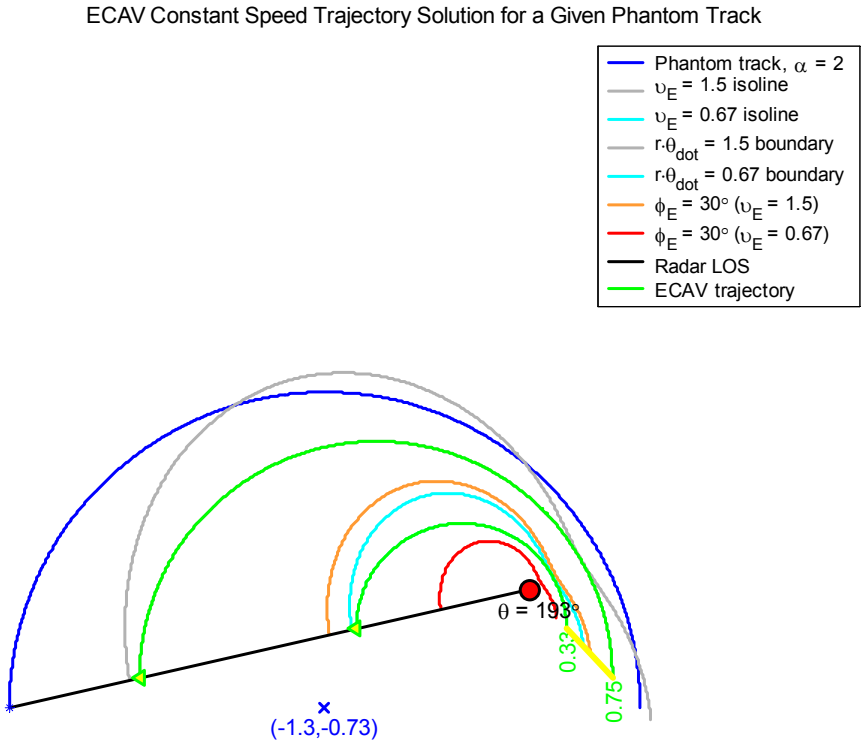

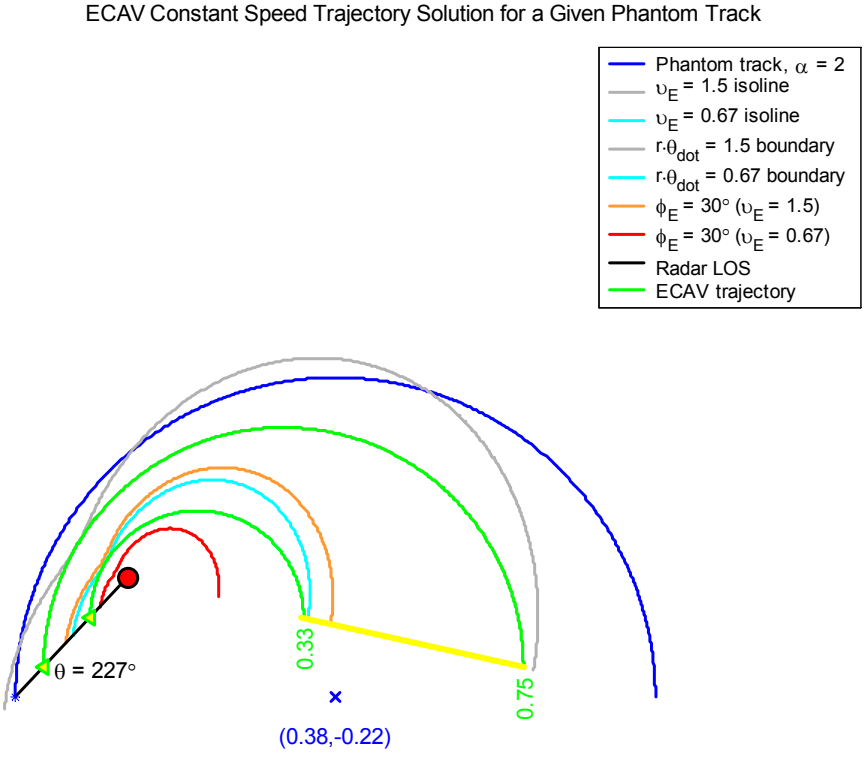

ECAV Constant Turn Rate Trajectory Solution for a Given Phantom Track

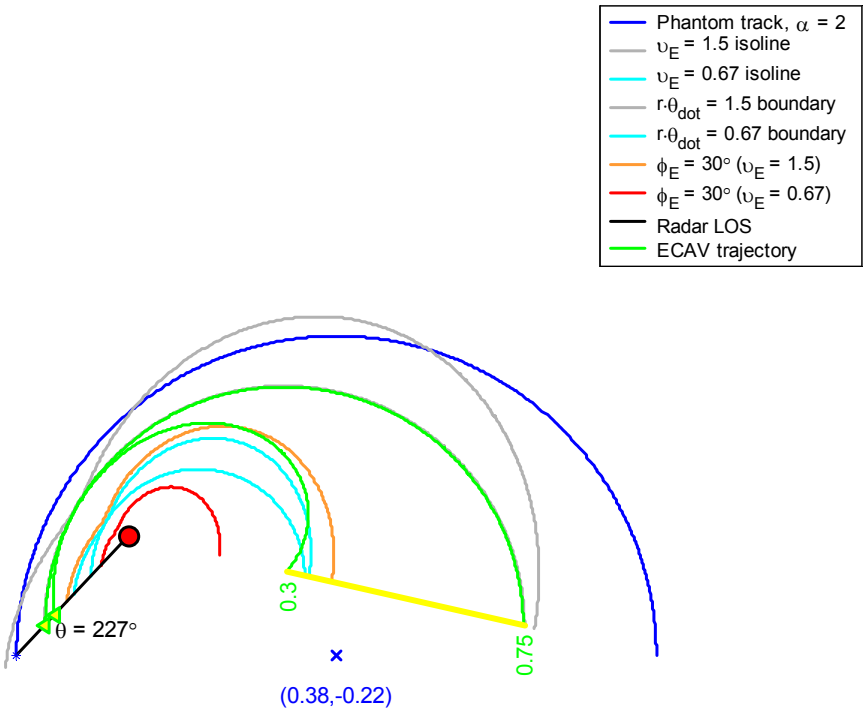

ECAV Constant Turn Rate Trajectory Solution for a Given Phantom Track

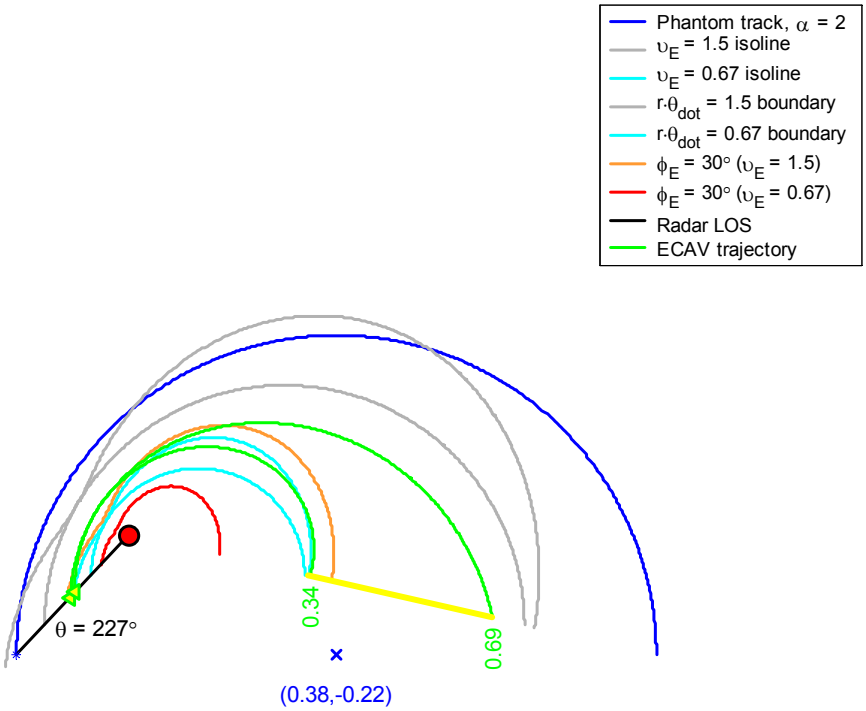

ECAV Constant Turn Rate Trajectory Solution for a Given Phantom Track

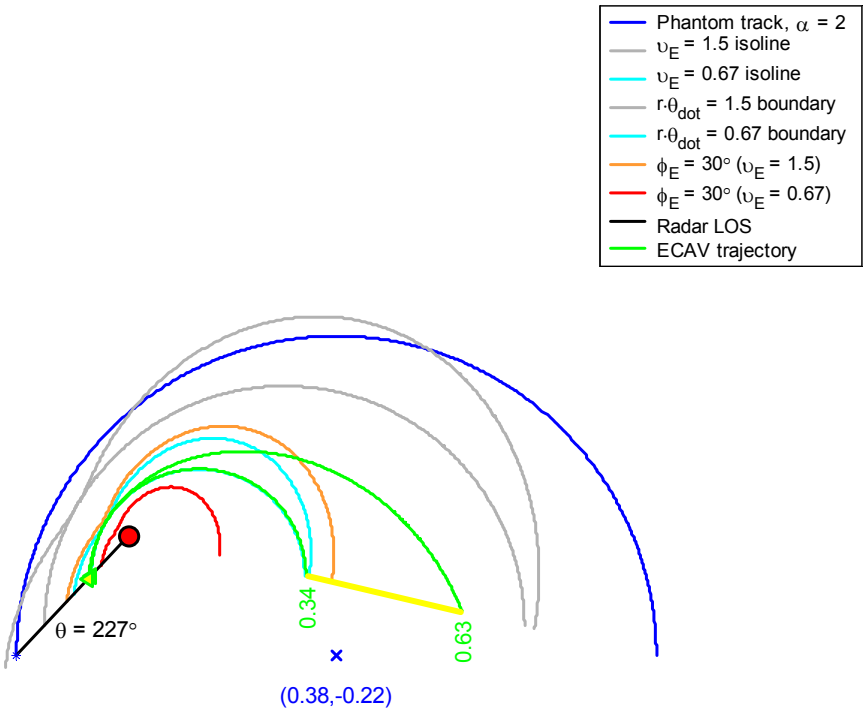

Appendix E: MATLAB code for ECAV trajectory solutions for a straight-line phantom track (MATLAB code for the trajectories corresponding to circular phantom tracks is not included, but is very similar to the code shown below; the main differences are the phantom track equations and axis/text adjustments)

```
%   ECAVPLOTRANGE
%
%   by Keith Purvis, August 2003
%
%   Shows a wide variety of ECAV trajectory solutions with different ECAV
%       systems (constant velocity, constant course, constant turn rate,etc.)
%       used for the solutions - all for a straight line phantom track and
%       theta = 90 degrees

clear all
close all

alpha=2;
psi=pi/4;
posnegEq=2;

%-------------------------------------------------------------------------
%Constant velocity, v_E
constraint=1;
constant=1.5;
r0=constant/alpha;
tstart=0;
tfinal=1/(alpha*cos(psi))-0.0001;
extras=0;
ecavsimrange(alpha,psi,constraint,constant,posnegEq,r0,tstart,tfinal,extras,0);
constant=2/3;
r0=constant/alpha;
ecavsimrange(alpha,psi,constraint,constant,posnegEq,r0,tstart,tfinal,extras,1);
plot([0.33 0.75],[0 0],'y','LineWidth',6)
hold off

%-------------------------------------------------------------------------
%Constant course, phi_E
constraint=2;
constant=pi/2;
r0=1.5*sin(psi)/alpha-0.0001;
tstart=0;
tfinal=1/(alpha*cos(psi))-0.0001;
extras=0;
ecavsimrange(alpha,psi,constraint,constant,posnegEq,r0,tstart,tfinal,extras,0);
r0=0.472;
```

```
ecavsimrange(alpha,psi,constraint,constant,posnegEq,r0,tstart,tfinal,extras,1);
plot([0.47 0.53],[0 0],'y','LineWidth',6)
hold off

%-------------------------------------------------------------------------
%Constant heading
constraint=3;
constant=pi-pi/4;
r0=0.75-0.0001;
tstart=0;
tfinal=1/(alpha*cos(psi))-0.0001;
extras=0;
ecavsimrange(alpha,psi,constraint,constant,posnegEq,r0,tstart,tfinal,extras,0);
constant=pi-pi/4-pi/25;
r0=0.5;
extras=0;
ecavsimrange(alpha,psi,constraint,constant,posnegEq,r0,tstart,tfinal,extras,1);
constant=pi-pi/4+pi/22.5;
r0=0.5;
extras=0;
ecavsimrange(alpha,psi,constraint,constant,posnegEq,r0,tstart,tfinal,extras,1);
constant=pi-pi/4;
r0=0.334;
extras=0;
ecavsimrange(alpha,psi,constraint,constant,posnegEq,r0,tstart,tfinal,extras,1);
plot([0.33 0.75],[0 0],'y','LineWidth',6)
hold off

%-------------------------------------------------------------------------
%Constant turn rate at the minimum of 1.5/theta_dot
constraint=4;
constant=5.18;
r0=[1.5*sin(psi)/alpha-0.0001;0];
tstart=cos(psi)/alpha;
tfinal=0;
extras=0;
ecavsimrange(alpha,psi,constraint,constant,posnegEq,r0,tstart,tfinal,extras,0);
tfinal=1/(alpha*cos(psi))-0.0001;
extras=0;
ecavsimrange(alpha,psi,constraint,constant,posnegEq,r0,tstart,tfinal,extras,1);

constant=0;
tfinal=0;
extras=0;
ecavsimrange(alpha,psi,constraint,constant,posnegEq,r0,tstart,tfinal,extras,1);
tfinal=1/(alpha*cos(psi))-0.0001;
```

```
extras=0;
ecavsimrange(alpha,psi,constraint,constant,posnegEq,r0,tstart,tfinal,extras,1);
plot([0.36 0.75],[0 0],'y','LineWidth',6)
hold off

%-------------------------------------------------------------------------
%Constant turn rate at the minimum of 1.35/theta_dot
constraint=4;
constant=5.18;
r0=[1.35*sin(psi)/alpha-0.0001;0];
tstart=cos(psi)/alpha;
tfinal=0;
extras=0;
ecavsimrange(alpha,psi,constraint,constant,posnegEq,r0,tstart,tfinal,extras,0);
tfinal=1/(alpha*cos(psi))-0.0001;
extras=0;
ecavsimrange(alpha,psi,constraint,constant,posnegEq,r0,tstart,tfinal,extras,1);

constant=3.6;
tfinal=0;
extras=0;
ecavsimrange(alpha,psi,constraint,constant,posnegEq,r0,tstart,tfinal,extras,1);
tfinal=1/(alpha*cos(psi))-0.0001;
extras=0;
ecavsimrange(alpha,psi,constraint,constant,posnegEq,r0,tstart,tfinal,extras,1);

constant=2.79;
tfinal=0;
extras=0;
ecavsimrange(alpha,psi,constraint,constant,posnegEq,r0,tstart,tfinal,extras,1);
tfinal=1/(alpha*cos(psi))-0.0001;
extras=0;
ecavsimrange(alpha,psi,constraint,constant,posnegEq,r0,tstart,tfinal,extras,1);

constant=-0.18;
tfinal=0;
extras=0;
ecavsimrange(alpha,psi,constraint,constant,posnegEq,r0,tstart,tfinal,extras,1);
tfinal=1/(alpha*cos(psi))-0.0001;
extras=0;
ecavsimrange(alpha,psi,constraint,constant,posnegEq,r0,tstart,tfinal,extras,1);
plot([0.32 0.42],[0 0],'y',[0.46 0.7],[0 0],'y','LineWidth',6)
hold off

%-------------------------------------------------------------------------
%Constant turn rate at the minimum of 1.01/theta_dot
```

```
constraint=4;
constant=5.18;
r0=[1.01*sin(psi)/alpha-0.0001;0];
tstart=cos(psi)/alpha;
tfinal=0;
extras=0;
ecavsimrange(alpha,psi,constraint,constant,posnegEq,r0,tstart,tfinal,extras,0);
tfinal=1/(alpha*cos(psi))-0.0001;
extras=0;
ecavsimrange(alpha,psi,constraint,constant,posnegEq,r0,tstart,tfinal,extras,1);

constant=1.01;
tfinal=0;
extras=0;
ecavsimrange(alpha,psi,constraint,constant,posnegEq,r0,tstart,tfinal,extras,1);
tfinal=1/(alpha*cos(psi))-0.0001;
extras=0;
ecavsimrange(alpha,psi,constraint,constant,posnegEq,r0,tstart,tfinal,extras,1);

constant=-0.61;
tfinal=0;
extras=0;
ecavsimrange(alpha,psi,constraint,constant,posnegEq,r0,tstart,tfinal,extras,1);
tfinal=1/(alpha*cos(psi))-0.0001;
extras=0;
ecavsimrange(alpha,psi,constraint,constant,posnegEq,r0,tstart,tfinal,extras,1);
plot([0.235 0.244],[0 0],'y',[0.43 0.57],[0 0],'y','LineWidth',6)
hold off

%--------------------------------------------------------------------------
%Constant turn rate at the minimum of 0.67/theta_dot
constraint=4;
constant=0;
r0=[0.67*sin(psi)/alpha-0.0001;0];
tstart=cos(psi)/alpha;
tfinal=0;
extras=0;
ecavsimrange(alpha,psi,constraint,constant,posnegEq,r0,tstart,tfinal,extras,0);
tfinal=1/(alpha*cos(psi))-0.0001;
extras=0;
ecavsimrange(alpha,psi,constraint,constant,posnegEq,r0,tstart,tfinal,extras,1);

constant=-0.74;
tfinal=0;
extras=0;
ecavsimrange(alpha,psi,constraint,constant,posnegEq,r0,tstart,tfinal,extras,1);
```

```
tfinal=1/(alpha*cos(psi))-0.0001;
extras=0;
ecavsimrange(alpha,psi,constraint,constant,posnegEq,r0,tstart,tfinal,extras,1);
plot([0.33 0.39],[0 0],'y','LineWidth',6)
hold off

%--------------------------------------------------------------------------
%Constant speed rate, v_Edot
constraint=5;
constant=-1.41;
r0=[1*sin(psi)/alpha-0.0001;-0.0001];
tstart=cos(psi)/alpha;
tfinal=0;
extras=0;
ecavsimrange(alpha,psi,constraint,constant,posnegEq,r0,tstart,tfinal,extras,0);
constant=1.41;
r0=[1*sin(psi)/alpha-0.0001;0.0001];
tfinal=1/(alpha*cos(psi))-0.0001;
extras=0;
ecavsimrange(alpha,psi,constraint,constant,posnegEq,r0,tstart,tfinal,extras,1);

constant=-2.02;
r0=[0.67*sin(psi)/alpha-0.0001;-0.0001];
tstart=cos(psi)/alpha;
tfinal=0;
extras=0;
ecavsimrange(alpha,psi,constraint,constant,posnegEq,r0,tstart,tfinal,extras,1);
constant=2.02;
r0=[0.67*sin(psi)/alpha-0.0001;0.0001];
tfinal=1/(alpha*cos(psi))-0.0001;
extras=0;
ecavsimrange(alpha,psi,constraint,constant,posnegEq,r0,tstart,tfinal,extras,1);

constant=0;
r0=[1.5*sin(psi)/alpha-0.0001;-0.0001];
tstart=cos(psi)/alpha;
tfinal=0;
extras=0;
ecavsimrange(alpha,psi,constraint,constant,posnegEq,r0,tstart,tfinal,extras,1);
constant=0;
r0=[1.5*sin(psi)/alpha-0.0001;0.0001];
tfinal=1/(alpha*cos(psi))-0.0001;
extras=0;
ecavsimrange(alpha,psi,constraint,constant,posnegEq,r0,tstart,tfinal,extras,1);

constant=0;
```

```
r0=[0.67*sin(psi)/alpha-0.0001;-0.0001];
tstart=cos(psi)/alpha;
tfinal=0;
extras=0;
ecavsimrange(alpha,psi,constraint,constant,posnegEq,r0,tstart,tfinal,extras,1);
constant=0;
r0=[0.67*sin(psi)/alpha-0.0001;0.0001];
tfinal=1/(alpha*cos(psi))-0.0001;
extras=0;
ecavsimrange(alpha,psi,constraint,constant,posnegEq,r0,tstart,tfinal,extras,1);
plot([0.33 0.75],[0 0],'y','LineWidth',6)
hold off
```

```
%   ECAVSIMRANGE
%
%   by Keith Purvis, August 2003
%
%   Plots an ECAV trajectory solution given the selected ECAV system (constant
%      velocity, constant course, constant turn rate, etc.) and the other
%      parameters listed below - all for a straight line phantom track
%
%   alpha is the relative speed of the phantom track
%   psi is the course of the phantom track
%   see the ode solution source code for details on constraint, constant, and r0
%   posneqEq is 1 for positive (increasing r) and 2 for negative (decreasing r)
%      when constraint = 1 (constant velocity) or 6 (constant acceleration)
%   tstart may be less than or greater than tfinal
%   extras is 0 for no extra graphs and 1 for extra graphs
%   multipleECAV is used for plotting multiple trajectories and is:
%      0 if starting the first segment of the first trajectory
%      1 otherwise
%      2 if no ECAV trajectories are desired (bounds only)
%   to end a plot of multiple trajectories, set hold off
%   to plot a single trajectory with multiple segments, set hold on in between

function [r,t]=ecavsimrange(alpha,psi,constraint,constant,posnegEq,r0,tstart,...
   tfinal,extras,multipleECAV)

if nargin==9
   multipleECAV=9;
end

%Constraints
v_Trange=0.2;
v_Erange=0.2;
v_Epseudomin=(1-v_Erange)/(1+v_Trange);
v_Epseudomax=(1+v_Erange)/(1-v_Trange);
phi_Erange=pi/3;
phi_Emin=pi/2-pi/3;
phi_Emax=pi/2+pi/3;

%Solution for the ode
tstep=0.001;
[t,r,ts,rs,is,R,theta,theta_dot,theta_ddot]=phantomline(tstart,tstep,tfinal,...
   r0,alpha,psi,constant,v_Epseudomin,v_Epseudomax,phi_Erange,posnegEq,...
   constraint);
Eq=['Eq. ',num2str(posnegEq)];
format compact
eval_is(is,ts,'')
```

```
%Check conditions for switching
if is(:)==1
   theta_ddot_minus=2*alpha^2*(sin(psi)*cos(psi)-alpha*sin(psi)*(ts(1)-...
      tstep))/((1+alpha^2*(ts(1)-tstep)^2-2*alpha*cos(psi)*(ts(1)-tstep))^2)
   theta_ddot_plus=2*alpha^2*(sin(psi)*cos(psi)-alpha*sin(psi)*(ts(1)+...
      tstep))/((1+alpha^2*(ts(1)+tstep)^2-2*alpha*cos(psi)*(ts(1)+tstep))^2)

   if is(:)==1 & ((theta_ddot_minus>0 & theta_ddot_plus<0) | constraint==5)
      posnegEq2=posnegEq+sign(1.5-posnegEq);
      if constraint==1
         r0=r(end);
         tstart=ts+sign(tfinal-tstart)*tstep;
      elseif constraint==5
         r0=[r(end);rs(2)+2*rs(2)];
         tstart=ts+sign(tfinal-tstart)*tstep;
      elseif constraint==6
         r0=[r(end);rs(2)+sign(rs(2))*2*tstep];
         tstart=ts+sign(tfinal-tstart)*tstep;
      end

      [t2,r2,ts2,rs2,is2,R2,theta2,theta_dot2,theta_ddot2]=phantomline(...
         tstart,tstep,tfinal,r0,alpha,psi,constant,v_Epseudomin,...
         v_Epseudomax,phi_Erange,posnegEq2,constraint);
      t=[t;real(t2)];
      r=[r;real(r2)];
      R=[R;R2];
      theta=[theta;theta2];
      theta_dot=[theta_dot;theta_dot2];
      theta_ddot=[theta_ddot;theta_ddot2];
      eval_is(is2,ts2,'After Switch, ')
      Eq=['Eqs. ',num2str(posnegEq),' and ',num2str(posnegEq2)];
      is=is2;
   end
end
theta_r=theta;
t_r=t;

%--------------------------------------------------------------------------

mainhandle=gcf;

%Calculate and plot other variables of interest
ic=2:length(t)-2;
ic2=2:length(t)-3;
r_dot=(diff(r,1))./tstep;
```

```
r_dot(ic)=(r_dot(ic)+r_dot(ic-1))/2;
r_ddot=(diff(r_dot(2:end),1))./tstep;
r_ddot(ic2+1)=(r_ddot(ic2-1)+r_ddot(ic2))/2;
phi_E=atan2(r(2:end-1).*theta_dot(2:end-1),r_dot(2:end));
phi_Edot=(diff(phi_E,1))./tstep;
phi_Edot(ic2+1)=(phi_Edot(ic2-1)+phi_Edot(ic2))/2;
v_E=sqrt(r_dot(2:end).^2+(r(2:end-1).*theta_dot(2:end-1)).^2);
v_Edot=(diff(v_E,1))./tstep;
v_Edot(ic2+1)=(v_Edot(ic2-1)+v_Edot(ic2))/2;
a_E=sqrt((r_ddot(3:end)-r(3:end-2).*theta_dot(3:end-2).^2).^2+...
   (r(3:end-2).*theta_ddot(3:end-2)+2.*r_dot(3:end-1).*theta_dot(3:end-2)).^2);
heading_E=phi_E+theta(2:end-1);
turnrate_E=phi_Edot(3:end)+theta_dot(3:end-2);

if extras==1
   figure;subplot(2,2,1)
   plot(t,theta_dot);grid on
   title('\theta_{dot} Versus Time')
   subplot(2,2,2)
   plot(t,theta_ddot);grid on;
   title('\theta_{ddot} Versus Time')
   subplot(2,2,3)
   plot(t(3:end-2),phi_E(2:end-1));grid on;
   title('\phi_E Versus Time')
   subplot(2,2,4)
   plot(t(4:end-3),phi_Edot(4:end-1));grid on;
   title('\phi_E_{dot} Versus Time')
   figure;subplot(2,2,1)
   plot(t,r);grid on;
   title('r Versus Time')
   subplot(2,2,2)
   plot(t(3:end-2),r_dot(3:end-1));grid on;
   title('r_{dot} Versus Time')
   subplot(2,2,3)
   plot(t,r.*theta_dot);grid on;
   title('r\cdot\theta_{dot} Versus Time')
   subplot(2,2,4)
   plot(t(4:end-3),r_ddot(4:end-1));grid on;
   title('r_{ddot} Versus Time')
   figure;subplot(2,2,1)
   plot(t(3:end-2),v_E(2:end-1),'b',t,v_Epseudomin*ones(size(t)),'r-.',...
      t,v_Epseudomax*ones(size(t)),'r-.');grid on;
   title('\upsilon_E Versus Time');legend('Actual','Bounds',0)
   subplot(2,2,2)
   plot(t(4:end-3),v_Edot(4:end-1));grid on;
   title('\upsilon_Edot Versus Time')
```

```
   subplot(2,2,3)
   plot(t(3:end-2),heading_E(2:end-1),t,phi_Emin+theta,'r-.',...
      t,phi_Emax+theta,'r-.');grid on;
   title('Heading Versus Time');legend('Actual','Bounds',0)
   subplot(2,2,4)
   plot(t(4:end-3),turnrate_E(2:end-1));grid on;
   title('Turn Rate Versus Time')
end

%Initialize the main plot figure
tfinal2=1/(alpha*cos(psi))-0.0001;
if multipleECAV==0
   t=0:tstep:tfinal2;
   R=sqrt(1+alpha^2.*t.^2-2*alpha*cos(psi).*t);
   theta=asin(alpha*sin(psi).*t./R);
   theta_dot=alpha*sin(psi)./(1+alpha^2.*t.^2-2*alpha*cos(psi).*t);
end

figure(mainhandle)
if ishold
   cla
else
   if get(gcf,'Color')==[1 1 1]
      figure
   end
   axis equal;axis([0 1 0 max(R(end),1)]);hold on;axis off
   set(gcf,'Color',[1 1 1],'MenuBar','figure','DoubleBuffer','on',...
      'Renderer','painters')
   title(['ECAV ',eval_constraint(constraint),...
      ' Trajectory Solution for a Given Phantom Track'],'FontSize',11)
end
if t_r(1)<=2*tstep
   if multipleECAV==9
      q=text(r(1),-0.01,['r_0 = ',num2str(r(1),3)],'Color','g',...
         'VerticalAlignment','top','HorizontalAlignment','left',...
         'FontSize',11);
      set(q,'HandleVisibility','callback')
   else
      q=text(r(1),-0.01,[num2str(r(1),2)],'Color','g',...
         'VerticalAlignment','middle','HorizontalAlignment','right',...
         'FontSize',11,'Rotation',90);
      set(q,'HandleVisibility','callback')
   end
end

if multipleECAV==0 | multipleECAV==9 | multipleECAV==2
```

```
%Plot of phantom track
d=plot(R.*cos(theta),R.*sin(theta),'b','LineWidth',1.5);

%Plots of r*theta_dot bounds, speed isolines, and phi_E bounds
f1v=plot(v_Epseudomax/alpha.*R.*cos(theta),...
   v_Epseudomax/alpha.*R.*sin(theta),'k:','Color',[0.7 0.7 0.7],...
   'LineWidth',1.5);
f2v=plot(v_Epseudomin/alpha.*R.*cos(theta),...
   v_Epseudomin/alpha.*R.*sin(theta),'c:','LineWidth',1.5);
f1=plot(v_Epseudomax./theta_dot.*cos(theta),...
   v_Epseudomax./theta_dot.*sin(theta),'k-.','Color',[0.7 0.7 0.7],...
   'LineWidth',1.5);
f2=plot(v_Epseudomin./theta_dot.*cos(theta),...
   v_Epseudomin./theta_dot.*sin(theta),'c-.','LineWidth',1.5);
f3=plot(v_Epseudomax*sin(phi_Emin)./theta_dot.*cos(theta),...
   v_Epseudomax*sin(phi_Emin)./theta_dot.*sin(theta),'y-.',...
   'Color',[1 0.6 0.2],'LineWidth',1.5);
f4=plot(v_Epseudomin*sin(phi_Emin)./theta_dot.*cos(theta),...
   v_Epseudomin*sin(phi_Emin)./theta_dot.*sin(theta),'r-.','LineWidth',1.5);

%Plots of radar LOS and ECAV trajectory
g=plot([0 R(end)*cos(theta(end))],[0 R(end)*sin(theta(end))],'k',...
   'LineWidth',1.5);
e=plot(r.*cos(theta_r),r.*sin(theta_r),'g','LineWidth',1.5);

%Markers for radar, ECAV, and phantom target
x=plot(0,0,'ko','LineWidth',1.5,'MarkerFaceColor','r','MarkerSize',10);
o=plot(R(end)*cos(theta(end)),R(end)*sin(theta(end)),'b*','MarkerSize',5);
h=plot(r(end)*cos(theta_r(end)),r(end)*sin(theta_r(end)),'g<',...
   'LineWidth',1.5,'MarkerFaceColor','y','MarkerSize',7);

%Text for theta= , psi= , and legend
p=text(0.15*cos(theta(end)),0.15*sin(theta(end)),['\theta = ',...
      num2str(theta(end)*180/pi,'%6.0f'),'\circ'],'VerticalAlignment',...
   'bottom','HorizontalAlignment','right','FontSize',11);
psiarray=pi-psi:psi/100:pi;
u=plot(1+0.07.*cos(psiarray),0.07*sin(psiarray),'b',[0.9 1],[0 0],'b',...
   [1+0.1*cos(psiarray(1)) 1],[0.1*sin(psiarray(1)) 0],'b');
v=text(1+0.07*cos(pi-psi),0.07*sin(pi-psi),['\psi = ',...
   num2str(psi*180/pi,2),'\circ'],'VerticalAlignment','bottom',...
   'FontSize',11,'Color','b');
w=legend(['Phantom track, \alpha = ',num2str(alpha)],...
   ['\upsilon_E = ',num2str(v_Epseudomax,2),' isoline'],...
   ['\upsilon_E = ',num2str(v_Epseudomin,2),' isoline'],...
   ['r\cdot\theta_{dot} = ',num2str(v_Epseudomax,2),' boundary'],...
   ['r\cdot\theta_{dot} = ',num2str(v_Epseudomin,2),' boundary'],...
```

```
        ['\phi_E = ',num2str(phi_Emin*180/pi,2),'\circ (\upsilon_E = ',...
            num2str(v_Epseudomax,2),')'],...
        ['\phi_E = ',num2str(phi_Emin*180/pi,2),'\circ (\upsilon_E = ',...
            num2str(v_Epseudomin,2),')'],'Radar LOS','ECAV trajectory');
    set([d e f1 f1v f2 f2v f3 f4 w],'HandleVisibility','callback')
    if multipleECAV==0 | multipleECAV==2
        set([g o p u(1) u(2) u(3) v x],'HandleVisibility','callback')
    end
elseif multipleECAV==1
    e=plot(r.*cos(theta_r),r.*sin(theta_r),'g','LineWidth',1.5);
    set(e,'HandleVisibility','callback')
    if t_r(end)>=tfinal2-2*tstep
        h=plot(r(end)*cos(theta_r(end)),r(end)*sin(theta_r(end)),'g<',...
            'LineWidth',1.5,'MarkerFaceColor','y','MarkerSize',7);
    end
end
hold off

if multipleECAV==0 | multipleECAV==1
    hold on
    if t_r(end)>=tfinal2-2*tstep
        set(h,'HandleVisibility','callback')
    end
end

if multipleECAV==2
    set([e h q],'HandleVisibility','on')
    cla
end
```

```
%   PHANTOMLINE
%
%   by Keith Purvis, August 2003
%
%   Solves for an ECAV trajectory solution given the input constraint and the
%      other inputs, which are described in ecavsimrange.m - all for a straight
%      line phantom track (phantom track functions are also calculated)
%   An events function at the end stops the ode solution at the defined zero
%      crossings, which relate to a possible switching function,
%      v_Epseudorange, phi_Erange, radar crossing, or phantom track crossing
%
%   for the last input - constraint,
%   1=constant speed, v_E; initial range required for r0
%   2=constant course, phi_E; initial range required for r0
%   3=constant heading;initial range required for r0
%   4=constant turn rate; initial range and range rate required for r0
%   5=constant speed rate, v_Edot; initial range and range rate required for r0
%   6=constant acceleration,a_E; initial range and range rate required for r0

function [t,r,te,re,ie,R,theta,theta_dot,theta_ddot]=phantomline(tstart,...
   tstep,tfinal,r0,alpha,psi,constant,v_Epseudomin,v_Epseudomax,phi_Erange,...
   posnegEq,constraint)

%Options, tspan, and r0 initialized
options = odeset('RelTol',1e-6,'AbsTol',1e-6,'MaxStep',tstep,'Events',@events,...
   'Refine',1);
if (tfinal-tstart)<0
   tstep=-tstep;
end
tspan=tstart:tstep:tfinal;
if constraint<=3 r0=r0(1);
end

%Ode solved
[t,r,te,re,ie]=ode45(@f,tspan,r0,options,alpha,psi,constant,v_Epseudomin,...
   v_Epseudomax,phi_Erange,posnegEq,constraint);

%If the switching function = 0, last solution value deleted since imaginary
if length(ie)>1
   ie=min(ie);
end
if ie(:)==1 | constraint==6
   re=r(end-1,:);r=r(1:end-1,1);
   te=t(end-1);t=t(1:end-1);
else
   re=r(end,:);r=r(1:end,1);
```

```
   te=t(end);t=t(1:end,1);
end

%Calculation of other variables dependent on the phantom track
R=sqrt(1+alpha^2.*t.^2-2*alpha*cos(psi).*t);
theta=asin(alpha*sin(psi).*t./R);
theta_dot=alpha*sin(psi)./(1+alpha^2.*t.^2-2*alpha*cos(psi).*t);
theta_ddot=2*alpha^2*(sin(psi)*cos(psi)-alpha*sin(psi).*t)./...
   ((1+alpha^2.*t.^2-2*alpha*cos(psi).*t).^2);

%Arrays reversed if ode was solved back in time
if (tfinal-tstart)<0
   for i=1:length(t)
      rr(i)=r(end+1-i);
      tr(i)=t(end+1-i);
      Rr(i)=R(end+1-i);
      thetar(i)=theta(end+1-i);
      theta_dotr(i)=theta_dot(end+1-i);
      theta_ddotr(i)=theta_ddot(end+1-i);
   end
   r=rr;t=tr;R=Rr;theta=thetar;theta_dot=theta_dotr;theta_ddot=theta_ddotr;
end

%-------------------------------------------------------------------------

function drdt=f(t,r,alpha,psi,constant,v_Epseudomin,v_Epseudomax,phi_Erange,...
   posnegEq,constraint)

R=sqrt(1+alpha^2*t^2-2*alpha*cos(psi)*t);
theta=asin(alpha*sin(psi)*t/R);
theta_dot=alpha*sin(psi)/(1+alpha^2*t^2-2*alpha*cos(psi)*t);
theta_ddot=2*alpha^2*(sin(psi)*cos(psi)-alpha*sin(psi)*t)/((1+alpha^2*t^2-...
   2*alpha*cos(psi)*t)^2);

if constraint==1    %v_E constant
   drdt=sign(1.5-posnegEq)*sqrt(constant^2-(theta_dot)^2*r^2);
elseif constraint==2    %phi_E constant
   drdt=r*theta_dot*cot(constant);
elseif constraint==3    %heading constant
   phi_E=constant-theta;
   drdt=r*theta_dot*cot(phi_E);
elseif constraint==4    %turnrate constant
   phi_Edot=constant-theta_dot;
   drdt=[r(2);(r(2)*(r(1)*theta_ddot+r(2)*theta_dot)-(r(2)^2+...
      (r(1)*theta_dot)^2)*phi_Edot)/r(1)/theta_dot];
elseif constraint==5    %v_Edot constant
```

```
    drdt=[r(2);(-r(1)*theta_dot*(r(1)*theta_ddot+r(2)*theta_dot)+...
        sqrt(r(2)^2+(r(1)*theta_dot)^2)*constant)/r(2)];
elseif constraint==6    %a_E constant
    drdt=[r(2);r(1)*theta_dot^2+sign(1.5-posnegEq)*sqrt(constant^2-...
        (r(1)*theta_ddot+2*r(2)*theta_dot)^2)];
end

%-------------------------------------------------------------------------

function [value,isterminal,direction]=events(t,r,alpha,psi,constant,...
    v_Epseudomin,v_Epseudomax,phi_Erange,posnegEq,constraint)

R=sqrt(1+alpha^2*t^2-2*alpha*cos(psi)*t);
theta=asin(alpha*sin(psi)*t/R);
theta_dot=alpha*sin(psi)/(1+alpha^2*t^2-2*alpha*cos(psi)*t);
theta_ddot=2*alpha^2*(sin(psi)*cos(psi)-alpha*sin(psi)*t)/((1+alpha^2*t^2-...
    2*alpha*cos(psi)*t)^2);

if constraint==1
    s=constant^2-(r*theta_dot)^2;
    vmin=1;
    vmax=1;
    a=r*theta_dot/constant-sin(pi/2-phi_Erange);
elseif constraint==2
    v_E=r*theta_dot/sin(constant);
    s=1;
    vmin=v_E-v_Epseudomin;
    vmax=v_E-v_Epseudomax;
    a=1;
elseif constraint==3
    phi_E=constant-theta;
    v_E=r*theta_dot/sin(phi_E);
    s=1;
    vmin=v_E-v_Epseudomin;
    vmax=v_E-v_Epseudomax;
    a=1;
elseif constraint==4
    v_E=sqrt(r(2)^2+(r(1)*theta_dot)^2);
    s=1;
    vmin=v_E-v_Epseudomin;
    vmax=v_E-v_Epseudomax;
    a=r(1)*theta_dot/v_E-sin(pi/2-phi_Erange);
elseif constraint==5
    v_E=sqrt(r(2)^2+(r(1)*theta_dot)^2);
    s=r(2);
    vmin=v_E-v_Epseudomin;
```

```
    vmax=v_E-v_Epseudomax;
    a=r(1)*theta_dot/v_E-sin(pi/2-phi_Erange);
elseif constraint==6
    v_E=sqrt(r(2)^2+(r(1)*theta_dot)^2);
    s=constant^2-(r(1)*theta_ddot+2*r(2)*theta_dot)^2;
    vmin=v_E-v_Epseudomin;
    vmax=v_E-v_Epseudomax;
    a=r(1)*theta_dot/v_E-sin(pi/2-phi_Erange);
end

value=[s;vmin;vmax;a;R-r(1);r(1)];
isterminal=[1;1;1;0;1;1];
direction=[0;0;0;0;-1;-1];
```

```
function eval_is(is,ts,string)

if length(is)==2
   is=is(1);
end

if is(:)==1
   disp([string,'Switching Function Reached Zero at t = ',num2str(ts,3),' sec'])
elseif is(:)==2
   disp([string,'Lower Velocity Bound Reached at t = ',num2str(ts,3),' sec'])
elseif is(:)==3
   disp([string,'Upper Velocity Bound Reached at t = ',num2str(ts,3),' sec'])
elseif is(:)==4
   disp([string,'Angle Bound Reached at t = ',num2str(ts,3),' sec'])
elseif is(:)==5
   disp([string,'ECAV Trajectory Reached Phantom Track at t = ',...
      num2str(ts,3),' sec'])
elseif is(:)==6
   disp([string,'ECAV Trajectory Reached Radar at t = ',num2str(ts,3),' sec'])
elseif is(:)==7
   disp([string,'No Events Occurred - Reached theta(end) at t = ',...
      num2str(ts,3),' sec'])
else
   disp([string,'No Events Occurred'])
end
```

```
function [string]=eval_constraint(constraint)

if constraint==1
   string='Constant Speed';
elseif constraint==2
   string='Constant Course';
elseif constraint==3
   string='Constant Heading';
elseif constraint==4
   string='Constant Turn Rate';
elseif constraint==5
   string='Constant Speed Rate';
elseif constraint==6
   string='Constant Acceleration';
end
```